Towards a Novel Process for Milking High Value Fatty Acids from Microalgae

A thesis submitted for the degree of Doctor of Philosophy in Biotechnology

Aidan Grimsley (Student ID: 4215101)

Supervised by: Prof. Gill Stephens, Dr. Anna Croft and Dr. Stephen Hall

18/12/2020

Table of Contents

List of Figures

List of Tables

List of Abbreviations

AG - acylglycerol/acylglyceride

BBM - Bold's basal modified

CHD - coronary heart disease

DAG - diacylglycerol

DHA- docosahexaenoic acid

DNA - deoxyribonucleic acid

EPA - eicosapentaenoic acid

EPAEE - eicosapentaenoic acid ethyl ester

EPAME - eicosapentaenoic acid methyl ester

ESI-MS - electrospray ionisation mass spectrometry

FA - fatty acid

FAEE - fatty acid ethyl ester

FAME - Fatty acid methyl ester

FID - flame ionisation detection

GC - gas chromatography

GCMS - gas chromatography mass spectrometry

HPLC - high performance liquid chromatography

HPLCUV - high performance liquid chromatography with ultraviolet detection

IL - ionic liquid

LoQ - limit of quantification

MAG - monoacylglycerol

MD - molecular dynamics

MIC - minimum inhibitory concentration

NADPH - nicotinamide adenine dinucleotide phosphate (reduced form)

NAG - *N*-acetylglucosamine

NAM - *N*-acetylmuramic acid

NMR - nuclear magnetic resonance

OD - optical density

PCB - printed circuit board

PEF - pulsed electric fields

PPFD - photosynthetic photon flux density

PUFA - polyunsaturated fatty acid

RNA - ribonucleic acid

ROS - reactive oxygen species

TAG - triacylglycerol

UV - ultraviolet

Acknowledgements

Special thanks go to my supervisors Professor Gill Stephens, Dr. Anna Croft and Dr. Stephen Hall. Without their help, encouragement, and guidance on matters scientific or otherwise, this never would have happened. I would also like to thank all members of the SPT research team, both for their technical help and for providing a great social environment in and outside of work. Thank you to Edward Kujawinski and Mark Birkin of the electrical engineering workshop team for their technical assistance in the design and construction of the electrode array PEF rig. Thank you to John Dodd of AlgaeCytes, for his assistance throughout.

Thank you to all my friends and family for their support provided during a difficult time. Every one of you helped lift my spirits at some point throughout this process, whether knowingly or not. Special thanks go to Steph Bowskill, without her emotional support I may not have made it. Thank you to Dr. Harriet(t) Day and Dr. Charlie Ducker, for their support and for providing a new home.

1. Abstract

The microalga *Trachydiscus minutus* produces high quantities of eicosapentaenoic acid (EPA), a valuable nutraceutical. However, the slow growing nature of *T. minutus* and the energy intensive processes of biomass concentration and EPA extraction significantly diminish the economic return of the whole bioprocess. A novel "milking" process, in which EPA can be extracted from cells while retaining their viability, was explored here. This enables repeated extractions from the same cells, reducing the time and energy cost of growing new algal cultures. A literature survey identified two promising milking methods; a biphasic system utilising a water immiscible, biocompatible solvent for product extraction, and pulsed electric fields (PEF) to produce transient pores in the cell membrane. Both methods were applied to dilute cultures, thus bypassing the need to concentrate biomass. The volatile organic compounds typically used in biphasic extractions are often hazardous to the environment and personnel. This project explored the use of water immiscible ionic liquids (ILs), which are salts in the liquid state, as an alternative for biphasic milking. ILs have a vast range of structures and properties, yet their potential in algal milking was relatively unexplored.

This project aimed to begin development of EPA milking processes by: (i) identifying solvents, including ILs, which are non-toxic towards *T. minutus* and could be used in a biphasic milking strategy, (ii) to develop methods for quantifying EPA present in these ILs, and (iii) to explore the ability of PEF to reversibly permeabilise *T. minutus* cells.

A tiered approach was used to screen for non-toxic ILs, using an adapted agar diffusion method, then a small scale liquid toxicity method, and finally a large scale toxicity experiment. This enabled 62 ILs to be screened at significantly reduced costs and time compared to direct large scale experiments. Imidazolium, pyridinium, pyrrolidinium and piperidinium ILs were generally toxic to *T. minutus*, while results from quaternary ammoniums and phosphoniums were more variable. Trihexyltetradecylphosphonium docusate ($[P_{6\,6\,6\,14}][AOT]$) and trihexyltetradecylphosphonium *bis*(2-ethylhexyl)phosphate ($[P_{6\,6\,6\,14}][iC_8PO_4]$), were found to be non-toxic to *T. minutus*, as were the conventional solvents dodecane and tetradecane. These are the first reports of ILs biocompatible with this alga, representing a significant step towards an IL-based biphasic EPA milking strategy for *T. minutus*.

Solvents for an EPA milking strategy must be capable of extracting EPA, so methods for quantifying EPA in ILs were developed. Gas chromatography analysis of fatty acids in conventional solvents is common in the literature. However, this method was deemed

unsuitable for analysing non-volatile ILs because they were shown to be introduced into the analytical column, thus restricting flow rate and causing peak broadening. Instead, a HPLC-UV method was developed to enable analysis of liquid samples. This provides a future means to assess the ability of non-toxic ILs to extract EPA from dilute cultures.

Using fluorescence staining and flow cytometry analysis, PEF treatments with an electric field strength greater than 3 kV/cm were demonstrated to permeabilise *T. minutus*. A cell counting method after culture recovery was suitable to assess cell viability after PEF treatment. A commercially available electroporator was unable to treat sufficient volume of *T. minutus* culture for accurate EPA quantification. A larger PEF chamber design is proposed, to enable treatment of greater volumes in a semi-continuous, more industrially relevant, process. Overall, these findings represent significant progress towards methods for milking EPA from *T. minutus* and could have applications in wider microbial bioprocesses.

2. Literature Review

2.1. Fatty Acids and Eicosapentaenoic Acid

Eicosapentaenoic acid (EPA) is an omega-3 polyunsaturated fatty acid (PUFA) commonly found in oily fish (Fig. 1). However, the initial producers of EPA and many other omega-3 fatty acids are microalgae, the predation of which results in the accumulation of EPA in the food chain. EPA has been shown to have significant preventative effects against cardiovascular diseases, including coronary heart disease (CHD) (Watanabe *et al.*, 2017). As a result, the American Heart Association and World Health Organisation recommend a combined EPA and docosahexaenoic acid (DHA) dose of 1 g day^{-1} in patients with a history of CHD, and 500 mg day^{-1} for patients with no history of cardiovascular diseases. This equates to approximately 2 oily fish meals per week (Lavie *et al.*, 2009). Other studies have suggested it may also assist in managing depression and schizophrenia (Peet and Stokes, 2005). Due to current concerns of overfishing, the potential for accumulation of toxins in fish, and the need for a vegetarian and halal source of EPA, there is a market for the sustainable production of EPA and DHA from microalgae for use as supplements or food and beverage enrichments (Lane *et al.*, 2013). There are currently at least 5 algae biotech companies commercialising EPA production; AlgaeCytes, Algisys, Veramaris, Qponics and Martek. AlgaeCytes, the industrial partner of this project, extract EPA from *Trachydiscus minutus*, which has been shown to produce EPA in high quantities. Under growth conditions optimal for EPA production, EPA accounts for around 4.6% of the total dry weight of *T. minutus* biomass. As a result, despite the relatively slow growth of this species, EPA production can reach 30 mg per litre of culture per day (Cepák *et al.*, 2014). Evidence suggests an EPA:DHA ratio in the region of 1:1 to 2:1 is particularly beneficial for reducing biomarkers of CHD (Dasilva *et al.*, 2015, Shang *et al.*, 2017). Critically, *T. minutus* does not produce DHA (Cepák *et al.*, 2014). This enables AlgaeCytes to supply an oil that can be easily mixed with other oils to achieve a specific EPA:DHA ratio for maximal efficacy, which separates AlgaeCytes' process from the competition. The global market value of omega 3 oils was estimated at $ 2.5 billion in 2019, has been growing year on year and is expected to continue growing by around 7 % annually for the next decade (GrandViewResearch, 2020).

The fatty acid profile of *T. minutus*, (and other alga) varies according to their cultivation conditions, *e.g.* light intensity, temperature, pH, nitrogen source, salinity. Since these variables also affect culture growth (*i.e.* overall biomass production), conditions in which the highest cellular EPA content is achieved do not necessarily coincide with highest EPA productivity due to reduced overall biomass production. Conditions for optimal

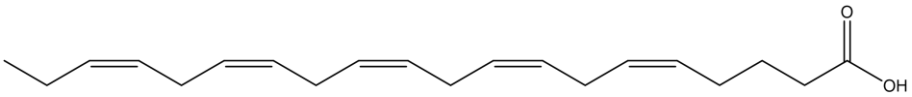

Fig. 1 - Structure of Eicosapentaenoic acid (EPA). Note that with a pKa of 4.8, the carboxyl group of EPA is typically deprotonated at physiological pH.

T. minutus growth and fatty acid production are well established (Cepák *et al.*, 2014, Gigova *et al.*, 2012). Briefly, EPA productivity of 30 mg L^{-1} day^{-1} can be achieved when growing *T. minutus* at 28 °C under a light intensity between 500 - 1000 µmol photons m^{-2} s^{-1}, with different common nitrogen sources (KNO_3, urea, NH_4NO_3) generally having little effect. However, lower light intensities and temperatures can yield an oil richer in EPA (up to around 50% of total FAs) at the cost of reduced culture growth rate and overall EPA productivity (Cepák *et al.*, 2014, Gigova *et al.*, 2012). AlgaeCytes balance EPA productivity with oil quality by typically growing *T. minutus* under a constant light intensity of 200 µmol m^{-2} s^{-1} and 25°C. Under these conditions, *T. minutus* cultures will enter stationary phase after 6 days of cultivation, at which point cellular EPA content is maximal and hence cells should be harvested for fatty acid extraction. AlgaeCytes currently harvest biomass using chemical flocculants, disrupt cells *via* mechanical methods, and extract algal oil using heptane.

Fatty acids are usually found esterified to glycerol, yielding acylglycerols (AGs, acylglycerides) (Fig. 2). Each glycerol molecule is capable of bonding with up to three fatty acids at each of its 3 carbon atoms: *sn*-1, *sn*-2, and *sn*-3. Not all *sn*- positions are necessarily bound with fatty acids, hence monoacylglycerols (MAGs), diacylglycerols (DAGs) and triacylglycerols (TAGs) exist. With so many variables, a huge range of AGs could be present within a cell; if any fatty acid can bond at any *sn*- position, the number of TAGs alone is equal to the cube of the number of different fatty acids available for esterification (Scrimgeour, 2005). This study focusses primarily on the extraction of EPA glycerides, since approximately 85% of EPA in *T. minutus* is found in the form of AGs; around 60% as TAGs and 25% as MAGs and DAGs (Stranska-Zachariasova *et al.*, 2016). The remaining 15% can be found across

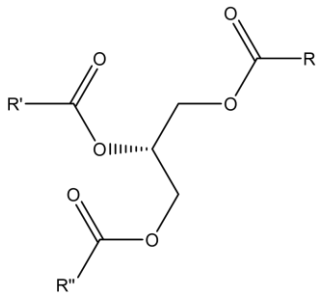

Fig. 2 - Structure of Triacylgycerols (TAGs). Fatty acids are usually found esterified to a glycerol backbone as depicted. A wide variety of TAGs can exist thanks to differing combinations of fatty acids.

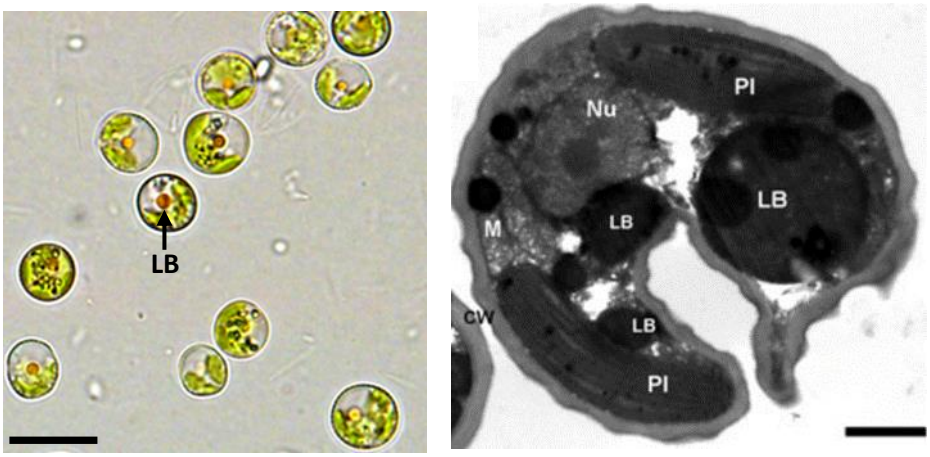

Fig. 3 - *Trachydiscus minutus* Morphology. Left - light micrograph of *T. minutus* cells, with visible yellow-brown lipid bodies (LB), scale bar 10 µm. Right - transmission electorn micrograph of a *T. minutus* cell. LB - lipid body, Nu - nucelus, Pl- plastid, M - mitochondrion, CW - cell wall, scale bar 1 µm. Image from Přibyl *et al.*, 2012.

various polar phospholipid classes, including phosphatidylglycerols, phosphatidylinositols, phosphatidylethanolamins, and phosphatidylserins, which are components of the cell membrane. Microalgal PUFA synthesis takes place in the chloroplast and endoplasmic reticulum (Mühlroth *et al.*, 2013). After synthesis, fatty acids are exported to the cytoplasm where they are attached to glycerol, yielding AGs. Here they agglutinate into a lipid body (Fig. 3) alongside other lipids and antioxidants such as β-carotene, vaucheriaxanthin and violaxanthin (Samek *et al.*, 2010, Přibyl *et al.*, 2012). The size of the lipid body typically increases over the course of culture growth, reaching maximal size (approximately 2 µm in diameter) in early stationary phase (Přibyl *et al.*, 2012). The main biological function of these AGs is to act as energy and carbon storage for times of environmental stress. Furthermore, AG biosynthesis may serve as an electron sink during photooxidative stress (Hu *et al.*, 2008). Excessive electron accumulation during the photosynthetic electron transport chain (*e.g.* under high light intensity) can result in increased levels of reactive oxygen species (ROS), which are capable of a myriad of biologically undesirable reactions (Auten and Davis, 2009). The production of a C18 fatty acid consumes 24 NADPH (from the electron transport chain), thus providing a means of lowering the electron excess (Hu *et al.*, 2008).

Exposure of fatty acids to oxygen can lead to their oxidative degradation. However, O_2 is in a triplet electronic state and cannot react directly with the singlet electronic state double bonds of a fatty acid (Chen *et al.*, 2011). Rather, for oxidation to occur the O_2 needs to be activated into ROS such as singlet oxygen ($^1O_2$), hydrogen peroxide (H_2O_2), superoxide anions ($O_2^{\bullet-}$), or hydroxyl radicals ($OH^{\bullet}$). These ROS can be introduced from a variety of endogenous reactions (*e.g.* oxidative phosphorylation) and exogenous sources (*e.g.* catalysis

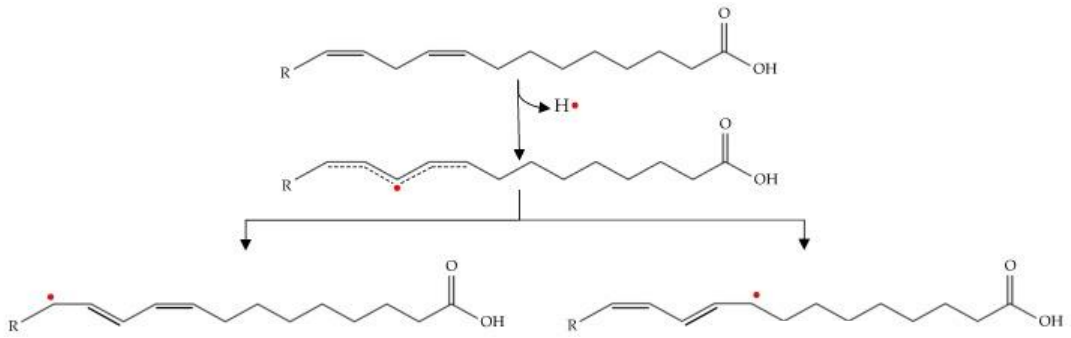

Fig. 4 - Initiation of Fatty Acid Oxidation. A reactive oxygen species (ROS) abstracts a hydrogen from an unsaturated fatty acid. The resultant alkyl radical can undergo rearrangement to yield conjugated dienes. Image adapted from Domínguez *et al*., 2019.

by heavy metal pollutants) (Min and Ahn, 2005). Of particular relevance to microalgae is fatty acid oxidation catalysed by light (photooxidation). In photooxidation, photosensitisers (*e.g.* chlorophyll) are excited into a singlet state by absorption of light (Foote, 1991). These excited photosensitisers can then initiate oxidation through direct interaction with a substrate (Type I photooxidation) or indirectly through interaction with oxygen to yield singlet oxygen (Type II photoxidation) (Bacellar and Baptista, 2019).

Oxidation can be considered to have 3 distinct phases: initiation, propagation, and termination. Initiation of fatty acid oxidation is still an area of active research but is thought to begin by the abstraction of a hydrogen from an unsaturated fatty acid by a ROS, yielding a free radical (Fig. 4). This occurs most readily to bisallylic carbon atoms. Hence fatty acids with greater extent of unsaturation, such as EPA with 5 double bonds, are more susceptible to oxidation. After hydrogen abstraction, the double bonds of the resulting alkyl radical can undergo rearrangement (Fig. 4) (Marchand and Rontani, 2001). This alkyl radical can react with molecular oxygen to generate a peroxy radical (ROO$^{\bullet}$) (Fig. 5). In the propagation phase the peroxy radical can abstract a hydrogen from a nearby lipid, generating a lipid hydroperoxide and a new alkyl radical (Fig. 5), enabling the process to continue. Furthermore, the lipid hydroperoxides can react with each other and metal ions to generate hydroxyl, peroxy and alkoxy lipid radicals (Fig. 5), themselves capable of abstracting hydrogen from more fatty acids, thereby creating a chain reaction (Domínguez *et al.*, 2019). Thus, while the initiation of the oxidation process is generally slow, propagation is comparatively rapid and can be extremely detrimental to maintaining fatty acid structure. However, the process can be terminated either by antioxidants, which donate a hydrogen to the radical and leave a much less reactive antioxidant radical (Ladikos and Lougovois, 1990), or through radical-radical coupling (Cheng, 2016). *T. minutus* is known to store high

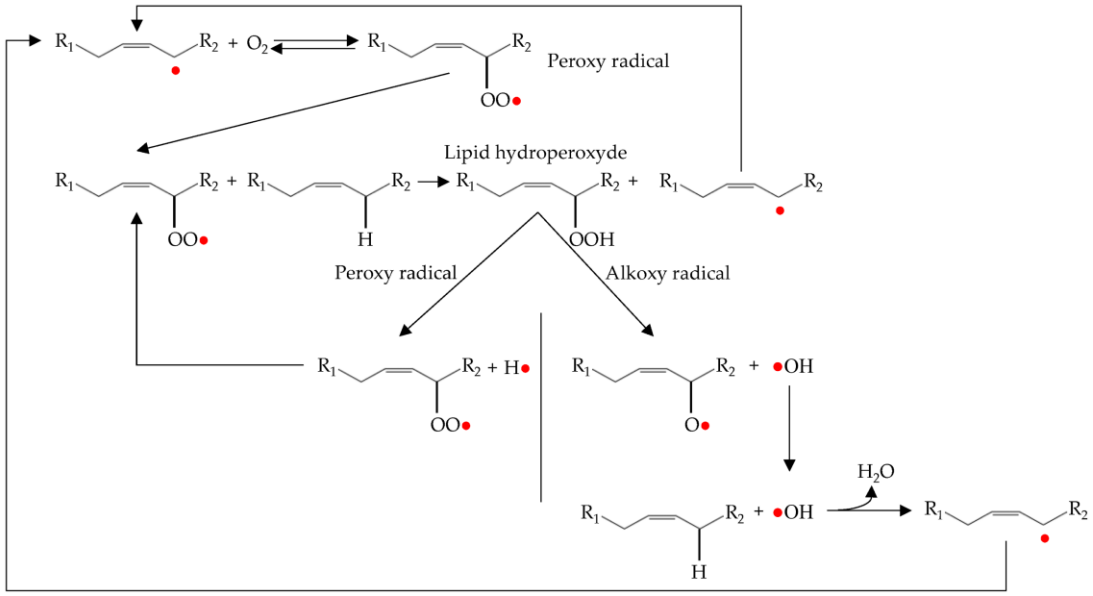

Fig. 5 - Propagation of Fatty Acid Oxidation. Further reaction of the alkyl radical with oxygen can generate peroxy radicals. These can themselves generate more alkyl radicals through reacting with unsaturated fatty acids, as well as alkoxy and hydroxy radicals which also further the propagation of fatty acid oxidation. Image from Domínguez *et al.*, 2019.

quantities of antioxidants (particularly β-carotene) alongside the AGs in the lipid body (Samek *et al.*, 2010). Extracting these antioxidants alongside the EPA AGs could prove an efficient means to provide continued oxidative protection.

2.2. Bottlenecks in Algal Biotechnology

Most successful algal bioprocesses are focussed on high-value low-volume products such as nutraceuticals. Low-value high-volume products from algae, such as biofuels, tend not to be economically viable. This is mainly due to current high cost, energy intensive biomass concentration and harvesting procedures (Boer *et al.*, 2012), as well as inefficient downstream extraction approaches. This is true for AlgaeCytes' process; dewatering and extraction approaches remain the greatest energetic and economic expense. Cultures of algae are particularly dilute, typically consisting of 0.02%-0.1% (w/v) suspended solids. For downstream extraction, the biomass usually needs to be concentrated into a slurry consisting of about 5-25% (w/v) solids (Uduman *et al.*, 2010). Once concentrated, a further hurdle is extraction of an intracellular product from the organism. Most algal species have some kind of cell wall, including common polysaccharide structures, silicon based layers of diatoms, and algaenans of certain Chlorophytes, Eustigmatophytes and Dinophytes (Versteegh and Blokker, 2004). Such structures are extremely tough, hence requiring high energy input to break or penetrate to access the intracellular compounds of interest.

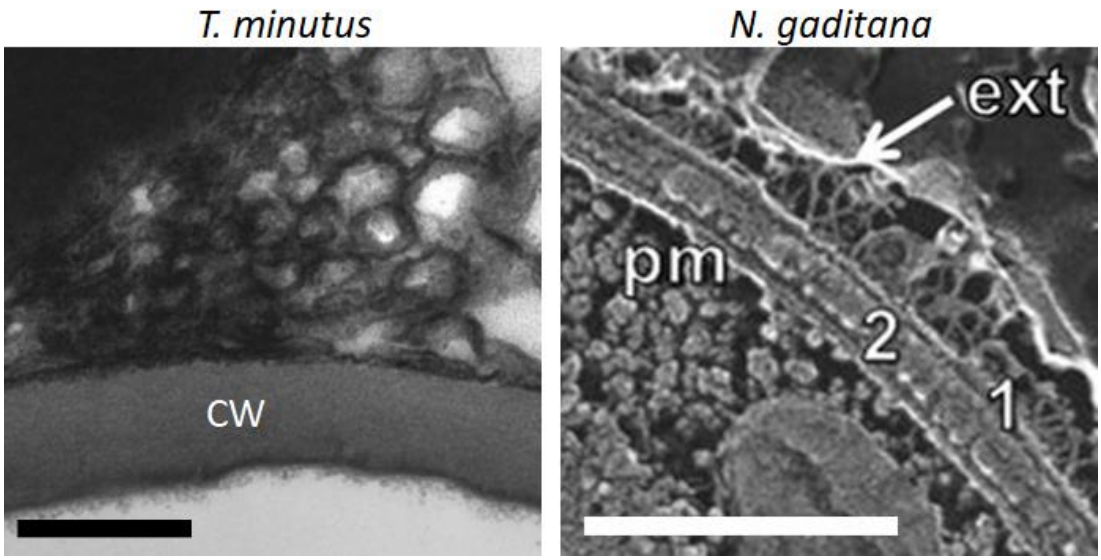

Fig. 7 - Cell wall structure of *T. minutus* and *N. gaditana.* The cell wall (CW) of *T. minutus* (left) appears to be a single structure consisting primarily of cellulose. The closely related *N. gaditana* (right) has been more extensively studied. Its plasma membrane (pm) is surrounded by a cell wall consisting of a predominantly cellulose layer (2) and an outer algaenan layer (1), with exterior extensions (ext) of an unknown composition. Both scale bars 250 nm. Images adapted from Přibyl *et al.*, 2012 (left) and Scholz *et al.*, 2014 (right).

For example, the cell wall of *T. minutus* is 150 - 250 nm thick (Fig. 7) (Přibyl *et al.*, 2012) and AlgaeCytes have communicated that it is composed predominantly of cellulose. Being a relatively obscure organism, no more is known about the *T. minutus* cell wall composition at the time of writing. However, *Nannochloropsis gaditana*, which belongs to the same taxonomic class as *T. minutus* (Eustigmatophyceae), has a cell wall consisting of 2 layers with a total thickness of 50 - 60 nm (Fig. 7). The inner layer consists of approximately 75% cellulose (glucose monosaccharides joined by β-1,4 glycosidic bonds (Fig. 6)). The

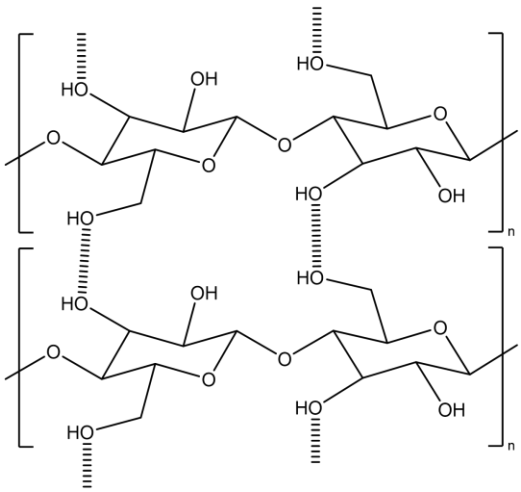

Fig. 6- Chemical Structure of Cellulose. Cellulose is a polymer of glucose connected by β-1,4 glycosidic bonds, forming long strands. Inter-strand hydrogen bonds (dashed lines) enable formation of fibres with high tensile strength.

remainder is comprised of other polysaccharides including 1,2-linked rhamnose and fucose, 1,4-linked mannose and 1,6-linked galactose, as well as around 6% protein (Scholz *et al.*, 2014). The outer wall is comprised of algaenan, a name given to a wide range of chemically recalcitrant aliphatic material formed of cross-linked carbon chains of varying structure found across many algal species. For example, the algaenan of *Nannochloropsis salina* is believed to be composed of straight chains around 30 carbons long (C_{30}), while *Scenedesmus communis* has an algaenan wall consisting of ≈C_{120} chains. The cross links and specific moieties present in algaenans are also highly variable between species and can include alcohols, carboxyls and aldehydes, as well as varying degrees of unsaturation (Scholz *et al.*, 2014). One group of microalgae, diatoms, have a silica (SiO_2) cell wall called a frustule. This is comprised of 2 joined halves, is very hard, and has a number of pores enabling flux (De Tommasi *et al.*, 2017) . The frustule is typically also coated in a polysaccharide sheath. A huge range of diatom shapes exist including circular, triangular, elliptical and square (Horner, 2002).

In comparison, bacterial cell membranes are protected by a peptidoglycan layer, and in Gram negative bacteria (*e.g. E. coli*), a subsequent outer lipopolysaccharide layer, with periplasm between each layer (Fig. 8). The peptidoglycan is the toughest layer and is the most responsible for bearing stress and maintaining cell shape (Huang *et al.*, 2008). It consists of β-1,4 linked *N*-acetylglucoasmine (NAG) and *N*-acetylmuramic acid (NAM) disaccharides, with a peptide chain of 3 to 5 amino acids attached to NAM subunits. These peptides can cross link with each other to create a mesh (Fig. 9) The thickness of the layer is variable between strains, species and growth conditions, but is generally substantially thicker in Gram positive bacteria. In *E. coli*, which is widely used in biotechnology, the peptidoglycan layer is

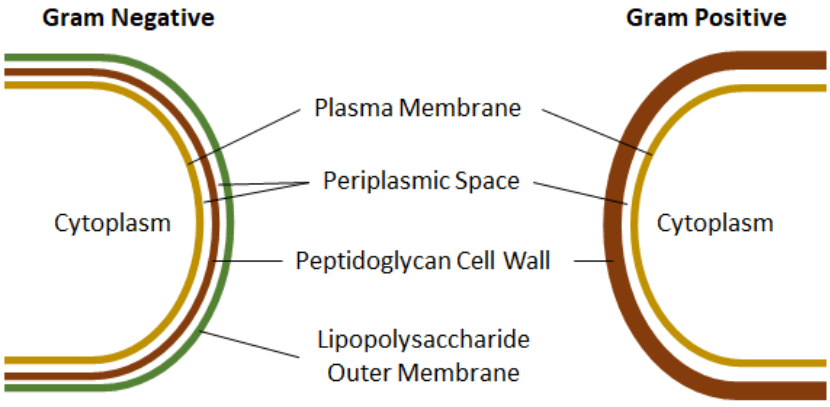

Fig. 8 - Schematic Representation of the Differences Between Gram Positive and Gram Negative Bacteria. Both cell types have a plasma membrane and peptidoglycan cell wall, but the cell wall is usually much thicker in Gram positive bacteria. Gram negative bacteria also have an outer membrane consisting primarily of lipopolysaccharides.

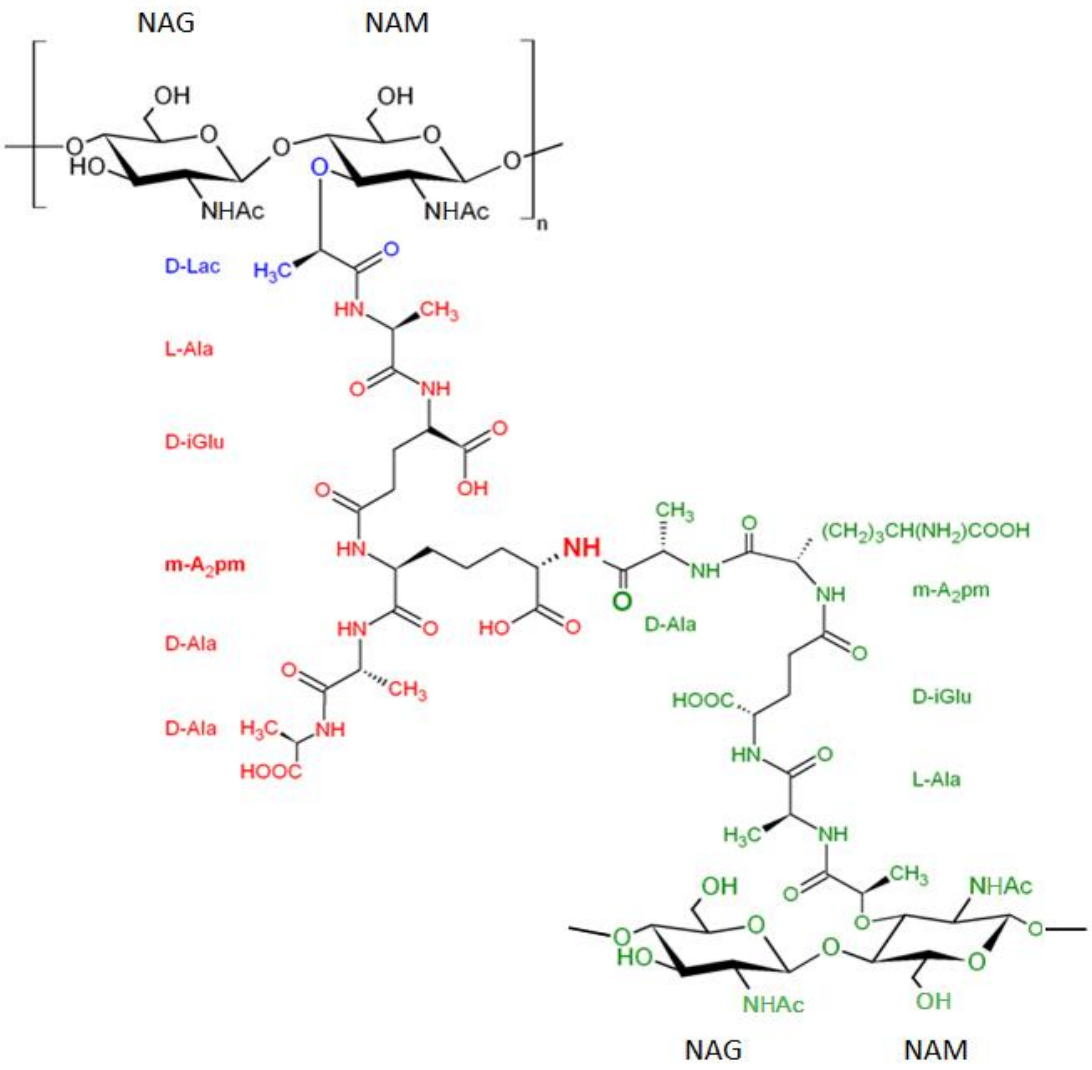

Fig. 9 - Chemical Structure of *E. coli* Peptidoglycan. Peptidoglycan is polymer of a disaccharide and pentapeptide motif. The disaccharide consists of β-1,4-linked N-acetylglucosamine (NAG) and N-acetylmuramic acid (NAM). The peptide chain (red) is linked to NAM residues *via* its D-lactyl group (blue). The peptide chain can form cross links with other peptidoglycan strands (green). In *E. coli*, the pentapeptide usually consists of L-alanine (L-Ala), D-isoglutamic acid (D-iGlu), meso-diaminopimelic acid (m-A_2pm), and 2 D-alanine (D-Ala) residues. Image adapted from Glycopedia (N. Jean, 2014).

around 4 nm thick (Gan *et al.*, 2008, Yao *et al.*, 1999), while in the widely used Gram positive bacterium, *Bacillus subtilis*, it is around 40 nm thick (Hayhurst *et al.*, 2008, Anné *et al.*, 2014).

Cell shape and size will also play a role in the energy required to break the cell wall, but it is often true that microalgal cells are tougher than bacteria due to their generally much thicker walls, which can comprise multiple chemically distinct and recalcitrant layers. For example when using high pressure homogenisation as a means of cell lysis, maximum lysis of *E. coli* is typically achieved at a pressure of around 500 bar (Pekarsky *et al.*, 2019), *B. subtilis* at around 900 bar (Geciova *et al.*, 2002), and *N. gaditana* at 1500 bar (Safi *et al.*, 2017). Unfortunately, equivalent data for *T. minutus* is unavailable.

2.3. Biomass Concentrating Technologies

Due to huge variations between microalgal species, including shape, size and motility, no individual algae concentrating technique can currently be universally regarded as the best. Centrifugation is a valid harvesting technique for small scale cultures that utilises centrifugal force to separate components based on their density and particle size. Hence, due to the vast range of cell sizes across species, different accelerations (*g*) are needed for different species (Heasman *et al.*, 2000). The effect of centrifugation on cell viability is also highly dependent on the species and applied acceleration (Molina Grima *et al.*, 2003). This technique is widely used in lab environments because it is fast (often 5-10 mins) and effective (usually recovering >90% of cells). However, it is very energy intensive, often making it unfavourable for use with very large volumes (Uduman *et al.*, 2010). Despite this, such a process is used at industrial scale, as exemplified by Alfa Laval's range of algae separators (AlfaLaval, 2015).

Chemical flocculation is a widely used means of concentrating algal biomass, even at industrial scales. There are two broad classes of flocculants; inorganic flocculants such as alum and ferric sulphate, and organic polymer flocculants such as polyamines and polyacrylamides (*e.g.* Praestol™ and Zetag™ flocculants) (Uduman *et al.*, 2010). Both classes are cationic and form electrostatic interactions with negative cell surface charges of multiple cells, thereby bridging them together (Fig. 10). Chemical flocculation allows large cultures to be treated easily, typically yielding 70-80% cell recovery (Uduman *et al.*, 2010). However,

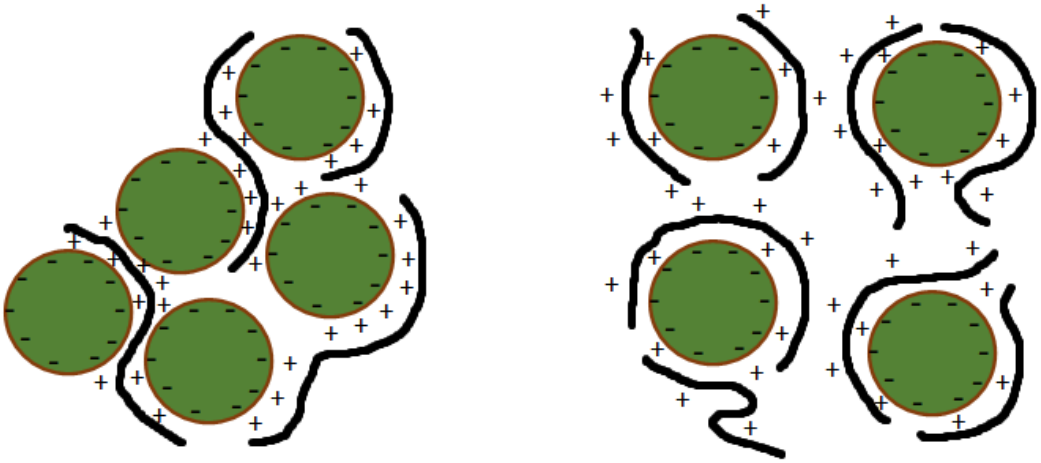

Fig. 10 - Diagram of Flocculation. Flocculants (black) are usually cationic and interact with negative algae cell (green) surface charges. At the correct dose (left) bridges form across multiple cells, forming a floc which can then be easily removed from the culture medium by flotation or sedimentation depending on the species and flocculant. If too much flocculant is added (right) then individual cells can become saturated with flocculant to the point that they repel one another.

their effectiveness (and therefore cost) varies with target species, media composition, cell concentration, pH and dose (Milledge and Heaven, 2013, Kucmanová and Gerulová, 2019). This variability arises due to the varying extent of cell bridging achieved under different conditions. A critical extent of cell bridging is required to sufficiently hold the cells together against any agitation. The pH will determine the extent of ionisation on cell surfaces and therefore the extent to which flocculants can interact with them, and ions in the growth medium can interact with both flocculants and cells. These conditions therefore determine the appropriate dose of a flocculant, and if too much is added then it is possible that cell surfaces become saturated with cationic flocculants which then repel each other (Fig. 10). The use of flocculants also adds a further contaminant to the biomass that usually needs to be separated from the extracted product.

Microbial flocculation, wherein a specific bacterium (*e.g. Alcaligenes cupidus*) is added which produces an extracellular polysaccharide flocculant, has also been demonstrated at laboratory scale for microalgae flocculation (Lee *et al.*, 2009). However, there is no benefit over simply adding a purified version of the bioflocculant. Autoflocculation of certain species can also occur, provided their medium contains sufficient phosphate and calcium ions. Autoflocculation is caused by an increase in pH, itself due to photosynthetic CO_2 consumption. This enables precipitation of cationic calcium phosphate which acts as the flocculant (Sukenik and Shelef, 1984). The viability of this process is dependent on species and media composition and is unfortunately not applicable to *T. minutus* cultures.

Electrocoagulation and flotation has shown promise as a means of treating wastewater (Chen, 2004), and is now receiving attention as a means to harvest microalgae. The process applies an electric current through an algal culture *via* electrodes. Oxidation reactions occur at a sacrificial anode, typically made of iron or aluminium, to yield metal cations (Table 1) which act as coagulants towards algal cells due to their negative surface charges (Gao *et al.*, 2010). Simultaneously, oxygen and hydrogen bubbles are produced at the anode and cathode, respectively (Table 1). These bubbles are typically very small (5 - 80 µm diameter), and well dispersed (100 - 1000 bubbles per mL) (Landels *et al.*, 2019). As the bubbles rise through the culture, they lift the flocculated cells to the surface where they can be easily collected. The remaining water can potentially be re-used for subsequent rounds of culture growth. Such a process is potentially more effective when using lower density and non-motile organisms. OriginOil's patented Electro Water Separation™ system (Eckelberry, 2013) provides an example of industrially available electrocoagulation and flotation

technology specifically designed for harvesting microalgae. Their system operates in a continuous flow manner, with electrocoagulation and flotation occurring in distinct chambers, and cell flocs harvested by a conveyor belt. They also claim their technology destroys unwanted organisms including 99% of bacteria, and is able to deliver algae cells intact or lysed depending on the strength of the electrical pulses applied (OriginOil, 2014a). The process is presented as low energy, though no values are provided.

Table 1 - Simplified Chemical Reactions of Iron and Aluminium Electrodes During Electrocoagulation and Flotation.

Electrode Material	Anode reaction	Cathode reaction
Iron	$Fe \rightarrow Fe^{2+} + 2e^-$ $2H_2O \rightarrow O_2 + 4H^+ + 4e^-$	$2H_2O + 2e^- \rightarrow H_2 + 2OH^-$
Aluminium	$Al \rightarrow Al^{3+} + 3e^-$ $2H_2O \rightarrow O_2 + 4H^+ + 4e^-$	$2H_2O + 2e^- \rightarrow H_2 + 2OH^-$

A similar technique is electro-flocculation, which does not use a sacrificial anode, but rather attracts the algae cells to the anode where they flocculate (Uduman *et al.*, 2010). Whilst these technologies have uses where the whole algal cell is the product (such as feeds), conventional, energy intensive, downstream selective extraction is still required to access high-value intracellular chemicals, such as PUFAs. Furthermore, the electrodes can be prone to fouling and require regular cleaning or replacement.

2.4. Irreversible Cell Disruption and Product Extraction Technologies

Conventional means of cell disruption through techniques such as bead milling, pressing, osmotic shock and rapid pressure decline are still used as a means of cell disruption in some microalgal bioprocesses. These methods are very effective (often destroying >90% of cells), but various life cycle analyses have shown them to have high energy consumption (Boer *et al.*, 2012). As a result, development of alternative techniques for cell disruption and extraction, particularly of lipids for biofuels, has become a focus of the academic community in this field.

Supercritical fluids, most notably CO_2, have shown some promise for algal lipid extraction (Bjornsson *et al.*, 2012, Cheng *et al.*, 2011, Mendes *et al.*, 2003, Santana *et al.*, 2012). Supercritical fluids are maintained at a temperature and pressure above their critical point, where phase boundaries no longer exist (Fig. 11). CO_2 is particularly suitable since it is non-toxic, readily available, and does not react with the functionality commonly found in

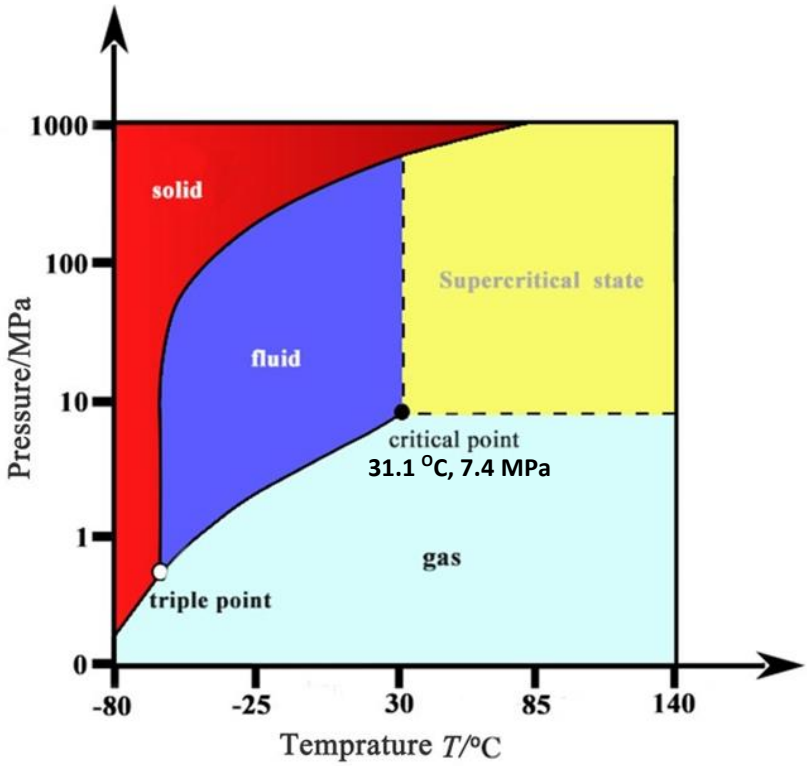

Fig. 11 - Phase Diagram of Carbon Dioxide. By maintaining CO_2 at a temperature and pressure above its critical point (31.1 ^{O}C, 7.4 MPa), a supercritical state can be achieved. Image adapted from (Yang *et al.*, 2018).

fatty acids. Furthermore, it has a relatively modest critical point of 31.1 ^{O}C and 7.4 MPa (Boer *et al.*, 2012), making it comparatively less expensive than alternative supercritical fluids (*e.g.* methanol, which can be used for in situ transesterification to fatty acid methyl esters, has a critical point of 239.5 ^{O}C and 8.1 MPa (Boer *et al.*, 2012)). This low temperature ensures products can be extracted without them denaturing (thermal decomposition of unsaturated TAGs can begin at around 160 ^{O}C (Vecchio *et al.*, 2008)). The pressure can be adjusted to alter the selectivity of extraction, and good selectivity for TAGs over other lipids has been reported, albeit with low overall yields in comparison to conventional solvent extractions

$$CO_{2(g)} \rightleftharpoons CO_{2(aq)}$$

$$CO_{2(aq)} + H_2O \rightleftharpoons H_2CO_3$$

$$H_2CO_3 \rightleftharpoons H^+ + HCO_3^-$$

$$HCO_3^- \rightleftharpoons H^+ + CO_3^{2-}$$

$$CO_3^{2-} + Ca^{2+} \rightleftharpoons CaCO_{3(aq)}$$

$$CaCO_{3(aq)} \rightleftharpoons CaCO_{3(s)}$$

Fig. 12 - Dissolution of CO_2 in Water. Dissolved CO_2 reacts with water, yielding carbonic acid (H_2CO_3). Dissociation of protons yields bicarbonate (HCO_3^-) and carbonate (CO_3^{2-}). If calcium is present, as it is in many growth media, calcium carbonate ($CaCO_3$) can form and precipitate.

(Bjornsson *et al.*, 2012, Cheng *et al.*, 2011). Finally, CO_2 is soluble in water (Fig. 12) yielding carbonic acid, bicarbonate, carbonate, and calcium carbonate (if Ca^{2+} is available as it is in many growth media (Mitchell *et al.*, 2010)). The solubility of CO_2 in pure water at room temperature and pressure is 14.3 g CO_2/L H_2O. The solubility of CO_2 at the increased temperatures and pressures required to reach its critical point is approximately 58.5 g CO_2/L H_2O (Diamond and Akinfiev, 2003). Thus, a portion of the extraction solvent is lost to a phase in which TAGs are insoluble. Therefore, efficient extraction requires that biomass be dried to less than 20% (*w/w*) water content beforehand (Boer *et al.*, 2012, Crampon *et al.*, 2013), which can be an energy intensive process.

Subcritical water extraction has also received recent attention from the academic community towards extraction of algal oils (Toor *et al.*, 2013, Jin *et al.*, 2013, Reddy *et al.*, 2014). The process utilises water at temperatures between 100 ^{O}C to 374 ^{O}C and high pressure to retain the liquid state. The increasing temperature significantly reduces the relative permittivity (permittivity relative to a vacuum, otherwise known as dielectric constant) of water. This can be considered a measure of a substances polarity, and hence adjusting it can greatly affect solvating capability (Herrero *et al.*, 2006). The relative permittivity of water is around 80 at 25 ^{O}C and can be as low as 6 (*i.e.* less polar) towards its critical point (Fig. 13) (Archer and Wang, 1990)**.** For comparison, the relative permittivity of hexane, commonly used in industrial scale algal oil extraction, is around 2 at 25 ^{o}C (Mopsik, 1967). This process advantageously uses the water in the algae culture as a solvent, thereby removing the need to dry the biomass, and avoiding use of solvents potentially harmful to

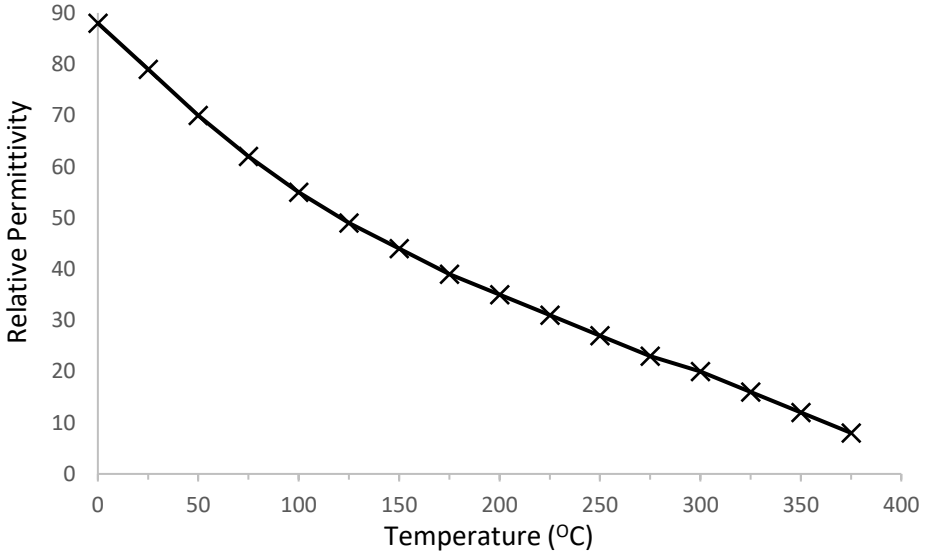

Fig. 13 - Relative Permittivity (dielectric constant) of Water at Varying Temperature. Data shown is at a constant pressure of 10 MPa. Adapted from Archer and Wang, 1990.

personnel and the environment. Whilst further studies would be required to accurately assess its energy requirements for algal oil extraction specifically, the required elevated temperatures and pressures should generally be avoided when trying to minimise costs.

Heating algal cultures can be considered a means of both dewatering and cell disruption, however, this is generally accepted to be very energetically unfavourable. Alternatively, the use of microwave heating has been explored to extract algal lipids. Compared to conventional heating approaches, microwave heating allows more rapid and evenly distributed heating, with an energy consumption that can be precisely controlled since energy input can be immediately stopped or started (Dai *et al.*, 2014). Cell disruption *via* microwave heating has been shown by some authors to be more effective than other approaches including conventional heating, bead milling, osmotic shock, sonication and autoclaving (Prabakaran and Ravindran, 2011, Lee *et al.*, 2010). Additionally, there is interest in using this rapid heating as a means to greatly increase rates of transesterification reactions for *in situ* production of biodiesel (Patil *et al.*, 2013, Patil *et al.*, 2012). However, the energy efficiency of this technique at an industrial scale is still in question (Gude *et al.*, 2013). It should also be noted that heating approaches will not be appropriate where a heat labile product is targeted.

Enzyme cocktails aimed at degrading algal cell walls have been utilised for the production of protoplasts and spheroplasts prior to DNA transformation for decades (Braun and Aach, 1975, Yamada and Sakaguchi, 1982). More recently, focus has been towards discovering enzymes for the degradation of cell walls of potential biofuel-producing species, such as *Chlorella vulgaris (Gerken et al., 2013)* and *Botryococcus braunii* (Ciudad *et al.*, 2014). Since algal cell walls are often multi-layered (Popper *et al.*, 2014), a mix of enzymes is usually required for full degradation, often including amylase, cellulase, lysozyme, pectinase, glucuronidases and sulfatases. Whilst such an approach can be very efficient at weakening cells for easier downstream extraction, significant drawbacks exist. Firstly, due to the huge range of cell wall structures in microalgae species, it is unlikely that a single cocktail will be successful for multiple species, but rather that a specific cocktail will need to be established for each, based on a previously developed understanding of the species' cell wall structure. Furthermore, the structure of cell walls can vary within species, often being dependent on growth conditions and development stage (Cheng *et al.*, 2015). In addition, producing and/or recycling large quantities of the desired enzymes can be expensive. However, such techniques have the advantage of not requiring that the biomass be dried, and can generally be considered environmentally friendly. Some bacterial species have shown promise as a

whole-cell approach towards microalgae cell wall degradation; *Flavobacterium aquatile* and *Flavobacterium yaeyamensis* have been shown to be able to degrade the cell walls of *Chlorella* species, either after death of the algae by heat shock (Afi *et al.*, 1996) or during live co-culture (Chen *et al.*, 2013). It is proposed that this degradation occurs through extracellular enzymes, and hence such processes are also likely to only be applicable to specific algae species. Furthermore, there is the potential for the bacteria to utilise the desired product as a nutrient, decreasing productivity.

Another approach to degrading algae biomass is with ionic liquids (ILs). ILs are salts in the liquid phase at temperatures <100 ^{o}C (and typically liquid at room temperature for ease of use in industrial applications). They are non-volatile, can be non-toxic and are extremely tuneable – allowing "designer solvents" for task-specific applications. It is important to remember that ILs are a broad class of chemicals (over a million combinations can be attained using currently available cations and anions (Rogers and Seddon, 2003)) and the generalisation should not be made that all ILs are safe, but rather that specific combinations may have the potential to replace traditional organic solvents. There are already some industrial uses of ILs, including their use as liquid pistons, as a storage medium (Markiewicz *et al.*, 2013) and in chemical processes such as "BASIL™" by BASF, in which ILs are produced during scavenging acid by-products (Fig. 14), thereby avoiding formation of a solid salt and enabling a simple liquid-liquid separation (BASF, 2021).

ILs of varying structures have been assessed for their ability to dissolve algal biomass. leaving a water immiscible lipid phase which can easily be removed form a waste hydrophilic phase (Teixeira, 2012, Choi *et al.*, 2014, Kim *et al.*, 2012, Fujita *et al.*, 2013). Teixeira *et al.* demonstrated that hydrophobic butylimidazolium hexafluorophosphate and butylimidazolium *bis*triflimide were not capable of dissolving whole algal cells of various species, while hydrophilic ethyl-, butyl-, and allylimidazolium chloride ILs were (Teixeira, 2012). However, these successes required temperatures above 100 ^{O}C, potentially reducing their industrial efficacy. However, Fujita *et al.* report greater success using hydrophilic

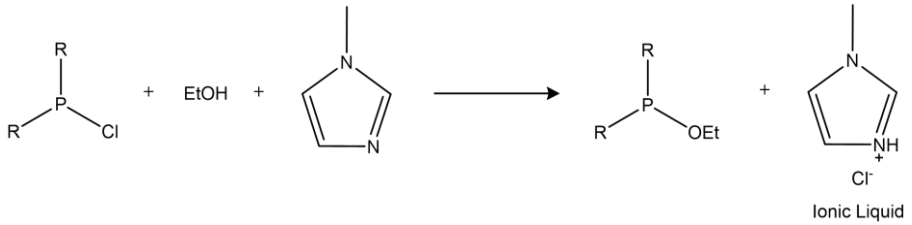

Fig. 14 - The BASIL™ process by BASF. Diethoxyphenylphosphine is produced from dichlorophenylphosphine and ethanol. This would usually produce HCl, which can in turn react with the product in an unwanted manner. The addition of 1-methylimidazole enables the HCl to be scavenged, producing methylimidizaloium chloride, an IL. An added benefit of this process is that the IL is more easily separated from the product than the solid HCl salt.

ethylimidazolium methylphosphate to dissolve *Synechocystis* spp. at room temperature in 30 minutes (Fujita *et al.*, 2013). They also used filtration and vacuum drying to demonstrate the feasibility of recycling the IL, but this may not be a viable approach at an industrial scale. Similarly, Kim *et al.* demonstrated the use of polar imidazolium IL - methanol mixtures to dissolve *Chlorella vulgaris* at 65 ^{O}C (Kim *et al.*, 2012). However, efficient separation and removal of the lipid layer required the addition of excess water followed by centrifugation, a high energy process unlikely to be industrially viable. Whilst this approach appears to show some promise, it is not without further drawbacks. Firstly, a relatively complicated lipid layer remains from which EPA AGs would need to be separated. Secondly, ILs are generally expensive and their efficient recycling would be required to make such a process industrially viable (discussed further in section 2.6.8). Despite this, some patents exist for such processes, although these are often unspecific as to the structure of the IL intended for use (Di Salvo *et al.*, 2012, Chew *et al.*, 2013, Chew *et al.*, 2011).

Pulsed electric fields (PEF) are another extraction technique receiving attention in this field. PEF of sufficient voltage can irreversibly disrupt the cell wall and membrane. Using a specific combination of electric field strength, pulse time and pulse duration, a transmembrane voltage above a critical irreversible threshold can be achieved, creating irreversible pores in the cell membrane (Teissie *et al.*, 2005). When carried out in an aqueous media this only allows the spontaneous release of water soluble compounds (Goettel *et al.*, 2013, Eing *et al.*, 2013, Grimi *et al.*, 2014). However, in conjunction with downstream ethanol extraction, it has been reported to increase lipid yields 3-fold on average in comparison to ethanol extraction alone, using the microalga *Auxenochlorella protothecoides (Eing et al., 2013)*. Whilst this technique generally has a very low energy cost (Boer *et al.*, 2012), combining it with current downstream extraction processes necessary for extraction of water-insoluble compounds would require an energy intensive biomass concentrating stage.

Ultrasound (sonication) can be used to disrupt cells through the production and cavitation of minute bubbles, causing pressure shockwaves throughout a solution (Greenly and Tester, 2015). Like PEF, this technique can also be used with wet algal biomass (Mubarak *et al.*, 2016, Hadrich *et al.*, 2018). However, excessive sonication can cause the oxidation of fatty acids (Gerde *et al.*, 2012). Many papers demonstrate that during sonication of water, the cavitation occurring is sufficiently high-energy to cause the dissociation of water molecules and produce hydroxyl free radicals ($^{\bullet}$OH) (Riesz and Kondo, 1992, Mason *et al.*, 1994, Riesz *et al.*, 1985). These can initiate fatty acid oxidation as discussed previously (Fig. 4). Furthermore, excessive sonication can cause temperature increases sufficient to enable

thermal decomposition of fatty acid AGs (Jahouach-Rabai *et al.*, 2008). Thus, this approach must be carefully controlled in order to be used effectively for PUFA extraction.

2.5. Milking

Most extraction techniques in development depend on some means of irreversible cell disruption. An alternative approach is to "milk" the biomass, extracting the compounds of interest whilst maintaining cell viability for further rounds of extraction. Milking processes are extremely promising, since they bypass the need to concentrate or harvest the biomass and allow its re-use. Furthermore, if cell viability is truly maintained there is potential for a cleaner product and less complicated waste streams due to the lack of cell debris. It has also often been reported that removal of a compound from a cell whilst retaining viability leads to increased production of that compound (Zhang *et al.*, 2011a), providing a further advantage over conventional extraction approaches. In conjunction with the most selective extraction solvents, this principle could prove extremely beneficial to a variety of bioprocesses using different organisms.

Growth of microorganisms in batch cultures occurs over four phases (Fig. 15). In the lag phase, the microorganisms are not actively reproducing but rather adjusting to their conditions by undergoing transcription and translation necessary for general metabolism

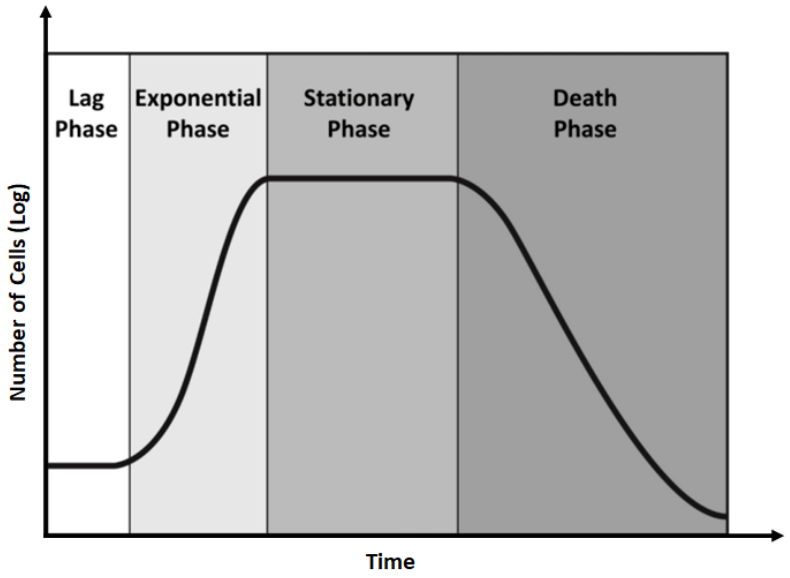

Fig. 15 - General Microbial Growth Curve in Batch Culture. Cells adjust to their conditions and prepare for division during the lag phase. The number of cells doubles per unit time during the exponential phase. As essential nutrients diminish and/or toxic metabolites accrue, cell death rate increases. Cell death rate is equivalent to cell growth during the stationary phase, and greater than cell growth in the death phase. Image adapted from (Garrison and Huigens, 2016)

and preparing for cell division. In the exponential phase (also called the logarithmic phase) cell division is unlimited, enabling the number of cells to double per a unit of time (doubling time). The specific growth rate of the organism under these conditions can be determined by the gradient of the line during exponential phase. Since the culture is in an enclosed environment, nutrients will gradually deplete and/or toxic metabolites will accumulate which will limit growth. Cultures enter a stationary phase when growth rate is equal to death rate, and a death phase (also called a decline phase) when death rate is greater than growth rate (Fig. 15) (Tortora *et al.*, 2019). There is some evidence to suggest that the cell wall structure of microalgae can vary throughout growth stages, typically becoming tougher over time (Gao *et al.*, 2016, Gerken *et al.*, 2013). It is currently unknown if this occurs in *T. minutus*. However, the average EPA content of *T. minutus* cells is maximal at the onset of stationary phase, when cell concentration is also highest (Cepák *et al.*, 2014). Therefore, this is the best stage to extract EPA triglycerides, since any potential slight increase in energetic expense of extraction arising from an increase in cell wall toughness is likely to be outweighed by increased EPA availability.

Growth rates of many algal species are often slow in comparison to bacteria, with full growth curves (from lag to stationary) often taking over a week (Cheng *et al.*, 2013, Cepák *et al.*, 2014). The doubling time of *T. minutus,* under conditions optimised for EPA production, is approximately 5 days (Cepák *et al.*, 2014). This is longer than most other microalgal species considered for industrial EPA production; the diatom *Phaeodactylum tricornutum* has a doubling time of 18 hours (Mann and Myers, 1968), while *Nannochlorposis spp*., *Dunaliella salina* and *Chlorella vulgaris* have approximate doubling times of 2.5 days, 3.9 days and 5 days, respectively (Sukarni *et al.*, 2014). In comparison, the doubling time of the widely used bacterium, *E. coli*, is just 20 minutes under optimal growth conditions (Gibson *et al.*, 2018). To potentially increase productivity, a milking process could be paired with a chemostatic system to maintain a culture in its stationary phase throughout extraction, allowing the repeated slow growth in lag phase to be bypassed. In a chemostatic system, fresh culture medium containing essential nutrients is continually added alongside the continuous removal of "used" medium containing live cells, debris and metabolites. Other culture conditions (*e.g.* pH, temperature, light intensity, air flow, mixing) are also maintained (Herbert *et al.*, 1956, Smith and Waltman, 1995). Since culture growth is dependent on the concentration of available nutrients and cell number, these systems enable the specific growth rate (and therefore cell density) of the microorganism to be

controlled and maintained as desired. This could be paired with a milking extraction, likely conducted in batches to enable cell recovery between extractions.

2.5.1. Reversible Electropermeabilisation

PEF for irreversible cell permeabilisation as a pretreatment for extraction was discussed earlier. However, PEF can also be used to generate transient pores in the membrane (Chang and Reese, 1990). This allows the influx and efflux of molecules normally impermeable to the membrane *via* diffusion, as well as allowing ions to be carried across the membrane *via* electrokinetic effects in the presence of the electric field (Movahed and Li, 2012). This process is most commonly used to transfer genetic material. These pores can reseal, allowing recovery of the cell (Escoffre *et al.*, 2008). Hence, this technique has the potential to be developed as a milking method.

The precise mechanisms of electropermeabilisation (also referred to as electroporation) are not fully understood. It is well known that pore formation occurs due to an increase in the resting transmembrane voltage ($\Delta\Psi$) of a cell (Escoffre *et al.*, 2008). Beyond a critical transmembrane voltage, $\Delta\Psi_{rev}$, transient pores are able to form in the membrane (Teissie *et al.*, 2005). A second, higher threshold, $\Delta\Psi_{irr}$, exists beyond which irreversible pores are formed (Gehl, 2003). The value of the electrically induced transmembrane voltage, $\Delta\Psi_E$, is given by equation 1:

Equation 1
$$\Delta\Psi_E(t) = -fg\lambda rE\cos\theta[1 - e^{-\frac{t}{\tau}}]$$

Where f is related to the shape of the cell, g is dependent on the conductivity, λ, of the extracellular medium, membrane and cytoplasm, r is the radius of the cell, E is the electric field strength, θ is the angle at a specific position on the membrane relative to the direction of the electric field, t is time and τ is the membrane charging time (Kotnik and Miklavcic, 2000). In the literature this equation is often simplified to:

Equation 2
$$\Delta\Psi_E = 1.5rE\cos(\theta)$$

by assuming the cell membrane to be a true dielectric (Schwan, 1957), when in reality it exhibits some limited conductivity.

From these equations, several interesting relationships between delivered pulse parameters and the extent of permeabilisation are notable, which have been shown

experimentally. Firstly, the value of the transmembrane voltage, $\Delta\Psi_E$, is dependent on the value of the applied electric field strength, E. Hence, the electric field strength has a threshold value, E_p, required to generate a transmembrane voltage sufficient to permeabilise cells (Escoffre *et al.*, 2008). Electric field strength is defined by the force exerted on a unit charge (expressed in equivalent units of N/C or V/m). Thus, its strength is dependant only on the applied potential difference (V) over a given distance (during electroporation, the distance between electrodes). Hence, assuming a fixed electrode gap distance, the only variable of the delivered electric pulse that determines if electroporation can occur is its amplitude (voltage). Further increasing the value of E beyond E_p increases the permeabilised area of the membrane (Schwister and Deuticke, 1985). Provided $E > E_P$ such that permeabilization can occur, pulse duration has been shown to affect the extent of permeabilization. Authors suggest this could be through an increase in pore density, pore diameter, or a combination thereof (Gabriel and Teissié, 1999). Pore formation also has a positional dependency, $cos\theta$, such that the poles of the cells nearest electrodes are the most permeabilised, and *vice versa* (Hibino *et al.*, 1993, Gabriel and Teissié, 1999).

Reversible elctropermeabilisation can be considered to have 5 discrete stages. The first stage is initial pore formation occurring as $\Delta\Psi$ reaches $\Delta\Psi_{rev}$. In the second stage of the process, the pore size can expand as long as $\Delta\Psi$ is maintained above $\Delta\Psi_{rev}$. During these stages the pore is thought to be hydrophobic due to the exposed phospholipid tails (Fig. 16). In the third stage, membrane phospholipids rearrange such that their heads are at the pore surface, yielding a hydrophilic pore (Fig. 16). This is a result of the electric pulse coming to conclusion, with $\Delta\Psi$ becoming lower than $\Delta\Psi_{rev}$. The fourth stage sees further rearrangement of the phospholipids to reseal the pore, and can last seconds to minutes. There is evidence to suggest that this is an active process, requiring ATP, mediated by the cytoskeleton (Rols and Teissie, 1992). The final stage can be thought of as membrane "memory"; the electropermeabilisation process leaves areas of the cell membrane prone to

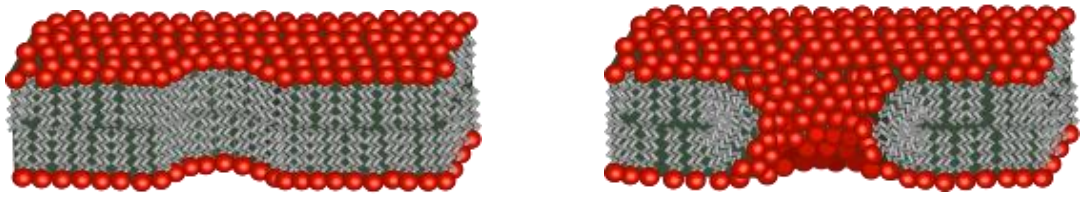

Hydrophobic pore Hydrophilic pore

Fig. 16 - Pores Formed in the Cell Membrane During Electropermeabilisation. The initial pore is hydrophobic (left), but as the pulse comes to conclusion the phospholipids rearrange to produce a hydrophilic pore (right). Over time, these pores can reseal.

subsequent pore formation, and can have further physiological effects including inducing endocytosis where such a property is not normally present in native cells (Teissie *et al.*, 2005).

Equations 1 and 2 demonstrate that aspects of cell morphology also play a role in electropermeabilisation. Firstly, the area of a cell membrane permeabilised by PEF depends upon the angle, θ, of the membrane relative to the electrodes (Schwister and Deuticke, 1985, Kotnik and Miklavcic, 2000). Membranes more parallel to the electrodes are more readily permeabilised, whilst those perpendicular are not permeabilised. Hence non-spherical cells, such as the discoid *T. minutus* (Fig. 17) with wider centre and tapered edges (Přibyl *et al.*, 2012), are permeabilised to varying extents depending on their orientation to the electrodes. This will make it harder to achieve a PEF treatment that can reversibly permeabilise enough cells for adequate EPA extraction without irreversibly permeabilising others. However, in bulk electroporation, a huge number of mobile cells are exposed to the electrical pulse, such that the effect of cell shape will likely be averaged. Secondly, cell radius plays a vital role in determining the electric field strength required to permeabilise cells, with larger cells generally requiring smaller electric field strengths to achieve permeabilisation (Teissié and Rols, 1993). In the case of algal cells, the effect of a cell wall must also be considered. Literature in this area is lacking, but there is a report that demonstrates the cell wall can restrict entry of molecules after PEF treatment, likely based on their size (Azencott *et al.*, 2007).

Furthermore, cell concentration has been shown to play a role in the extent of cell permeabilization; if two cells are near each other during a PEF treatment, the cell closest to the electrodes can "shield" the other, increasing the field strength required for its

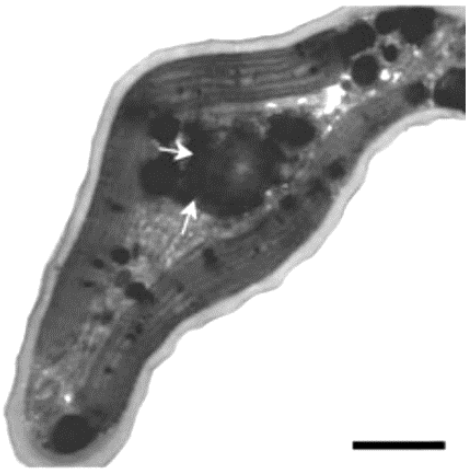

Fig. 17 - A Transmission Electron Micrograph Image of a Transverse Section of a *T. minutus* Cell. Image adapted from Přibyl *et al.*, 2012. Arrows point to the lipid body. Scale bar = 0.1 µm.

permeabilization by 5-10% (Henslee *et al.*, 2014). This has implications for the development of the final milking process; shielding effects could be bypassed by increasing the strength of the applied electric field, but this will likely lead to a higher percentage of non-viable cells, as well as increase overall process costs and potentially cause arcing. Alternatively, cultures could be diluted prior to treatment, but this could also increase process costs and reduce the quantity of EPA that can be extracted in a given duration.

Finally, the effect of the medium should be considered. Conventional electroporation for the transfer of genetic material is usually conducted in water rather than culture media, because the lower ion concentration reduces the likelihood of arcing and can increase cell survivability (Pucihar *et al.*, 2001). However, it would be impractical to harvest cells and resuspend them in water for subsequent milking, especially considering a significant advantage of the proposed milking process is avoiding dewatering of the algal culture. Therefore, it is important that milking strategies are developed to be compatible with the algal growth medium used.

A patent from OriginOil based on the principle of reversible electropermeabilisation with the aim of extracting lipids was published in 2012 (Reep and Green, 2012). Whilst there is no data currently available to assess the success of this "Live Extraction™" invention, it claims to use an aqueous media, despite previous research suggesting this will not allow spontaneous lipid release. Furthermore it is implied that the process is selective for "ripe" oil-rich algae cells, leaving "unripe" cells to continue to grow and produce lipids despite not giving any evidence as to how these cells are distinguished (OriginOil, 2014b). Due to the lack of any scientific evidence as to the invention's success in the time since the patent's publication, it seems unlikely that this process is industrially viable. However, combining reversible PEF with a biphasic system utilising a hydrophobic solvent may be a viable means to encourage algal lipid release whilst maintaining cell viability.

2.5.2. Genetic Engineering for Product Secretion

It could be argued that an alternative means to establish an algal milking process would be through genetically engineering organisms to secrete compounds of interest. EPA secretion could potentially be achieved by the expression of fatty acid exporters in the plasma membrane. This concept has been demonstrated for other free fatty acids in engineered *E. coli* (Meng *et al.*, 2013). Some promising ABC transporters for fatty acids, wax esters and alkanes have been identified in higher plants (Panikashvili *et al.*, 2007, Pighin *et al.*, 2004), but a challenge remains in transferring these genes to microalgae. A more attractive

approach would be to identify the endogenous fatty acid transporters present in the endoplasmic reticulum of wild type microalgae, and express a version with a signal peptide instead targeting them to the plasma membrane. The genes and proteins responsible for fatty acid export from chloroplasts and endoplasmic reticulum are beginning to be identified in certain microalgae species (predominantly *Chlamydomonas reinhardtii*) (Li *et al.*, 2019). One potential downside to this approach is that contaminating organisms in the culture might utilise the highly nutritive compounds being secreted, thereby lowering their yields (Radakovits *et al.*, 2010). This is particularly relevant for certain algal species, including *T. minutus,* which only grow alongside bacterial symbionts or mutualists. Furthermore, a significant advantage of extracting high value consumer products from microalgae is their "green" and eco-friendly perception, which will likely be greatly diminished if the algae have been genetically modified.

Such an approach would also likely need to be conducted in a model organism such as *C. reinhardtii* or *Phaeodactylum tricornutum*, rather than in *T. minutus* since it is far less understood and no previous attempts of its genetic modification have been reported. These model algae have comparably unfavourable fatty acid profiles; *C. reinhardtii* doesn't naturally produce EPA (Pflaster *et al.*, 2014), and *P. tricornutum* produces DHA alongside EPA, (Popko, 2016) which is undesirable in AlgaeCytes' process. Hence, further genetic modifications targeting fatty acid metabolism would be necessary to achieve an oil with desirable characteristics. Over 30 microalgae strains have been successfully transformed (Suttangkakul *et al.*, 2019), so a more appropriate organism could present itself in the near future, or tools could be developed for *T. minutus* specifically.

However, genetic engineering of microalgae is still in its infancy in comparison to bacteria, with technical difficulties slowing its development. Critically, transformation of the chloroplast genome is generally preferred (where appropriate) over the nuclear genome. This is because genetic modification of the chloroplast genome can be targeted to a specific location through homologous recombination (Fig. 18). Unfortunately, nuclear transformation in microalgae (and most other photosynthetic eukaryotes) very rarely occurs *via* homologous recombination (Sodeinde and Kindle, 1993). The exact alternative mechanism of DNA integration into the nuclear genome is ultimately unknown. However, it likely involves the use of the non-homologous end joining repair pathway in which double stranded DNA breaks are ligated. Crucially, this occurs with no apparent sequence specificity (*i.e.* randomly throughout the genome), often being lethal due to direct genetic disruption and/or reading frame shifts in neighbouring genes. Furthermore, the transforming DNA can

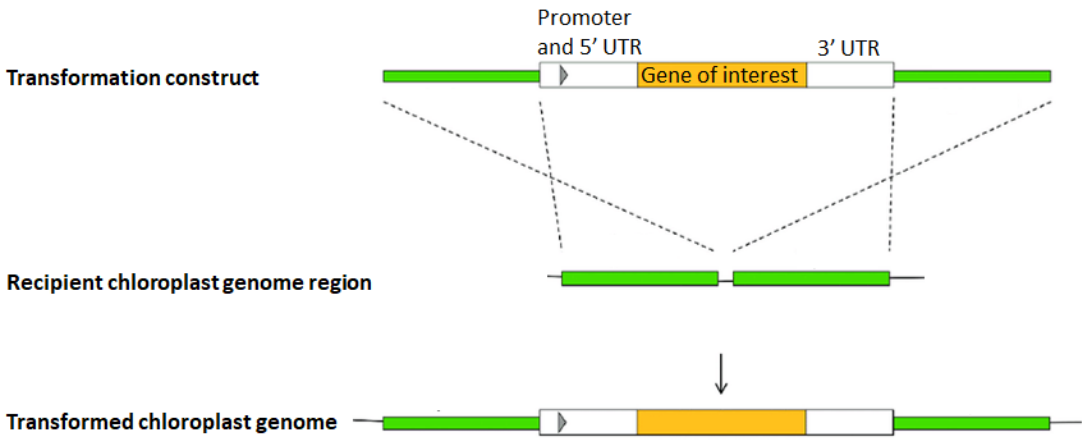

Fig. 18 Targeted Transformation of the Chloroplast Genome. The gene cassette, itself consisting of the gene of interest, 3' untranslated region (UTR), promoter and 5' UTR, is flanked by DNA arms identical to regions of the chloroplast genome (green). This enables the targeted integration of the gene cassette *via* homologous recombination, a process which rarely occurs in the nuclear genome of most photosynthetic organisms. Image adapted from (Yefremova and Purton, 2018).

break into multiple fragments and be integrated at different locations, resulting in no transgene expression. Finally, the extent of intact transgene expression can be affected by neighbouring genes and epigenetic effects, so successful transformants can have varying extents of expression (Doron *et al.*, 2016). Thus, many transformants generally need to be produced and screened to identify the best.

There are many proven means of selecting microalgal transformants, including the use of antibiotic resistance (although many algae are naturally resistant and require initial transformation for susceptibility) (Gutiérrez *et al.*, 2012, Bateman and Purton, 2000, Xie *et al.*, 2014), herbicide resistance (Newman *et al.*, 1992), recovery of photosynthetic or heterotrophic growth (Kindle *et al.*, 1991, Cheng *et al.*, 2005) and auxotrophic selection markers (Remacle *et al.*, 2009). Metabolic selection is generally favourable at an industrial scale since herbicides and antibiotics are more expensive and could be considered less environmentally friendly. Typically, the precise means of selection needs to be tailored to the organism and process. Unfortunately, selection often needs to be continued indefinitely, since a second significant disadvantage of nuclear transgene expression is its frequent transience. It is thought this could be due to RNA mediated gene silencing, since the necessary machinery is known to exist in many species of microalgae (Schroda, 2006). In such a system non-coding RNAs are produced with complementary base pairing towards target mRNAs. This yields double stranded RNA which is targeted for degradation by the RISC (RNA induced silencing complex) enzyme complex (Pratt and MacRae, 2009).

Whilst chloroplast transformation is often favoured, it has disadvantages. Firstly, transformation can sometimes be difficult due to the need for DNA to cross extra membranes. However, a number of relatively simple transformation protocols, including glass bead milling, exist for *C. reinhardtii* (Economou *et al.*, 2014). Secondly, the chloroplast lacks machinery to conduct certain post translational modifications, most notably glycosylation (Ahmad *et al.*, 2016). Thirdly, the chloroplast stroma is a different environment than the cytosol, being a slightly higher pH and containing many proteases. This environment can be unfavourable for expression of certain proteins, particularly if they are exogenous (Ahmad *et al.*, 2016). Finally, and most importantly regarding this project, the chloroplast lacks the machinery to export proteins to the cytosol and beyond (Siddiqui *et al.*, 2020, Bogorad, 2000). It is therefore unfortunately entirely unsuitable for production of a transporter protein that needs to be targeted to the plasma membrane. In conclusion, tools for the genetic transformation of microalgal chloroplast genomes are generally robust, but not applicable to this concept. Stable nuclear transformation of microalgae generally remains a challenge, with further development of genetic tools being necessary before such an approach to algal milking could be pursued.

2.5.3. Biphasic Milking Approaches

The idea of milking microorganisms has been realised for some time, with the milking of extracellular hydrocarbons from the microalga *B. braunii* being reported as early as 1989 by Frenz *et al.*(Frenz *et al.*, 1989a). Their technique involved harvesting cells, contacting them for a short time with hexane for extraction, followed by replacing the cells in the growth media. A similar approach was adopted by Sauer and Galinski, who successfully milked ectoines from the halophilic bacterium *Halomonas elongata*. The term ectoines refers to ectoine and hydroxyectoine (Fig. 19), which many halophilic bacteria accumulate intracellularly to achieve osmotic equilibrium with high extracellular salt concentrations. These molecules have industrial uses in moisturising skin care products (Graf *et al.*, 2008).

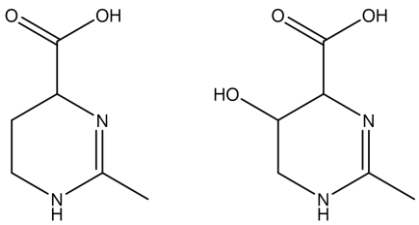

Fig. 19 - Ectoine (left) and Hydroxyectoine (right). These molecules are produced by many halophilic bacteria as osmoprotectants and can be “milked” by adjusting media salinity.

Their milking process takes advantage of the cell's need to maintain osmotic equilibrium: the cells are cycled between a high salinity medium where they produce ectoines, and a low salinity medium where they are released (Sauer and Galinski, 1998).

Whilst these early studies demonstrate the feasibility of milking, they are not particularly efficient processes due to the need to exchange the media (and hence harvest cells) for separate growth and extraction periods. Instead, biphasic systems can be used thereby allowing continuous growth alongside extraction, and these approaches tend to be the focus of more recent milking attempts. Such an approach was adopted by Hejazi and colleagues for the milking of β-carotene from *Dunaliella salina,* and they suggest that the partition coefficient (P) of a solvent is critical for successful milking (Hejazi *et al.*, 2004). This value is the ratio of concentrations of a molecule between two immiscible phases, typically octanol and water, and is usually expressed logarithmically ($logP_{(O/W)}$). From this value the relative solubility of the compound can be inferred. For example, hexane has a logP of 3.9; the concentration of hexane is $10^{3.9}$ times higher in octanol than water. Hejazi *et al.* illustrated that organic solvents with logP > 6 are compatible with *D. salina*, and that pigment extraction ability of a solvent is inversely proportional to its logP value (Hejazi *et al.*, 2002). Hence, they suggest dodecane (logP 6.8, boiling point of 216 ^{o}C and density of 750 kg/m^3) as an appropriate solvent for the process, compromising well between biocompatibility and extractability. Their approach is to grow cells under optimal initial conditions and later stress them *via* excess light to produce increased quantities of β-carotene. Using light microscopy and flow cytometry, they report that cell viability was >90% after 47 days of milking, and that the cell population remained constant after an initial growth phase.

However, Kleinegris *et al.* later demonstrated that the dodecane-water phase interface is highly toxic to *D. salina* cells, likely *via* membrane disruption. They suggest that the majority of β-carotene extracted originates from these lysed cells, since fluorescence microscopy revealed little loss of carotenoids from live cells (Kleinegris *et al.*, 2011). They attribute the previous viability results by Hejazi *et al.* to their flow cytometry method only being used to distinguish intact live and dead cells, and not accounting for ruptured cells. The constant population of cells reported by Hejazi *et al.* was explained by simultaneous cell death and growth; Kleinegris *et al.* measured cell death through arresting cell growth *via* the addition of hydroxyurea (Kleinegris *et al.*, 2011). Hydroxyurea inhibits DNA synthesis (and therefore cell division) by inhibiting ribonucleotide reductase, an enzyme responsible for producing deoxyribonucleotides (Koç *et al.*, 2004). Whilst these results may disprove that this is a true milking process, *in situ* extraction in a continuous manner is still highly

advantageous over conventional harvesting and extraction techniques, reducing costs and potentially allowing a higher productivity to be achieved (Hejazi *et al.*, 2004).

The marine alga *Botryococcus braunii* can produce and accumulate hydrocarbons at high levels (30-40% of the dry biomass weight (Eroglu and Melis, 2010)). Different strains of *B. braunii* produce a wide variety of different hydrocarbons (Fig. 20), including odd carbon numbered (C_{23} to C_{33}) dienes and trienes, a wide range of triterpenoids often referred to as "botryococcenes" (Fig. 21), methylated squalenes (C_{31} to C_{34}) and tetraterpenoids (Metzger and Largeau, 2005). These hydrocarbons can be used as a feedstock for hydrocracking to produce transportation fuels (Hillen *et al.*, 1982). This species is colonial, and exports liquid hydrocarbons into the intracolonial extracellular matrix, which is hardened *via* a network of cross-linked hydrocarbons. A final barrier is provided by a polysaccharide sheath surrounding

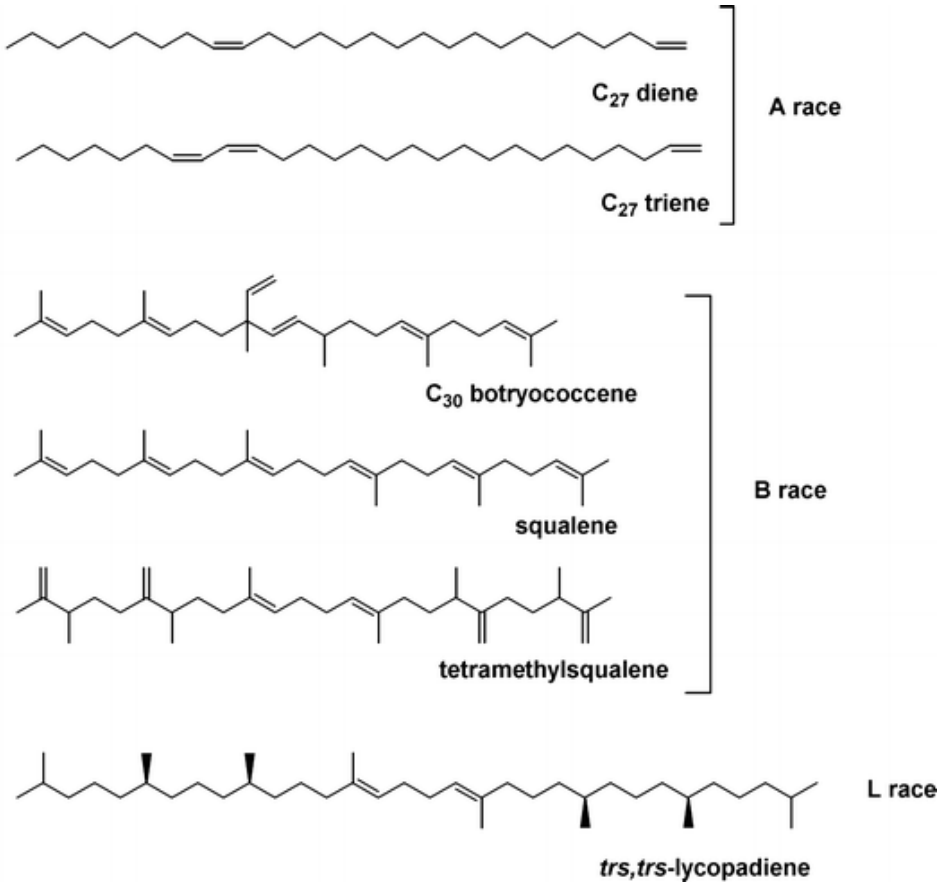

Fig. 20 - Examples of Hydrocarbons Produced by *B. braunii*. Different strains of *B. braunii* produce different hydrocarbons and are grouped into three distinct races accordingly. Race A produce predominantly dienes and trienes, each of an odd number of carbons between and including C_{23} to C_{33}. Race B produce squalene, methylated sqaulenes, and "botryococcenes" - a wide range of triterpenoids containing 30 to 37 carbon atoms. The L race only produces lycopadiene. Image modified from Metzger and Largeau, 2005.

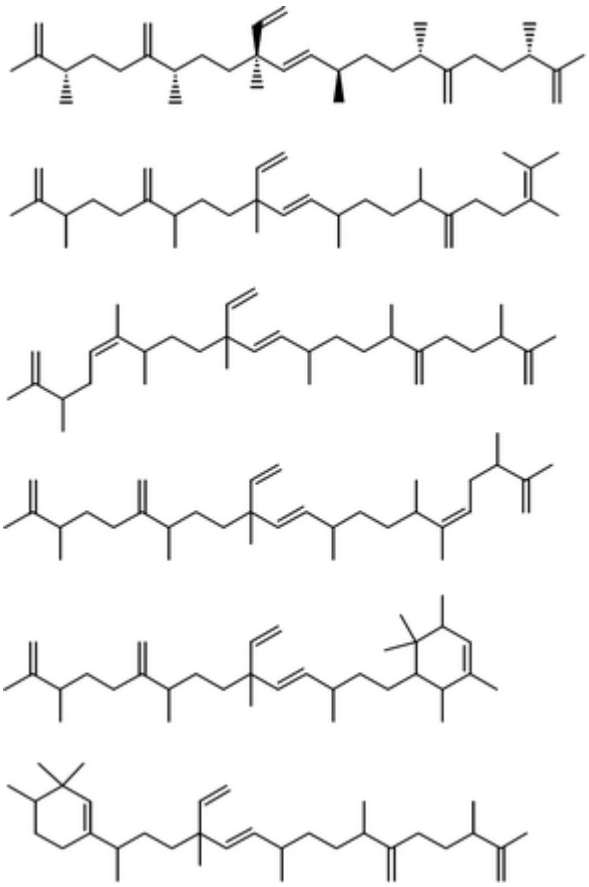

Fig. 21 - Examples of Botryococcene Structures. B race *B. braunii* strains can produce triterpenoid "botryococcenes" of varying structure, containing 30 to 37 carbon atoms. Illustrated above are 6 identified C_{34} isomers. Image Modified from Metzger and Largeau, 2005.

the entire colony (Fig. 22) (Weiss *et al.*, 2012). There are many reports of using biocompatible organic solvents to extract the extracellular liquid hydrocarbons from *B. braunii* cultures whilst maintaining cell viability (Zhang *et al.*, 2011a, Zhang *et al.*, 2013a, Samorì *et al.*, 2010b, Eroglu and Melis, 2010, Frenz *et al.*, 1989a, Frenz *et al.*, 1989b, Moheimani *et al.*, 2013, Moheimani *et al.*, 2014). Most of these approaches use a water immiscible alkane, typically hexane or heptane, to produce a biphasic system. Short contact times (≤ 20 mins) with the organic solvent are often necessary to maintain cell viability. Interestingly, Moheimani *et al.* demonstrated that very small quantities of the extracellular lipids can be harvested, whilst maintaining cell viability, through application of gentle pressure *via* means of a cover slip in a solvent-free "blotting" process (Moheimani *et al.*, 2013). The relative success of milking attempts utilising this algal species could in part be due to the extracellular location of the hydrocarbons.

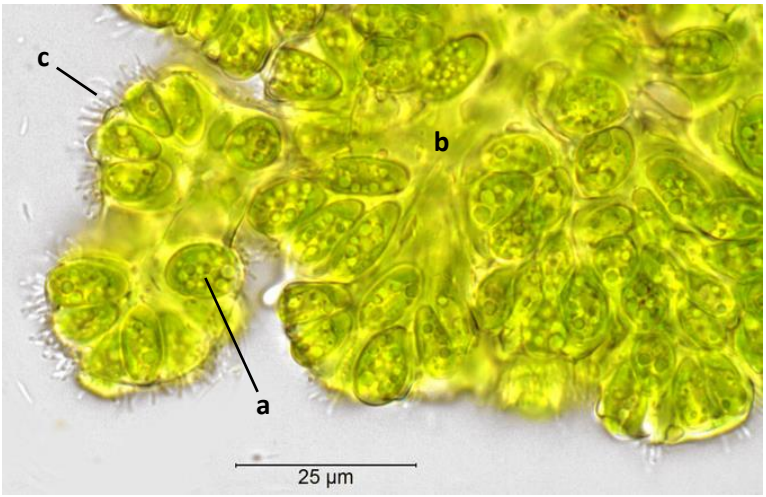

Fig. 22 - Micrograph of a *B. braunii* colony. Whilst intracellular lipids (a) accumulate in these algae, liquid hydrocarbons are exported into an extracellular matrix (b), facilitating the milking process. The whole colony is surrounded by a comparatively loose polysaccharide sheath (c). Image adapted from (Weiss *et al.*, 2012).

2.6. Ionic Liquids as Designer Solvents for Milking Processes

2.6.1. Advantages and Desirable Properties of ILs

Whilst the previously discussed milking approaches are somewhat successful, they have thus far relied upon the use of volatile, environmentally unfriendly organic solvents. It is proposed here that ILs could be used as a potentially safer, designer alternative for use in an algal milking process. ILs for an EPA milking process must be water immiscible, allowing a biphasic system to be established, biocompatible towards *T. minutus*, allowing high levels of cell viability to be maintained throughout extraction, and ideally selective, since a product with a high percentage EPA content is desired. Additional advantageous characteristics would include increased safety compared to traditional organic solvents and ease of separation from the product, allowing the IL to be recycled.

2.6.2. IL Structures and Synthesis

Due to the cumbersome nature of the IUPAC names of many ILs, most authors utilise a shorthand naming system. The abbreviations and detailed structure of IL cations and anions which are discussed throughout this thesis are presented in Table 2 and Table 3, respectively.

Table 2 - Structure and Abbreviations of IL Cations Used in this Project.

Class and Description	Abbreviation	Structure
1-Alkyl-3-methylimidazolium	[C$_n$MIM]	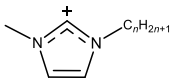
1-Alkyl-3-butylimidazolium	[C$_n$BIM]	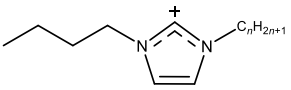
1-Alkyl-3-methylpyridinium	[C$_n$py]	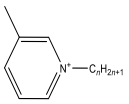
1-Alkyl-1-methylpyrrolidinium	[C$_n$pyrro]	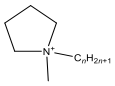
1,1-Dialkylpiperidinium	[Pip$_{n\ m}$]	
Tetraalkylammonium (hydrocarbon chains)	[N$_{m\ n\ p\ q}$]	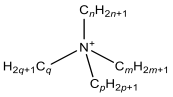
Tetraalkylammonium (hydroxylated)	[N$_{m\ n\ p\ q\text{-OH}}$]	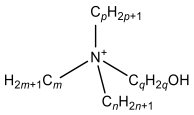
Tetraalkylphosphonium (hydrocarbon chains)	[P$_{m\ n\ p\ q}$]	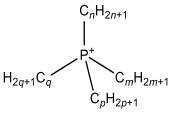
N-Benzyl-*N*,*N*-dimethyl-2-(2-(4-(2,3,3-trimethylbutan-2-yl)phenoxy)ethoxy)ethan-1-aminium	[N$_{1\ 1\ 1\text{-Bn}\ 2\text{-O-}2\text{-O-Bn}}$]	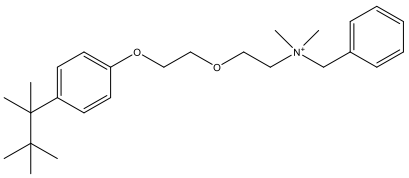
N-Ethyl-*N*,*N*-dimethyl-2-(2-(naphthalen-1-yloxy)ethoxy)ethan-1-aminium	[N$_{1\ 1\ 2\ 2\text{-O-}2\text{-O-Bn}}$]	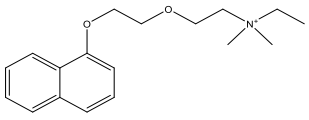
N-Ethyl-*N*,*N*-dimethyl-2-(2-(quinolin-2-yloxy)ethoxy)ethan-1-aminium	[N$_{1\ 1\ 2\ 2\text{-O-}2\text{-O-NBn}}$]	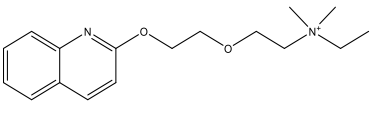

Table 3 - Structure and Abbreviations of IL Anions Used in this Project.

Class and Description	Abbreviation	Structure
Chloride	Cl^-	
Bromide	Br^-	
bis{(trifluoromethyl) -sulfonyl}imide	[NTf_2]	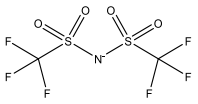
Docusate	[AOT]	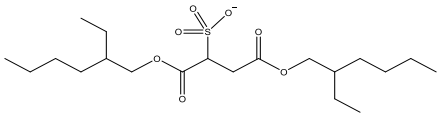
Alkyl sulphate	[C_nSO_4]	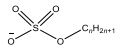
Isobutylsulphate	[iC_4SO_4]	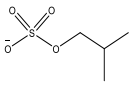
Trifluoroacetate	[TFA]	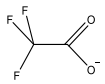
Thiocyanate	[SCN]	
bis(2,4,4-Trimethylpentyl)phosphinate	[iC_5PO_2]	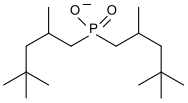
di-Isobutylphosphate	[iC_4PO_4]	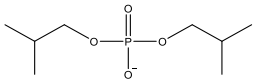
bis(2-Ethylhexyl)phosphate	[iC_8PO_4]	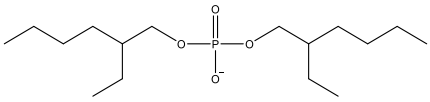
Acesulfamate	[Ace]	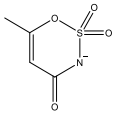
Saccharinate	[Sac]	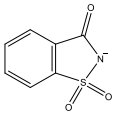
Salicylate	[Sal]	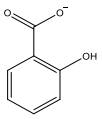
Cyclamate	[Cyc]	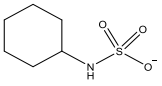
Linoleate	[Lin]	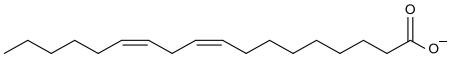
Decanoate	[Dec]	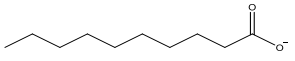

The core structures of IL cations are typically imidazolium, pyridinium, pyrrolodinium, piperidinium, quaternary ammonium or quaternary phosphoniums. The alkyl chains attached to these structures vary in length, saturation, oxidation and cyclisation to provide a huge range of structurally distinct cations. Typical anions include simple halides, *bis*triflimide and docusate. More recently, artificial sweeteners including acesulfamate, saccharinate and cyclamate have also been used. Greater anion variability can be achieved by using phosphates or sulphates with differing alkyl chains.

Many ILs, particularly those with imidazolium, pyridinium, pyrrolodinium, quaternary ammonium and quaternary phosphonium cations, and halide, bistriflimide, docusate, phosphinate and phosphate anions are currently available "over the counter" from general chemical suppliers such as Sigma-Aldrich or more specialised IL suppliers such as Iolitec. More unusual ILs can be synthesised either in house or by order. Broadly speaking, IL synthesis usually takes place in two steps: creating a halide salt of the desired cation, and anion exchange. Often, the desired halide salt can be purchased directly. If its synthesis is required, one can begin with the phosphine or amine structure (e.g. methylimidazole or methylpyridine), which are often readily available commercially, and undergo alkylation through reaction with a haloalkane(Fig. 23). This reaction only requires heating and mixing. The specific reaction temperature and time required will depend on the haloalkane used, since the halide will vary in reactivity ($I^- > Br^- > Cl^-$), but typically ranges around 50 - 80 ^oC and 1 - 3 days. This general synthesis is similar for several common IL cations including imidazoliums, pyridines, pyrrolidines, and quaternary amines. Usually, the reactants are miscible liquids, whilst the halide salt product is a denser solid immiscible in the reactants, allowing easy separation of the product by decantation. Excess reactants are removed by heating under vacuum, although temperatures above 80 ^OC should generally be avoided to prevent reversal of the quaternisation. The products are often highly hygroscopic, so it can be desirable to take care to keep the reaction and product free of water (Gordon *et al.*, 2007).

Having created a (typically solid) halide salt, anion exchange can be performed to achieve the desired cation-anion pairing. When synthesising water immiscible ILs, an aqueous solution of the halide salt is usually produced and then mixed with either the free acid of the

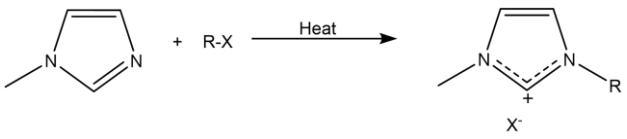

Fig. 23 - Synthesis of 1-alkyl-3-methylimidazolium halide. A haloalkane (R-X) is mixed with methylimidazole (which is readily available commercially) and heated to yield the desired cation in the form of a halide salt.

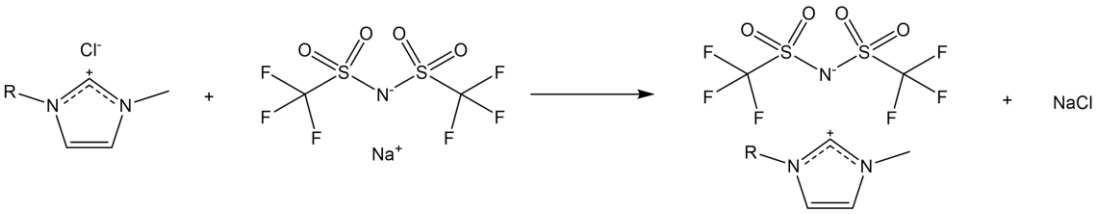

Fig. 24 - Anion Metathesis with a Halide Salt to Yield a Desired IL. The halide salt of a desired cation (in this example, 1-alkyl-3-methylimidazolium chloride) is mixed with the alkali metal salt of the desired anion (in this example, sodium *bis*(trifluoromethanesulfonyl)imide) in equimolar quantities. This yields the desired IL (here, 1-alkyl-3-methylimidazolium *bis*(triflouromethanesolfonyl)imide) and an alkali halide (here, NaCl).

desired anion, or alkali metal (*e.g.* Na, K) or ammonium salt of the anion (Fig. 24). This yields the IL with the desired cation-anion pairing, and a simple byprodcut (*e.g.* HCl, NaCl) which can be removed by water washes. When synthesising water miscible ILs, a similar approach is usually conducted but with extraction of the IL into an organic phase (often dichloromethane, CH_2Cl_2) and successive small-scale water washes. The dichloromethane (and residual water, if desired) can then be removed by rotary evaporator. Thus, sufficient removal of halide impurities can be harder to achieve for water miscible ILs than water immiscible ILs. In both cases washes can be tested with $AgNO_3$, which yields a coloured precipitate if halides are present, providing a means to determine if sufficient washing has been conducted (Gordon *et al.*, 2007). Notably, the use of Na^+ salts appears to yield higher remaining Cl^- levels in water miscible ILs than Ag^+ salts (Seddon *et al.*, 2000). However, silver is particularly antimicrobial so it is important to consider which impurity would be of greater hindrance to the intended task, and ensure residual silver is fully removed when producing an IL for a bioprocess. Furthermore, silver is comparatively expensive. Finally, IL purity is usually analysed qualitatively by ^1H NMR spectroscopy. Quantitative analysis can be conducted by electrospray ionisation mass spectrometry (ESI-MS), UV-Vis spectroscopy, capillary electrophoresis or hydrophilic interaction liquid chromatography, depending on the IL and potential impurities being analysed (Stark *et al.*, 2008).

2.6.3. Identifying Biocompatible Ionic Liquids

The use of ionic liquids in bioprocesses utilising microorganisms has already been demonstrated at lab scale, including the previously described uses of ILs to dissolve algal biomass, and their use in biphasic systems using bacteria as whole-cell catalysts (Pfruender *et al.*, 2006, Lou *et al.*, 2006, Cornmell *et al.*, 2008). However, there appears to only be one example of a study aimed at the development of a process for milking algae using ILs; Lovejoy *et al.* screened the ability of 7 ILs, varying greatly in structure, to extract extracellular

hydrocarbons from *B. braunii* cultures. They also assessed the effect these ILs had on cell viability, and all were found to be more toxic than hexane. However, a multitude of studies have been conducted that assess the ecotoxicity of ionic liquids to various organisms, to determine their effect as a potential effluent during industrial processes. Such data could prove useful in identifying biocompatible ILs suitable for use in an algal milking process. Unfortunately, algal species are still underrepresented in these studies in comparison to other organisms, and those studies that have been conducted typically assess the toxicity of the most well-known IL structures such as those with imidazolium and pyridinium cations. These studies use widely varying methods, including assessment of cell growth *via* optical density (Cho *et al.*, 2007, Cho *et al.*, 2008), fluorometry (Kulacki and Lamberti, 2008) or electrical conductance, cell counting (Wells and Coombe, 2006, Stolte *et al.*, 2007) and measurement of photosynthetic activity (Pham *et al.*, 2008). Such studies also vary greatly in their endpoint and algal species studied. This can make the data difficult to interpret or accurately compare, particularly since it appears there can be large species differences in response to ILs. As an example, the reported EC_{50} values of 1-butyl-3-methylimidazolium bromide ($[C_4MIM][Br]$) for different microalgae vary drastically between studies using different methods of toxicity assessment (Table 4). It is also noteworthy that results of repeated experiments can vary (Cho *et al.*, 2008, Cho *et al.*, 2007) (Table 4), providing further uncertainty as to the reliability of reported results. It has even been shown that media composition can affect IL toxicity (Latala *et al.*, 2010, Matzke *et al.*, 2008, Kulacki and Lamberti, 2008), providing a further variable between studies.

Table 4 - Toxicity of 1-butyl-3-methylimidazolium bromide ($[C_4MIM][Br]$) to Different Microalgae.

Organism	Method	Timescale (h)	EC_{50} (μM)	Reference
S.capricornutum	OD_{438}	96	1047	Cho *et al.*, 2007
S.capricornutum	OD_{438}	96	2137	Cho *et al.*, 2008
S. quadricauda	Chlorophyll *a* fluorometry	96	60	Kulacki *et al.*, 2008
C.reinhardtii	Chlorophyll *a* fluorometry	96	9766	Kulacki *et al.*, 2008
P. subcapitata	Photosynthetic Activity	2	23990	Pham *et al.*, 2008

2.6.4. Toxicity of Common Ionic Liquids Towards Microalgae

Despite these issues, some general trends are apparent for the most tested ILs. Imidazolium based ILs have been extensively studied, particularly with reference to differing anion

combinations and overall lipophilicity. Increasing lipophilicity, *via* extending alkyl chain length, generally increases toxicity of these ILs (Pham *et al.*, 2008) whilst introducing ether, hydroxyl or nitrile groups into the chain decreases lipophilicity and toxicity (Stolte *et al.*, 2007). Pyridinium based ILs appear to show similar trends, with increasing alkyl chain length increasing toxicity (Pham *et al.*, 2008). It is not possible to say if pyridinium ILs are any more or less toxic than imidazolium ILs to microalgae, since the data are inconsistent, with notable species differences. For example, Pham *et al.* demonstrated that various pyridinium ionic liquids ([C_xPy]) were more toxic than corresponding imidazolium ionic liquids (with respect to alkyl chain length and anion) to *P. subcapitata* (Pham *et al.*, 2008), whilst Latala *et al.* report a greater toxicity of [C_4MIM][Cl] over [C_4Py][Cl] toward *C. vulgaris*, and no significant difference in toxicities between these ILs towards *O. submarina* (Latala *et al.*, 2009). Stolte and co-workers report EC_{50} values of imidazolium and pyridinium halide ILs an order of magnitude lower (*i.e.* more toxic) than corresponding piperidinium and pyrrolidinium ILs, and 2 orders of magnitude lower than corresponding morpholinium and quaternary ammonium ILs, toward *S. vacuolatus* (Stolte *et al.*, 2007) (Table 5). Such results could again be due to the increased lipophilicity of the aromatic cations versus the aliphatic cations.

Table 5 - Effect of Cation Structure on IL toxicity Towards *S. vacuolatus*. The EC_{50} values of ionic liquids with varying cationic cores, but equivalent alkyl chain lengths and halide anions are presented. Results are from a cell counting approach, as presented by Stolte *et. al*, 2007. A clear ranking of toxicities is apparent, with the more lipophilic cations being more toxic.

Ionic Liquid	Ec_{50} (μM)
[C_4MIM][Cl]	180
[C_4Pyridinium][Cl]	390
[C_4Piperidinium][Br]	1850
[C_4Pyrrolidinium][Cl]	2340
[C_4Morpholinium][Br]	>10 000*
[$N_{1\,1\,2\,4}$][Cl]	>10 000*

Cho *et al.* assessed the toxicity of ILs with a C_4MIM cation and varying anions toward the alga *S. capricornutum (Cho et al., 2008)*. The toxicity of the anions tested was ranked as follows: $SbF_6^- > PF_6^- > BF_4^- > CF_3SO_3^- > C_8H_{17}OSO_3^- > Br^- \approx Cl^-$, [$C_4$MIM][$SbF_6^-$] and [$C_4$MIM][$PF_6^-$] were reported to produce fluoride ions, likely contributing to their toxicity. Interestingly, [C_4MIM][BF_4^-] was not reported to produce fluoride ions. The toxicity of the *bis*triflimide anion ([NTf_2]) towards *S. vacuolatus* is demonstrated in the work by Stolte *et al.*, where the

reported EC_{50} values of a morpholinium, pyrrolidinium and pyridinium cation paired with a halide (either Cl^- or Br^-) were all an order of magnitude higher than the same cation paired with the *bis*triflimide anion (Stolte *et al.*, 2007). The notable toxicity of this anion was also reported by Pretti *et al.* towards *P. subcapitata* (Pretti *et al.*, 2009). The toxicity arising from an ILs anion has been shown by many authors to be more pronounced when paired with less toxic cations (Stephens and Licence, 2011).

2.6.5. Ionic Liquids Untested with Microalgae: Toxicity Towards Bacteria

Many interesting ionic liquids with structures based on natural substances or artificial sweeteners have been developed on the principle that they could be less toxic. Examples include acesulfamate, saccharinate, amino acid, linoleate, docusate and cyclamate anions, as well as cholinium cations ($[N_{1\,1\,1\,2\text{-}OH}]$). However, whilst some of these have shown promise in bacteria toxicity screens, all are yet to be tested with any microalgae. Cholinium based ILs use the quaternary ammonium cation based on choline. Whilst no data on their toxicity towards algae is available, the toxicity of 10 different cholinium ILs towards the marine bacterium *Vibrio fischeri* was tested by Ventura *et al.* They demonstrated that this class of cations is certainly not devoid of toxicity, and is largely dependent upon the anion with which it is paired. Of the 10 ILs tested, cholinium bicarbonate was the only one with an EC_{50} higher than the conventional ILs $[C_2MIM][Cl^-]$, $[N_{1\,1\,2\,4}][Cl^-]$ and $[C_4Pyrr][Cl^-]$ (Ventura *et al.*, 2014). The ecotoxicity of ILs comprised of cholinium paired with various natural amino acid anions was assessed by Hou *et al.* The minimum inhibitory concentration (MIC) of these ionic liquids against three different bacteria ranged from approximately 20 mM to 500 mM, compared to 2.3 mM reported for $[C_4MIM][BF_4]$. However, all ILs using amino acid anions were more toxic than cholinium chloride (Hou *et al.*, 2013). Various imidazolium, quaternary ammonium and pyridinium cations were combined with cyclamate anions by Pernak *et al.*, and their toxicity towards 10 different bacteria was assessed (Pernak *et al.*, 2012). Unfortunately, no direct comparison was made using the same cations and different anions within the study, making it difficult to assess the toxicity resulting from the cyclamate anion. However, the MICs reported against *E. coli* range from approximately 0.2 to 1300 µM, with $[C_4MIM]$[Cyclamate] having an MIC of 788 µM. This is slightly lower than that reported for $[C_4MIM][BF_4]$ by Hou *et al.(Hou et al., 2013)*, who used the same method, despite the general proposal that the $[BF_4]$ anion is relatively toxic.

Wood *et al.* screened the toxicity of a multitude of ILs toward *E. coli* using agar diffusion and liquid growth inhibition assays. Four different ILs containing the saccharinate anion were tested. Whilst no growth in liquid media was observed for these ILs, the results

are inconclusive of anion toxicity since the cations used were also shown to be highly toxic when paired with halide anions (Wood *et al.*, 2011). Some ILs with docusate anions were also tested, with greatly varying results from complete growth inhibition to increased growth rates compared to control, depending on the paired cation. A single linoleate IL, $[N_{1148}][Lin]$, was also tested in this study, and was shown to completely inhibit growth of *E. coli* in liquid media. However, the same result was apparent for the $[N_{1148}]$ cation when paired with $[Br^-]$, $[I^-]$, $[NTf_2]$, and [Sac] anions, suggesting that the cation is particularly toxic. ILs containing a fatty acid anion, such as linoleate, could be particularly useful when applied to lipid extraction, and it would be worthwhile exploring other fatty acids for this application. ILs containing linoleate are typically solid at room temperature, or very viscous, due in part to the single double bond. By using more unsaturated fatty acids, such as arachidonic or linolenic acid (with 4 and 3 double bonds, respectively), it may be possible to produce an ionic liquid with high lipid extracting capability and low melting temperature. Whilst these ILs based on natural structures show varying degrees of toxicity in bacteria, their toxicity towards microalgae species is yet to be examined, and as such they should be considered during the search for compatible ILs.

2.6.6. Mechanisms of IL Toxicity

The toxicity of large groups of compounds to multiple species suggests a general mechanism of toxicity, and it is largely proposed that this occurs through cell membrane disruption (Latała *et al.*, 2005, Sena *et al.*, 2010, Samorì *et al.*, 2010a, Evans, 2006). This is supported by the observation that IL toxicity usually increases with lipophilicity (Stolte *et al.*, 2007). Sufficient membrane disruption will result in rupture, the loss of intracellular components, and ultimately cell death. However, it is important to remember that the cell membrane is not just a simple phospholipid barrier between the cell interior and exterior, but a complex organelle that is responsible for regulating flux (by direct absorption or through protein channels). Thus, disruptions that appear less drastic, such as small changes in fluidity and elasticity, can still have noticeable and even lethal effects. Evidence that various ILs can interfere with membrane structure, and how they do this, has been reported and reviewed (Benedetto, 2017). Most research into the mechanisms of membrane disruption have utilised $[C_xMIM]$ halide ILs. Far less data is available for other cation and anion classes.

Light and X-ray scattering methodologies have led authors to suggest that $[C_xMIM][Cl^-]$ cations can insert directly into a phospholipid membrane, with the polar headgroup at the phospholipid surface and alkyl chain extended into the hydrophobic region (Jing *et al.*, 2016). These observations are supported by computational molecular dynamics

(MD) simulations of [C_4MIM][Cl^-] (Bingham and Ballone, 2012). One study reported that [C_4MIM] cations were only found in the exposed exterior layer of the phospholipid bilayer (Yoo *et al.*, 2016), indicating they are unable to diffuse or "flip flop" to the interior layer as phospholipids can (Kol *et al.*, 2002). At a point of saturation (0.6 cations per phospholipid in the upper layer), this asymmetric insertion caused a bending of the membrane which led to

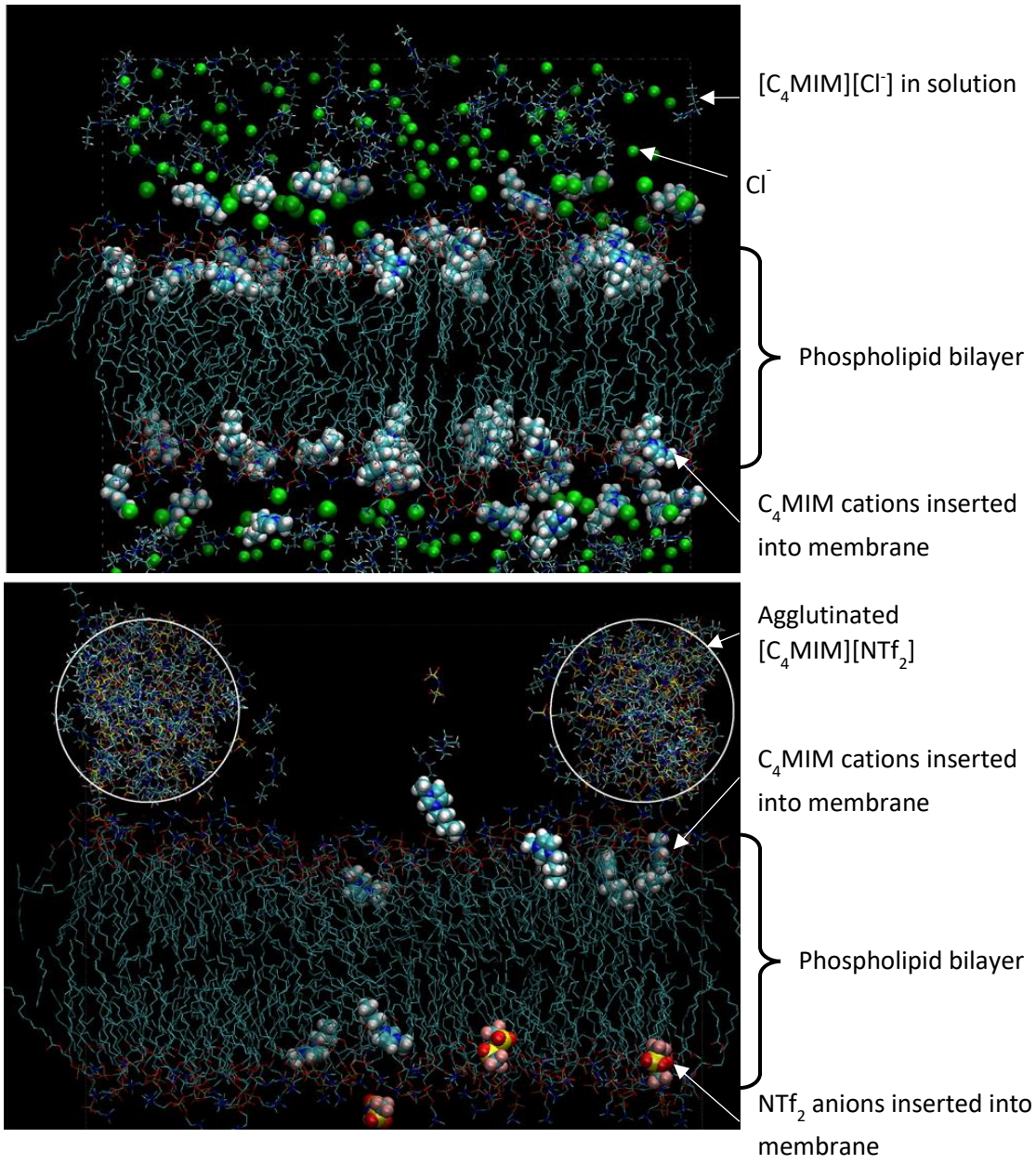

Fig. 25 Molecular Dynamics Snapshot of [C_4MIM][Cl^-] and [C_4MIM][NTf_2] Interacting with a Phospholipid Bilayer. For clarity, ions inserted into the membrane are represented by the space-filling model whilst those remaining in solution are shown by the stick model. Water was present but is not shown. [C_4MIM][Cl^-] (top) can dissociate and the cations can insert into the phospholipid membrane. The same can happen with [C_4MIM][NTf_2] (bottom), but this IL will preferentially agglutinate into droplets which interact with the polar phospholipid surface. Image adapted from Bingham and Ballone, 2012.

micelle nucleation. Other studies using this cation have demonstrated that its insertion throughout the membrane causes membrane thinning (Jeong *et al.*, 2012). Furthermore, this structural change can be sufficient to alter the efficacy of certain protein channels, specifically demonstrated with Gramicidin A (Lee *et al.*, 2015). Notably, the pairing of [C_4MIM] with the hydrophobic [NTf2] anion results in very different MD simulations. [C_4MIM][NTf_2] largely appears to agglutinate into a droplet that interacts with the membrane surface (Fig. 25), with very little dissociation of the IL or insertion of the ions into the

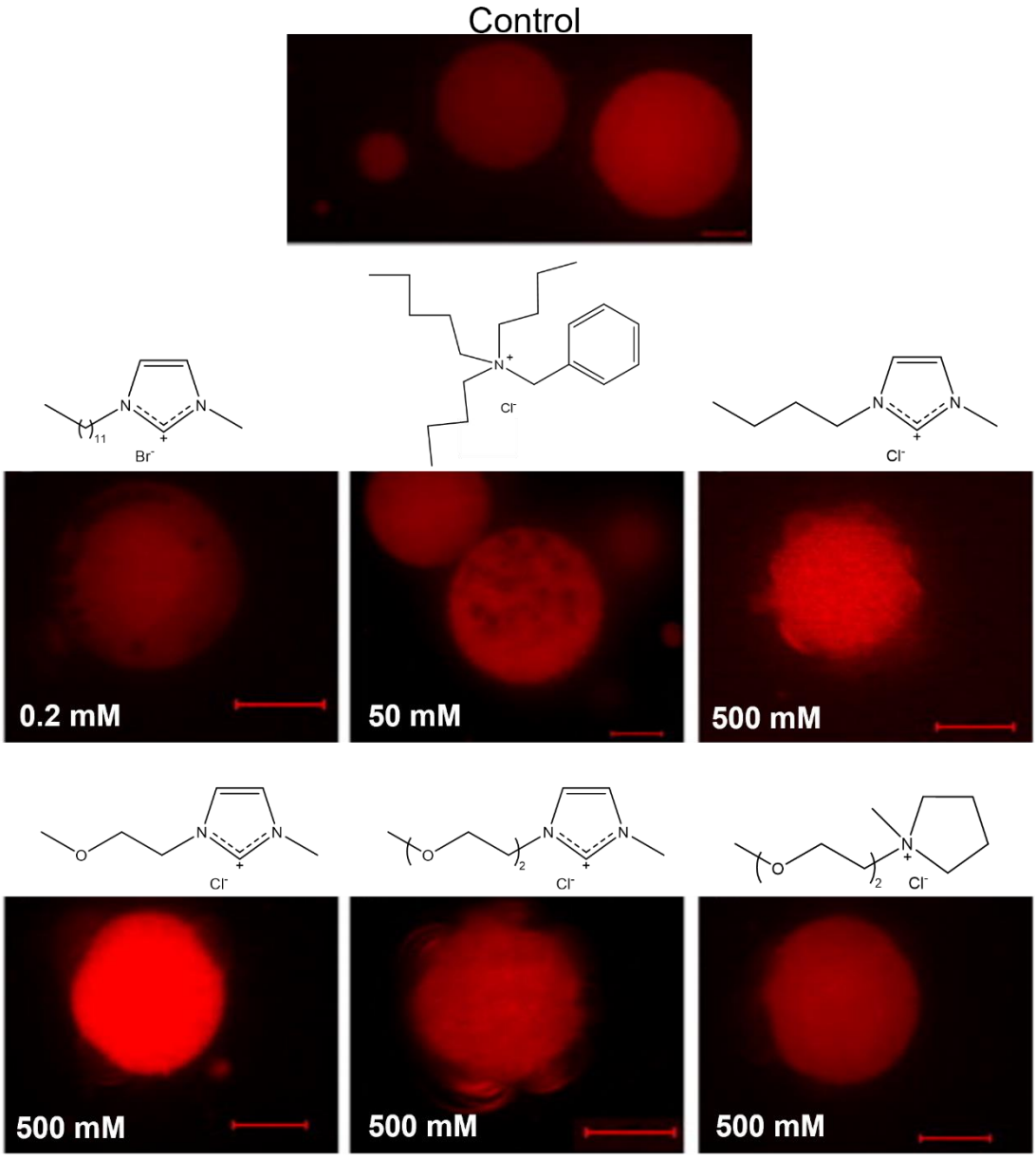

Fig. 26 - Different ILs Cause Visually Distinct Membrane Perturbations on Giant Vesicles. Gal *et al.* incubated giant vesicles with various ILs (structures given above corresponding image) and observed the resultant vesicle structure by confocal fluorescence microscopy. Note the differences in IL concentration as indicated. All scale bars 10 µm. Image adapted from Gal *et al.*, 2012.

membrane, unlike with [C_4MIM][Cl^-] (Bingham and Ballone, 2012). Clearly, more research is required to better understand how other hydrophobic ILs interact with a membrane.

Different cation classes also appear to have varying effects on membrane structure. Microscopic observation of giant vesicles in contact with imidazolium, quaternary ammonium, and pyrrolodinium chlorides yielded visually distinct membrane perturbations (Gal *et al.*, 2012) (Fig. 26). Interestingly, the extent of visible membrane disruption (although admittedly subjective), did not always correlate with extent of leakage of a fluorescent probe from the vesicles. Phosphonium acetate and phosphonium chloride ILs have been reported to be able to cross phospholipid bilayers, and cations with longer alkyl chains were generally more disruptive to membrane structure (Kontro *et al.*, 2016). Interestingly, cholesterol content was also demonstrated to provide some measure of protection against membrane disruption caused by certain ILs (Kontro *et al.*, 2016). This provides evidence that membrane composition can play some role in determining the toxicity of different ILs, perhaps partially explaining species differences. Benedetto *et al.* used neutron reflectometry to demonstrate that the cation of a cholinium chloride IL ([$N_{1\,1\,1\,2\text{-}OH}$][Cl^-]) was able to insert into the phospholipid membrane at the head-tail interface (Benedetto *et al.*, 2014), a result also predicted by MD simulations (Benedetto *et al.*, 2015). They report that insertion of the cations is initially driven by coulombic interaction between the negatively charged phospholipid head groups and positively charged IL cations. Our understanding of the mechanisms by which ILs can disrupt membrane structure is advancing but is ultimately lacking when considering the array of IL structures remaining to be studied.

Clearly where algae are concerned, the effect of the cell wall should also be considered. Sena *et al.* demonstrated that the toxicity of [C_4Py][Br^-], [$N_{2\,2\,2\,2}$][Br^-] and [$N_{4\,4\,4\,4}$][Br^-] was more pronounced in a cell-wall lacking mutant of *C. reinhardtii* in comparison to the wild-type (Sena *et al.*, 2010), suggesting that the cell wall acted as a barrier to prevent access to the membrane. Importantly however, there was little difference between the strains when using [C_4MIM][Br^-] and [C_8MIM][Br^-], perhaps suggesting that certain ILs can readily bypass the cell wall. As previously discussed, certain ILs ([$C_{1\text{-}10}$IM] cations with halide, [BF_4] and [PF_6] anions) are capable of dissolving cell wall structures, particularly cellulose (Pinkert *et al.*, 2009), and this may in fact be the means by which these ILs are toxic. Again, these interactions go some way towards explaining observed species difference across microalgae, since they can have very diverse cell wall compositions. Finally, since ILs span a huge range of chemical structures, some specific actions of toxicity such as enzyme inhibition are likely, and will also vary greatly amongst species. For example,

alkylimidazolium ILs are known to inhibit certain laccases (Sun *et al.*, 2017) and cellulases (Summers *et al.*, 2017).

2.6.7. Methods for Screening IL Toxicity and Cell Viability

The notable species and media differences in response to ILs highlights the need to conduct high throughput screens to assess their toxicity toward the specific organism used for a given bioprocess. The agar diffusion method has been shown to be a viable high throughput technique to assess the toxicity of water miscible ILs toward various bacteria (Rebros *et al.*, 2009, Ventura *et al.*, 2012, Wood *et al.*, 2011). This method entails soaking a filter paper disc in the compound to be tested, which is then placed on an agar surface spread with the microorganism (Fig. 27). If the compound is toxic, a clear zone of growth inhibition around the disc is apparent after sufficient incubation, and the width of this inhibition zone can be measured to estimate the extent of toxicity. Wood *et al.* also demonstrated the viability of this method to assess toxicity of water immiscible ILs (Wood *et al.*, 2011). Whilst these compounds are not readily soluble in the aqueous agar medium, they were able to spread over the agar surface in a film, typically resulting in larger inhibition zones than water miscible ILs. Notably, the size of an inhibition zone could thus potentially be related to the viscosity of an IL as well as its toxicity. However, except for some docusate ILs, the results from this method generally correlated well with results from a liquid growth rate method utilising OD measurements.

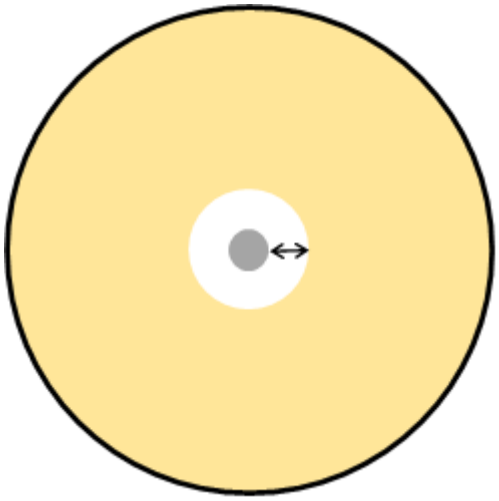

Fig. 27 - Schematic of the Agar Diffusion Method of Toxicity Assessment. A filter paper (grey) is soaked in a test substance and placed atop an agar surface spread with the test microbe (tan). Plates are incubated to allow microbial growth. If the test substance is toxic, a region of growth inhibition will be apparent (white) and can be measured (arrows). More toxic compounds generally give rise to larger inhibition zones.

The use of OD measurements, in conjunction with micro culture well-plate readers is another viable high throughput method to assess IL toxicity. However, Wood *et al.* demonstrated that the results for water immiscible ILs are often more variable than for water miscible ILs, since some cause high levels of light scattering (Wood *et al.*, 2011). Whilst these methods may not be precise enough to accurately rank the toxicity of ILs, they provide a rapid, high throughput means to identify the most (and least) biocompatible ILs. Cell viability in the presence of these ILs could then be more accurately investigated by other techniques.

2.6.8. IL Recycling and Product Recovery

When considering the use of ILs in a milking process, it is imperative that the product (EPA AGs) can be recovered sufficiently from the IL solvent. Furthermore, it is necessary to efficiently recover and re-use ILs since they are generally estimated to cost 5 – 20 times more than conventional solvents (Plechkova and Seddon, 2008). This expense is usually the greatest barrier to their commercial use. An overview of processes by which products and undesirable contaminants can potentially be separated from ILs is given here.

Owing to the negligible vapour pressure of ILs, distillation is a convenient means of extracting heat stable, volatile products from an IL solution (Sklavounos *et al.*, 2016). EPA esters are volatile, but the likelihood of adverse oxidation reactions occurring (as previously discussed in section 2.1) significantly increases with temperature. As such, conventional distillation can be unsuitable for purifying PUFAs. However, molecular distillation utilises a short path and extremely low pressures (often <1 Pa), thereby largely removing the potential for oxidation to occur. This technique has been used successfully to concentrate EPA AGs from complex fish oils (Rossi *et al.*, 2011, Solaesa Á *et al.*, 2016). Authors used pressures of 1 - 40 Pa and temperatures between 110 - 150 ^{O}C for this process, reporting that higher temperatures caused thermal degradation of the PUFAs. Theoretically, this technique should be applicable to EPA glycerides dissolved in ILs, but research is needed to confirm this. Appropriate economic analyses would also be required to determine if the process would be commercially viable; molecular distillation requires a specialised still capable of withstanding the pressure differential (a potentially high capital cost), and the operating costs associated with maintaining the high vacuum are likely to be higher than conventional distillation, despite the lower temperatures required.

Although the volatility of ILs is often referred to as “negligible” in the scientific literature, ILs can in fact vaporise under sufficiently high temperature and low pressure, and can therefore be distilled (Sklavounos *et al.*, 2016). For example, Earle *et al.* distilled

[C_2MIM][NTf_2] at 10 Pa and 300 °C using short-path distillation apparatus (a Kugelrohr) (Earle *et al.*, 2006). A BASF patent claims 98% recovery of methylimidazolium octanoate ([C_1MIM][Oct]) can be achieved by distillation at 1 Pa and 250 °C using a specialised still (Lang *et al.*, 2013). However, this process will not be applicable to every IL since such conditions are often close to the decomposition limits of the IL, thus limiting their recovery. Furthermore, achieving and maintaining these conditions is expensive, so the economic viability of IL distillation should be carefully considered. A similar approach to purify ILs is through reactive distillation, whereby the IL undergoes reactions to yield volatile products which can be distilled and subsequently used in further reactions to regenerate the original IL. A patented example of this is the decomposition of 1,3-dimethylimidazolium dimethylphosphate ([C_1MIM][C_1PO_4]) to 1-methylimidazole and trimethylphosphate, both of which are more volatile, allowing easier distillation. These products can then be used as reactants to yield the starting IL (Maase, 2005).

Where distillation is inappropriate, liquid-liquid extraction is frequently used to extract products from, and purify, ILs. The solvent used must be immiscible with the IL, enabling phase separation, and solvate the product (and contaminants, for IL recovery). These streams can then be further purified individually. Where EPA glycerides are concerned, this solvent could for example be hexane, heptane, chloroform, or diethyl ether, depending on the IL. There are examples in the literature of back extraction of lipids (including fatty acids) from various ILs using such solvents (To *et al.*, 2018, Kilulya *et al.*, 2014). This method is simple, low energy and easy to conduct. However, the benefits of using ILs over traditional solvents are rendered moot if those traditional solvents are used in a liquid-liquid back extraction. That said, if traditional solvents are found to be unsuitable for a milking process, where ILs are shown to work, then there is still value in exploring an IL milking strategy with traditional solvent back extraction. In a similar fashion, supercritical CO_2 may be inappropriate for a milking strategy, but it could be explored as a means of extracting products and contaminants from ILs. Blanchard and Brennecke used supercritical CO_2 to recover 96% of naphthalene from [C_4MIM][PF_6] (Blanchard *et al.*, 1999).

Membrane separation has also been used to purify ILs and recover solvated products (Blanchard *et al.*, 1999). For example, bromophenol blue was effectively separated from [C_4MIM][BF_4], and lactose from [C_1MIM][C_1SO_4] using membrane filtration, with >90% of IL being removed from the mixtures (Kröckel and Kragl, 2003). These processes have the potential to be low energy, without requiring additional solvent. Since nanofiltration membranes can enable the separation of charged and neutral compounds, they could

potentially be used to separate ILs and EPA esters, although there are no reports of this in the literature yet. However, membrane technologies have been developed for the purification of fatty acids and fatty acid ethyl esters from complex oils (Aghapour Aktij *et al.*, 2020), and may be worth exploring for IL-fatty acid separation. Similarly, electrodialysis through an ion-exchange membrane could potentially be used. The capital cost and reusability of the membranes will likely determine if such processes are economically viable.

Crystallisation can be used to purify certain ILs. However, not all ILs readily crystallise and those that do can require too low a temperature to provide an economically viable means of purification. Where this method has been used, extremely pure (>99%) IL can be recovered, as has been demonstrated with imidazolium chlorides (König *et al.*, 2008) and $[C_6Py][NTf_2]$ (Choudhury *et al.*, 2005). Another means of sequestering ILs could be through their adsorbance to certain materials. Activated carbon is a very popular adsorbent used predominantly in wastewater treatment. However, researchers have found that it is generally inefficient at adsorbing ILs (at best adsorbing 1g IL/g activated carbon), particularly hydrophilic ILs (Palomar *et al.*, 2009). Acetone washes have been used to separate activated carbon and ILs ($[C_{1\text{-}12}MIM]$ cations paired with $[Cl^-]$, $[BF_4]$, $[PF_6]$ or $[NTf_2]$ anions), with subsequent evaporation of the acetone to regenerate pure IL (Lemus *et al.*, 2012). However, activated carbon can lose adsorption efficiency and may not be suitable for prolonged re-use. Research is ongoing in this area with other adsorbents being explored. For example, Qi *et al.* recovered $[C_4MIM][Cl^-]$ from aqueous solution using a functional carbonaceous material (Qi *et al.*, 2013).

Water-immiscible ILs can easily be removed from a culture medium thanks to their phase separation, while water-miscible ILs present a greater challenge. However, certain hydrophilic ILs (*e.g.* $[C_4MIM][Cl^-]$) can be "salted out" of an aqueous solution and form a separate phase by the addition of kosmotropic salts (*e.g.* K_3PO_4), enabling easy IL recovery by phase separation (Gutowski *et al.*, 2003). However, one must then consider the cost of the salt and its recovery during this process. Furthermore, it is likely to be an inappropriate means of IL recovery from a culture medium in a milking process, since the salts will likely be toxic to the cells. Aqueous biphasic systems of normally water miscible ILs ($[C_xMIM]$ halides) have also been induced using carbohydrates (Wu *et al.*, 2008b, Wu *et al.*, 2008a), which may be more environmentally friendly than kosmotropic salts. Given these issues in separating water miscible ILs from culture medium, and considering that hydrophobic ILs are more likely to solubilise hydrophobic EPA glycerides, water-immiscible ILs are most likely to be successful in a milking strategy.

In conclusion, a number of methods are already available to recycle ILs and enable product recovery, each having its own advantages, disadvantages and operational requirements. Ultimately, the best method will likely depend on the specific IL used. It is hence proposed that ILs suitable for a milking process should be identified first and means with which to recycle these ILs considered subsequently.

2.7. Conclusions

Currently used dewatering and extraction methods are the greatest energetic and economic expense of most algal bioprocesses, and limit the use of microalgae to production of low-volume high-value chemicals. Algal milking provides an alternative approach through *in situ* extraction whilst maintaining cell viability, allowing a continuous extraction process without the need to concentrate the biomass. Additionally, slow algae growth can be bypassed, and increased cellular production of the target compound can be achieved, increasing overall productivity. Current milking approaches have utilised organic solvents, typically alkanes, and have been met with mixed success. Hydrocarbons have been successfully extracted from *B. braunii* cultures whilst maintaining cell viability, however, the target compounds were extracellular. Continuous processes have been demonstrated for extraction of intracellular compounds of interest, but cell viability is not usually retained.

An alternative approach could be developed through the use of pulsed electric field to generate reversible pores in the cell membrane, whilst providing a hydrophobic environment for the extraction of lipids in a biphasic solvent-culture system. Due to the toxic and environmentally unfriendly nature of volatile organic solvents, ILs could be a safer alternative. ILs offer a versatile and diverse range of properties, and could allow a biocompatible solvent to be developed that also has high EPA extractability. However, the current literature on IL toxicity towards algae is sparse, and what data is available illustrates that broad species differences are apparent.

3. Research Aims

The aims of this research were to:

- Identify water immiscible solvents, including ILs, that are biocompatible with *T. minutus* and could hence be used in an EPA milking strategy.

- Develop methods to quantify EPA present in these ILs

- Explore the ability of PEF treatments to reversibly permeabilise *T. minutus*, and the effect this has on cell viability and EPA extraction.

4. Materials and Methods

4.1. Materials

Bold's basal modified (BBM) medium, fatty acid standards, hexane, methanol and hydrochloric acid were purchased from Sigma-Aldrich (UK). Electroporation cuvettes were purchased from Bio-Rad Laboratories (UK). SYTOX Green was purchased from Thermo Fisher Scientific (UK). $[P_{4\,4\,4\,4}][Cl^-]$, $[P_{8\,8\,8\,8}][Br^-]$, $[P_{6\,6\,6\,14}][Cl^-]$, $[P_{4\,4\,4\,14}][Cl^-]$, $[P_{6\,6\,6\,14}][NTf_2]$ Cyphos 104 and $[P_{6\,6\,6\,14}][iC_8PO_4]$ were purchased from Iolitec (Heilbronn, Germany). $[P_{6\,6\,6\,14}][Sac]$, $[P_{6\,6\,6\,14}][cyc]$, $[P_{6\,6\,6\,14}][ace]$ and $[P_{6\,6\,6\,14}][sal]$ were provided by Dr. Angela Tether, University of Nottingham. The remaining ILs ($[C_6MIM][Sac]$, $[C_8MIM][Sac]$, $[C_2MIM][NTf_2]$, $[C_4MIM][NTf_2]$, $[C_8MIM][NTf_2]$, $[C_4MIM][AOT]$, $[C_6MIM][AOT]$, $[C_4MIM][Cl^-]$, $[C_6MIM][Cl^-]$, $[C_4MIM][Br^-]$, $[C_2BIM][C_2SO_4]$, $[C_2MIM][C_8SO_4]$, $[C_4MIM][C_3SO_4]$, $[C_4MIM][iC_4SO_4]$, $[C_6py][Br^-]$, $[C_6py][Cl^-]$, $[C_4py][AOT]$, $[C_4py][Sac]$, $[C_6py][TFA]$, $[C_8py][Lin]$, $[C_6py][AOT]$, $[C_8py][AOT]$, $[C_4pyrro][NTf_2]$, $[C_4pyrro][AOT]$, $[Pip_{1\,3\text{-}O\text{-}1}][NTf_2]$, $[P_{6\,6\,6\,14}][iC_4PO_4]$, $[P_{6\,6\,6\,14}][Br^-]$, $[P_{6\,6\,6\,14}][Dec]$, $[P_{8\,8\,8\,14}][Br^-]$, $[P_{1\,4\,4\,4}][NTf_2]$, $[P_{6\,6\,6\,14}][SCN]$, $[P_{8\,8\,8\,14}][AOT]$, $[P_{8\,8\,8\,14}][Cl^-]$, $[N_{1\,1\,4\,8}][Cl^-]$, $[N_{1\,1\,2\,2\text{-}OH}][NTf_2]$, $[N_{1\,1\,2\,4}][NTf_2]$, $[N_{1\,1\,4\,8}][Sac]$, $[N_{1\,4\,8\,8}][Lin]$, $[N_{1\,8\,8\,8}][Cl^-]$, $[N_{1\,1\,2\,2\text{-}O\text{-}2\text{-}O\text{-}Bn}][NTf_2]$, $[N_{1\,1\,2\,2\text{-}O\text{-}2\text{-}O\text{-}1\text{-}Bn}][NTf_2]$, $[N_{1\,1\,4\;\;2\text{-}OH}][AOT]$, $[N_{1\,2\text{-}OH\;2\text{-}OH\;12}][NTf_2]$, $[N_{1\,1\,4\,8}][NTf_2]$, $[N_{1\,1\,2\,2\text{-}OH}][AOT]$, $[N_{4\,4\,4\,4}][AOT]$ and $[N_{1\,1\,1\text{-}Bn\;2\text{-}O\text{-}2\text{-}O\text{-}Bn}][NTf_2]$) were a donation from the late Prof. Kenneth Seddon, Queen's University Belfast.

4.2. Culture Growth and Preparation

Cultures containing *T. minutus* and mutualist bacteria were grown in autoclave-sterilised Bold's Basal Modified (BBM) medium, at room temperature (21-24 ^{O}C), under a panel of 100 LEDs (consisting of 60 at 660 nm, 15 at 630 nm, 18 at 425 nm, 5 white, 1 at 730 nm and 1 at 380 nm) providing a photosynthetic photon flux density (PPFD) of 200 µmol/m^2/s. Agitation was provided for liquid cultures by shaking at 150 rpm. Stock cultures were maintained by harvesting cells by centrifugation (3000 rpm/1560 *g*, 3 min) once every 2 weeks, and aseptically (by use of a Bunsen) resuspending half the biomass in fresh, sterile BBM medium.

For all experiments, fresh experimental cultures were produced unless otherwise stated; cells from stock cultures in stationary growth phase were harvested by centrifugation (3000 rpm/1560 *g*, 3 mins) and pellets resuspended in fresh, sterile BBM medium to the desired concentration, as determined either by measurement of optical density at 750 nm (OD_{750}), or by cell counts.

4.3. Cell Counts

Algae cell counts were performed using a haemocytometer and an Olympus CX41 microscope; four counts were conducted, each containing a minimum of 100 cells, and the mean result was calculated and corrected for the dilution factor. The bacteria present in the culture were not counted.

4.4. Toxicity Screening

4.4.1. IL Growth Inhibition by an Agar Method

Plates were prepared *via* a top agar method. Aliquots (2 ml) of molten BBM agar (1.5% agar *w/v*) were incubated at 40 °C. To each, *T. minutus* culture (1 ml, OD_{750} = 1.5) was added. The solution was briefly vortexed and poured onto pre warmed (37 °C) BBM agar (1.5% agar *w/v*) in a plastic Petri dish. Petri dishes were gently tilted to achieve an even spread and left to set. Filter paper circles (5 mm diameter) were cut using a hole punch and autoclave-sterilised before being placed in triplicate on the media, approximately equidistant from each other and the edge of the plate, using flame-sterilised forceps. IL (10 µl) was added to all filter papers, with each plate receiving a different IL, and the three filter papers of each Petri dish serving as triplicates. ILs were allowed to absorb into filter papers before Petri dishes were incubated upside-down for 5 days under a PPFD of 150-200 µmol/m^2/s. Inhibition zones were measured from the edge of the filter paper to the edge of the zone, with maximum and minimum distances recorded for non-circular zones. Where two differently coloured zones were apparent, the maximum and minimum distance of each zone from the edge of the filter paper was recorded.

4.4.2. IL Growth Inhibition in Multi-well Plates

Bioscreen 100-well plates were used. Water (300 µl) was added to edge wells to reduce evaporation of inner wells. All tests were conducted in triplicate across the same plate, with their positions randomised. Controls consisted of *T. minutus* culture (300 µl, OD_{750} = 0.5) in fresh BBM media. Blanks consisted of BBM media (300 µl). Test wells contained IL (69 µl) and *T. minutus* culture (231 µl, OD_{750} = 0.26), yielding a final OD_{750} of 0.2 and 23% (*v/v*) IL, a phase ratio within what has previously been reported as suitable for biphasic systems applied to biocatalysis (León *et al.*, 1998). Plates were incubated, shaking vigorously (250 - 480 rpm), under a PPFD of 250 µmol/m^2/s. Once a day, plates were removed and the OD_{750} of each well measured using a Bioscreen C plate reader (Thermo Labsystems). Sterile plate lids were

exchanged before and after OD measurements to avoid condensation obscuring measurements.

4.4.3. IL Growth Inhibition in Flask Cultures

Fresh *T. minutus* cultures (10 ml, OD_{750} = 0.5) were added to sterile 25 ml Erlenmeyer flasks. IL (100 µl, yielding 1% *v/v*) was added to test cultures. This lower phase ratio was chosen to minimise the quantity of potentially expensive ILs used. The pH of the media in the presence of ILs was tested using pH papers. The pH difference with control cultures was found to be less than one unit in every case. Cultures were established in triplicate and incubated shaking at 220 rpm with a PPFD of 200 µmol photons m^{-2} s^{-1}. Culture positions were randomised. Each batch of experiments included triplicate controls for direct growth comparison. Every 24 h, culture aliquots (100 µl) were removed (avoiding the IL phase) and diluted in BBM media (900 µl). The solution was mixed by pipetting, and the OD_{750} recorded.

Specific growth rates (µ) were calculated using the formula:

$$\mu = \frac{\ln(N_2/N_1)}{(t_2 - t_1)}$$

Where N1 and N2 = OD_{750} at time 1 (t1) and time 2 (t2), respectively. Points were chosen such that they covered the exponential phase of growth. Specific growth rates were first calculated for control cultures and averaged. Specific growth rates for individual IL-containing cultures were then calculated and expressed as a percentage of the average control culture specific growth rate:

$$\frac{\mu \text{ of individual culture}}{\text{Average } \mu \text{ of controls}} \text{x}100$$

Finally, the percentages for triplicate ILs were averaged and their standard deviation determined.

4.4.4. Large Scale Solvent Toxicity

Cultures were grown in a photobioreactor (Multi-cultivator, Photon System Instruments) at 25 ^{O}C with a constant light intensity of 200 µmol/m^2/s. OD_{680} measurements were taken every 30 mins and cultures were grown for a total of 240 h from an initial OD_{680} of 0.5. Except

for control cultures, solvents were added at 120 h to a final volume of 20% (v/v). The total volume in each tube was 80 ml (16 ml IL + 64 ml culture).

4.5. Producing Permeabilised Controls

Heat shocked controls were produced by heating 10^7 algae cells/ml at 90 ^{O}C in a heating block for 1 h, and then allowing the sample to cool to room temperature. To produce isopropanol controls, *T. minutus* cells (10^7/ml) were separated from BBM medium by centrifugation (3000 rpm/600 *g*, 5 mins) and resuspended in 70% isopropanol for 1 h, after which they were re-harvested and resuspended in fresh BBM medium. Both controls were stained for 1 h in the dark with an equivalent volume of SYTOX Green (3 µM) in BBM media, yielding final concentrations of 5 x 10^6 cells/ml and 1.5 µM SYTOX Green.

4.6. Optimisation of SYTOX Green (SG) Cell Staining

SYTOX Green (SG) and heat-shocked cell suspensions were diluted in BBM medium to desired concentrations. Aliquots (50 µl) of each were added to wells of a Nunc 96 well plate throughout 3 experiments; varying SYTOX Green concentration, varying SG incubation time, and varying heat shocked control cell concentration. For each experiment, other variables remained constant (1 h incubation time, 1.5 µM SG, 5 x 10^6 algae cells/ml). Plates were incubated in the dark. After given incubation times well contents were mixed by gentle pipetting, and the fluorescence intensity of each well was measured by fluorescence spectroscopy as described in analytical methods.

4.7. Electroporation Protocols

All electroporation was conducted using a Bio-Rad Gene Pulser Xcell II using electroporation cuvettes with an electrode gap distance of 2 mm. In every experiment, the final volume present in a cuvette was 300 µl, with an algae cell concentration of 5 x 10^6 cells/ml and resistance of approximately 200 Ω. Each cuvette received a square wave pulse, but further pulse parameters (amplitude, duration and frequency), as well as the time of addition of SYTOX Green, were individually varied across experiments. Triplicate cell suspensions were produced for each PEF treatment. Cuvettes were allowed to stand for 1-2 mins after PEF treatment, after which their contents were mixed by gentle pipetting, and aliquots transferred to the wells of a microplate. The plate was kept in the dark between addition of samples, and allowed to incubate in the dark for 1 h after the addition of the final sample. Heat shocked, lysed cell controls were produced as previously described, and served as a

benchmark for maximal fluorescence intensity. Live cell controls consisted of a fresh cell suspension of 5 x 10^6 cells/ml, 1.5 µm SG, and were used to determine background fluorescence.

4.7.1. Determining Extent of Permeabilization from Varying PEF Treatments

Cell suspensions contained 1.5 µM SG and were exposed to either: a single 5 ms square wave pulse of varying voltage, a single pulse of 1.8 kV of varying duration, or a varying number of 1.6 kV pulses with 1 min pulse intervals. Aliquots (200 µl) were transferred to individual wells of a microplate. Triplicate aliqouts (100 µl) of heat-shocked and live cell controls were also added, and mixed with aliquots of SG (100 ul, 3 µM). Each well contained the same final volume (200 µl), SYTOX Green concentration (1.5 µM) and algae cell concentration (5 x 10^6 cells/ml). Plates were analysed by fluorescence spectroscopy or flow cytometry as described in analytical methods.

4.7.2. Determining Cell Resealing using SYTOX Green

Cell suspensions were exposed to a single 5 ms, 1.8 kV, square wave pulse without SYTOX Green present. At varying times after the pulse (1-60 min), aliquots (100 µl) were transferred to a microplate, containing an aliquot of SYTOX Green solution (100 µl, 3 µM) in BBM medium. In addition, triplicate suspensions were electroporated in the presence of SYTOX Green (1.5 µM) under the same conditions. After the pulse, an aliquot (100 µl) of each was transferred to wells containing SYTOX Green solution (100 µl, 1.5 µM). Heat shocked and live cell controls were diluted to 5 x 106 cells/ml, and triplicate aliquots (100 µl) were mixed with SYTOX Green (3 µM, 100 µl) in the wells of the same microplate. Each well contained the same final volume (200 µl), SYTOX Green concentration (1.5 µM) and algae cell concentration (2.5 x 106 cells/ml). Plates were analysed by fluorescence spectroscopy as described in analytical methods. The same procedure was used for further experiments, with analysis by flow cytometry (see analytical methods), and faster addition of SYTOX Green (10 s – 20 min).

4.7.3. Cell Counts After PEF Treatments

Cell suspensions were exposed to single 5 ms pulses of varying voltages. After the pulse, aliquots (200 µl) were transferred to a well of a 24-well plate. Aliquots of the same, untreated cell suspension (200 µl, 5 x 10^6 cells/ml) were also transferred in triplicate to individual wells of the same plate to serve as controls. To every well, sterile BBM medium (200 µl) was added. The plate was incubated (as described in culture growth and preparation), for 96 h. After

incubation, cell counts of cultures from each well were performed as previously described. These data were averaged to determine the cell concentrations in each well, from which the original cell concentration (2.5 x 10^6 cells/ml) was subtracted, and the result expressed as a percentage of the mean cell concentration of control cultures:

$$\frac{(Cell\ concentration\ of\ well - 2.5 \times 10^6 cells/ml)}{(Mean\ cell\ concentration\ of\ control\ wells - 2.5 \times 10\ cells/ml)} \times 100$$

The mean and standard deviation of triplicate culture samples exposed to the same pulse was then determined.

4.8. Fatty acid Extraction and Derivatisation for Analysis by GCMS

Chloroform/methanol (2:1 v/v, 0.2 ml) and HCl in methanol (5% v/v, 0.3 ml) were added to freeze-dried algal biomass for combined fatty acid (FA) extraction and *in situ* transesterification to fatty acid methyl esters (FAMEs). Tridecanoic acid methyl ester and heptadecanoic acid dissolved together in chloroform (20 µl) were added as recovery and transesterification standards, respectively. The solution was briefly vortexed before heating at 65 ^{O}C for 1 h. The solution was allowed to cool, after which hexane (1 ml) was added to extract FAMEs for 1 h at room temperature. The organic layer was removed *via* pipette and diluted 10-fold in hexane.

4.9. Analytical Methods

4.9.1. Fluorescence Spectroscopy

The contents of each microplate, prepared as previously described, were gently mixed by pipetting before being placed into a FLUOstar® Optima plate reader (BMG Labtech, Germany). The gain required to provide 90% of maximal fluorescence (65 000 rfu) was determined across the entire plate, after which the fluorescence intensity of each well was measured using 485 nm and 520 nm excitation and emission filters, respectively. Fluorescence was measured in a series of 20 orbital flashes per well (orbit diameter 4 mm), with the average fluorescence of each well expressed in relative fluorescence units (rfu).

For each electroporation experiment, the mean fluorescence intensity of live cell controls (n = 3) was determined. This was assumed to be equal to the background fluorescence present in all samples, and was hence subtracted from the raw fluorescence

intensity of every reading to give corrected fluorescence intensities for all samples and further controls:

$$Corrected\ fluorescence = Raw\ fluorescence - Mean\ of\ live\ cell\ fluorescence$$

Subsequently, the mean fluorescence intensity of the (heat-shocked) lysed cell controls was calculated. The fluorescence intensity (assumed to equate to the extent of permeabilisation) of each individual sample was then described as a percentage of this mean:

$$\%\ permeabilization = \frac{Corrected\ sample\ fluorescence}{Mean\ of\ corrected\ lysed\ cell\ control\ fluorescence} \mathrm{x}100$$

Across triplicate samples, the mean and standard deviation of these percentages were then determined.

4.9.2. Flow Cytometry

Samples were analysed by flow cytometry using a FACS CANTO II (Beckton Dickinson) equipped with a 488nm laser using a 530/30nm band pass filter for detection of SYTOX Green. The data were then analysed using Kaluza Analysis Software (Beckman Coulter), allowing the visualisation of cell populations and their fluorescence intensities. A distinct algae cell population was identified based on their larger size (producing a larger forward scatter), with a further population likely only containing smaller bacterial cells and cell debris. Subsequent analysis was conducted on events (individual algae cells) only within the designated algae cell population. A stained, heat-shocked lysed cell population was used to set a threshold fluorescence intensity at or above which cells were considered "fully stained". An unstained live cell population was used to set a florescence threshold below which cells were considered "not stained" (autofluorescing). Any events exhibiting fluorescence between these thresholds were considered "partially stained". The number of events belonging to each designated fluorescence intensity (not stained, partially stained, fully stained) were expressed as a percentage of the total events within the whole algae cell population.

4.9.3. Gas Chromatography – Mass Spectrometry (GC-MS)

An Agilent HP-5 column (30 m x 320 µm x 0.25 µm) was used in conjunction with an Agilent 7820 GC. The oven temperature program was as follows: held at 70 ^{O}C for 3 mins, ramped at 20 ^{O}C/min to 230 ^{O}C, held for 1 min, ramped at 20 ^{O}C/min to 300 ^{O}C and held for 3 mins. Inlet temperature was 280 ^{O}C, using a 1 µl splitless injection and helium carrier gas. Peaks were identified *via* their percentage match with NIST 2008 library spectra.

4.9.4. Gas Chromatography-Flame Ionisation Detection (GC-FID)

An Agilent HP-5 column (30 m x 320 µm x 0.25 µm) was used in conjunction with a 10 m deactivated fused silica guard column, used to trap non-volatile ILs, on an Agilent 7820 GC. The oven temperature program consisted of 70-300 ^{O}C at 20 ^{O}C/min, held for 1 min at 70 ^{O}C, 230 ^{O}C and 300 ^{O}C. The detector was held at 280 ^{O}C. Split injection (1 µl, 10:1) was used.

4.9.5. UV-vis Spectroscopy

Aliquots of ILs ($[P_{6,6,6,14}][NTf_2]$, $[N_{1,8,8,8}][NTf_2]$, $[P_{6,6,6,14}][iC_8PO_4]$) were added to pre – weighed HPLC vials in triplicate. Their mass was recorded prior to addition of acetonitrile to a total volume of 1 ml. Triplicate EPAEE solutions were prepared form a stock solution of 2.5mg/ml in acetonitrile. Further dilutions in acetonitrile were then conducted to achieve $0.1 < \lambda max < 0.8$ for every solution. A Shimadzu UV-2600 UV-Vis spectrophotometer was used to measure the absorbance of each sample every 0.5 nm from 190 nm to 400 nm. Samples were in quartz cuvettes and the instrument was blanked using acetonitrile. Molar extinction coefficients were calculated for each individual sample according to the Beer-Lambert law:

$$A = \varepsilon cl$$

4.9.6. HPLC-UV

A range of EPA standards were produced (at 0.5, 1.25, 2.5, 5, 12.5, 25, 50 and 100 µg/ml) in 1:1 IL:acetonitrile for each IL. Analysis was conducted with an Agilent 1200 fitted with an Extend C-18 column (150 x 4.6 mm, 3.5 µm) and guard column at 30 °C, using an isocratic mobile phase of acetonitrile (95%), water (5%), and formic acid (0.1%) at a flow rate of 1 ml/min and injection volume of 10 µl. UV detection was at 197nm.

5. Results - Solvent Toxicity towards *T. minutus*

A successful biphasic milking strategy requires a biocompatible solvent, making it necessary to assess the toxicity of a range of solvents towards *T. minutus*. Most reported biphasic extractions from cell cultures utilise phase ratios of ≥ 20% (*v/v*) of solvent (Hejazi *et al.*, 2004, Lovejoy *et al.*, 2013). Clearly, it is most valuable to know the toxicity of a solvent at the concentration at which it will be used during biphasic extraction (20 % *v/v* in this study). However, ILs are generally very expensive in comparison to most conventional organic solvents, making it undesirable to utilise large quantities of ILs that could be toxic. To avoid this, it was proposed that a tiered toxicity screening approach would be adopted in which small volumes of IL could be used initially, with promising ILs subsequently tested at a larger scale. Such an approach was suggested by Wood *et al.*, who demonstrated the effective use of agar diffusion and small-scale well plate screens for assessing the toxicity of a range of water miscible and water immiscible ILs towards *E. coli* (Wood *et al.*, 2011). Based on this work, the agar diffusion method was used as an initial screen in this study, since it is fast, easy to setup and uses very small quantities of IL (10 µl). Promising ILs were subsequently screened using a small scale (1% *v/v*) liquid/liquid method, providing liquid environment more like the proposed milking strategy than the solid-media agar diffusion screen, but requiring slightly larger quantities (100 µl) of IL. Finally, the best ILs from the small-scale liquid screen were used in larger scale (20% *v/v* IL, 80 ml total volume) biphasic experiments.

5.1. Assessment of IL Toxicity by an Agar Method

The agar diffusion method has been used for decades to assess the toxicity of water soluble compounds towards bacteria (Heatley, 1944, Reller *et al.*, 2009). It has also been used with ILs (Wood *et al.*, 2011, Ventura *et al.*, 2012). The method involves the application of the test substance to a filter paper on top of a lawn of the test species spread over agar medium. The test substance then diffuses throughout the agar and may inhibit growth around its point of application, with more toxic compounds producing larger zones of growth inhibition. However, the water immiscible ILs used in this study are unable to diffuse through the agar, and would instead likely form films over the agar surface, as has been reported previously (Wood *et al.*, 2011). It was therefore hypothesised that the size of an inhibition zone produced by a water immiscible IL may be as much due to its viscosity as its toxicity, *i.e.* a toxic but very viscous IL could produce a small inhibition zone. However, large inhibition zones should only be produced by toxic ILs. A library of 62 ILs was tested (Table 6 - Table 9).

The general structures of their component cations and anions are illustrated in Table 2 and Table 3 (subchapter 2.6.2), respectively, alongside their designated abbreviations.

Fig. 28 - Comparison of *T. minutus* Lawn Achieved by Spreading Cells Over the Agar Surface (left) *vs.* Cells Within a Top Agar (right).

Table 6 - Effect of Imidazolium Ionic Liquids on Growth of *T. minutus* on Solid Media. *T. minutus* cells suspended in a top agar were exposed to IL-soaked filter papers for five days, causing zones of growth inhibition.

	Inhibition Zone	
Ionic Liquid	Size (mm)	Colour
$[C_6MIM][Sac]$	Whole plate	Clear
$[C_8MIM][Sac]$	Whole plate	Clear
$[C_2MIM][NTf_2]$	Whole plate	Clear
$[C_4MIM][NTf_2]$	Whole plate	Clear
$[C_8MIM][NTf_2]$	Whole plate	Clear
$[C_4MIM][AOT]$	Whole plate	Clear
$[C_6MIM][AOT]$	Whole plate	Clear
$[C_6MIM][Cl^-]$	Whole plate	Clear
$[C_8MIM][Cl^-]$	Whole plate	Clear
$[C_4MIM][Br^-]$	Whole plate	Clear
$[C_2BIM][C_2SO_4]$	Whole plate	Clear
$[C_2MIM][C_8SO_4]$	Whole plate	Clear
$[C_4MIM][C_3SO_4]$	Whole plate	Clear
$[C_4MIM][iC_4SO_4]$	Whole plate	Clear

Liquid *T. minutus* cultures were incapable of producing uniform lawns when directly added to, and spread over, an agar surface (Fig. 28). Hence, the method was adapted to use a top-agar approach. Briefly, aliquots of molten agar were incubated at 40 ^{O}C to which liquid *T. minutus* cultures were added and mixed. These were then rapidly poured onto pre-warmed (37 ^{O}C) BBM agar plates, and the plates gently tilted to achieve a uniform spread (Fig. 28).

ILs containing imidazolium cations completely inhibited growth across the entire plate (Table 6), making them the most toxic of the cation classes tested with this method.

Similarly, 6 of the 8 pyridinium based ILs tested inhibited growth across the entire plate, with only [C_6py][AOT] and [C_8py][AOT] producing smaller, measurable inhibition zones of 11 mm and 3-4 mm, respectively (Table 7). These data, together with the whole-plate growth inhibition produced by [C_4py][AOT], may suggest that the toxicity of [$C_x$py][AOT] ILs increases with decreasing alkyl chain length. Only one piperidinium IL ([$Pip_{1\ 3\text{-}O\text{-}1}$][$NTf_2$]) and 2 pyrrolidinium ILs ([C_4pyrro][NTf_2] and [C_4pyrro][AOT]) were tested, and only [C_4pyrro][AOT] produced inhibition zones smaller than the whole plate (5-7 mm, Table 7).

Table 7 - Effect of Pyridinium, Pyrrolidinium and Piperidinium Ionic Liquids on Growth of *T. minutus* on Solid Media. *T. minutus* cells suspended in a top agar were exposed to IL-soaked filter papers for five days, causing zones of growth inhibition. For non-uniform inhibition zones the minimum and maximum distance between their edge and the edge of the filter paper is given.

	Inhibition Zone	
Ionic Liquid	Size (mm)	Colour
[C_6py][Br^-]	Whole plate	Clear
[C_6py][Cl^-]	Whole plate	Clear
[C_4py][AOT]	Whole plate	Clear
[C_4py][Sac]	Whole plate	Clear
[C_6py][TFA]	Whole plate	Clear
[C_8py][Lin]	Whole plate	Clear
[C_6py][AOT]	11	Clear
[C_8py][AOT]	3-4	Clear
[C_4pyrro][NTf_2]	Whole plate	Clear
[C_4pyrro][AOT]	5-7	Clear
[$Pip_{1\ 3\text{-}O\text{-}1}$][$NTf_2$]	Whole plate	Clear

Several ILs were tested which contained the [$P_{6\ 6\ 6\ 14}$] cation paired with various anions. The size of the inhibition zones they produced ranked [iC_4PO_4] > [Br^-] > [iC_8PO_4] > [Sal] > [Dec] > [AOT] > [Sac] > [Ace] > [iC_5PO_2] > [SCN] > [Cyc] > [NTf_2] = [Cl^-]. Phosphonium ILs containing [Cl^-] anions generally produced small inhibitions zones (0.5 – 4 mm). Of 18 quaternary phosphonium ILs tested, [$P_{6\ 6\ 6\ 14}$][iC_4PO_4] was the only one to completely inhibit growth across the whole plate (Table 8). The structurally related [$P_{6\ 6\ 6\ 14}$][iC_8PO_4] produced a measurable inhibition zone of 20mm, suggesting that toxicity of this anion may decrease with increasing alkyl chain length. Only 3 [$P_{8\ 8\ 8\ 14}$] ILs were tested, but the size of the inhibition zones they produced ranked [Br^-] > [AOT] > [Cl^-] as with [$P_{6\ 6\ 6\ 14}$] ILs. It is perhaps unsurprising that the [Br^-] anion appears to be much more toxic than [Cl^-], given the comparative abundance of the latter anion within nature. In every case, [$P_{8\ 8\ 8\ 14}$] ILs produced smaller

inhibition zones than [$P_{6\,6\,6\,14}$] paired with the same anions. However, it is not possible to say if this is a result of decreased toxicity, or increased viscosity.

Table 8 - Effect of Quaternary Phosphonium Ionic Liquids on Growth of *T. minutus* on Solid Media. *T. minutus* cells suspended in a top agar were exposed to IL-soaked filter papers for five days, causing zones of growth inhibition. For non-uniform inhibition zones the minimum and maximum distance between their edge and the edge of the filter paper is given. Additionally, in some circumstances distinct zones of different colours were produced. In such instances the maximum and minimum distance of the far edge of each zone from the edge of the filter paper is given alongside the colour of the zone.

	Inhibition Zone 1		Inhibition Zone 2	
Ionic Liquid	Size (mm)	Colour	Size (mm)	Colour
[$P_{6\,6\,6\,14}$][iC_4PO_4]	Whole plate	Clear		
[$P_{6\,6\,6\,14}$][Br^-]	1-4	White	17-22	White
[$P_{6\,6\,6\,14}$][iC_8PO_4]	4	Clear	8-20	Light Green
[$P_{6\,6\,6\,14}$][Sal]	2-4	White	10-11	Clear
[$P_{6\,6\,6\,14}$][Dec]	2-6	Clear	4-8	White
[$P_{6\,6\,6\,14}$][AOT]	3-8	Clear		
[$P_{6\,6\,6\,14}$][Sac]	1-3	White	4-6	Clear
[$P_{8\,8\,8\,14}$][Br^-]	1-3	White	4-6	Clear
[$P_{1\,4\,4\,4}$][NTf_2]	2-6	Clear		
[$P_{6\,6\,6\,14}$][Ace]	1-4	White	4-5	Clear
Cyphos® 104 (90% [$P_{6\,6\,6\,14}$] [iC_5PO_2], 10% [$P_{6\,6\,6\,14}$][Cl^-])	3-5	Clear		
[$P_{6\,6\,6\,14}$][SCN]	3-4	Clear		
[$P_{6\,6\,6\,14}$ [Cyc]	1-2	White	3-4	Clear
[$P_{8\,8\,8\,14}$][AOT]	0.5-1	White	2-4	Clear
[$P_{8\,8\,8\,8}$][Cl^-]	1-2	White	2-4	White
[$P_{4\,4\,4\,6}$][Cl^-]	0.5-2	Clear		
[$P_{6\,6\,6\,14}$][NTf_2]	1	Clear		
[$P_{6\,6\,6\,14}$][Cl^-]	1	White		
[$P_{8\,8\,8\,14}$][Cl^-]	<0.5-1	White		

Results were more varied for ILs with quaternary ammonium cations (Table 9). Of the 18 tested, 5 ([$N_{1\,1\,4\,8}$][Cl^-], [$N_{1\,1\,2\,2\text{-}OH}$][NTf_2], [$N_{1\,1\,2\,4}$][NTf_2], [$N_{1\,1\,4\,8}$][Sac] and [$N_{1\,1\,4\,8}$][Lin]) completely inhibited growth across the whole plate. In contrast to the phosphonium ILs, ammonium ILs containing chloride anions ([$N_{1\,1\,4\,8}$][Cl^-] and [$N_{1\,8\,8\,8}$][Cl^-]) produced some of the largest inhibition zones. Of the non-aromatic ammonium-*bis*triflimide ILs ([$N_{1\,1\,2\,2\text{-}OH}$][NTf_2], [$N_{1\,1\,2\,4}$][NTf_2] [$N_{1\,8\,8\,8}$][NTf_2] and [$N_{1\,1\,4\,8}$][NTf_2]), those with shorter-alkyl chains and hydroxylated species produced much larger inhibitions zones. Given the varied nature of the ILs tested, further conclusions on the effect of different cation-anion pairing or alkyl chain

length on the size of produced inhibition zones cannot be reliably drawn. Notably, $[N_{1\,1\,1\text{-}Bn\,2\text{-}O\text{-}2\text{-}O\text{-}Bn}][NTf_2]$ was the only IL of all 62 tested to have no visible effect on *T. minutus* growth.

Table 9 - Effect of Quaternary Ammonium Ionic Liquids on Growth of *T. minutus* on Solid Media. *T. minutus* cells suspended in a top agar were exposed to IL-soaked filter papers for five days, causing zones of growth inhibition. For non-uniform inhibition zones the minimum and maximum distance between their edge and the edge of the filter paper is given. Additionally, In some circumstances distinct zones of different colours were produced. In such instances the maximum and minimum distance of the far edge of each zone from the edge of the filter paper is given alongside the colour of the zone.

	Inhibition Zone 1		Inhibition Zone 2	
Ionic Liquid	Size (mm)	Colour	Size (mm)	Colour
$[N_{1\,1\,4\,8}][Cl^-]$	Whole plate	Clear		
$[N_{1\,1\,2\,2\text{-}OH}][NTf_2]$	Whole plate	Clear		
$[N_{1\,1\,2\,4}][NTf_2]$	Whole plate	Clear		
$[N_{1\,1\,4\,8}][Sac]$	Whole plate	Clear		
$[N_{1\,4\,8\,8}][Lin]$	Whole plate	Clear		
$[N_{1\,8\,8\,8}][Cl^-]$	0-1	Clear with white halo	20	Clear
$[N_{1\,1\,2\,2\text{-}O\text{-}2\text{-}O\text{-}NBn}][NTf_2]$	11-20	Clear		
$[N_{1\,8\,8\,8}][TFA]$	1-2	White	16-18	Clear
$[N_{1\,8\,8\,8}][Sac]$	13-15	Clear		
$[N_{1\,1\,2\,2\text{-}O\text{-}2\text{-}O\text{-}Bn}][NTf_2]$	13-14	Clear		
$[N_{1\,1\,2\,2\text{-}O\text{-}2\text{-}O\text{-}1\text{-}Bn}][NTf_2]$	13-14	Clear		
$[N_{1\,1\,4\,2\text{-}OH}][AOT]$	7-12	Clear		
$[N_{1\,8\,8\,8}][NTf_2]$	7	Clear		
$[N_{1\,2\text{-}OH\,2\text{-}OH\,12}][NTf_2]$	1-2	White	6	Clear
$[N_{1\,1\,4\,8}][NTf_2]$	5	Clear		
$[N_{1\,1\,2\,2\text{-}OH}][AOT]$	2-5	Clear		
$[N_{4\,4\,4\,4}][AOT]$	0.5-1	Clear		
$[N_{1\,1\,1\text{-}Bn\,2\text{-}O\text{-}2\text{-}O\text{-}Bn}][NTf_2]$	0 (as control)	-		

Inhibition zones were generally uniform in shape and size across triplicates for most ionic liquids. However, $[N_{1\,1\,4\,2\text{-}OH}][AOT]$, $[N_{1\,1\,2\,2\text{-}O\text{-}2\text{-}O\text{-}NBn}][NTf_2]$, $[P_{6\,6\,6\,14}][Dec]$, $[P_{6\,6\,6\,14}][AOT]$ and $[P_{1\,4\,4\,4}][NTf_2]$ produced highly irregularly shaped zones, the size of which varied between triplicates (Fig. 29 A-C, Table 8 and Table 9). This could perhaps be caused by a non-uniform top agar surface, as a result of its application at a lower temperature and rapid setting, paired with comparatively fluid ILs. Such asymmetrical inhibition zones make these results difficult to interpret and compare with other ILs, and further highlight the need for more reliable subsequent experiments. $[N_{1\ 8\ 8\ 8}][Cl^-]$, $[N_{1\,8\,8\,8}][TFA]$, $[P_{6\ 6\ 6\ 14}][Br^-]$, $[P_{6\,6\,6\,14}][iC_8PO_4]$, $[P_{6\,6\,6\,14}][Sal]$, $[P_{6\,6\,6\,14}][Dec]$, $[P_{6\ 6\ 6\ 14}][Sac]$, $[P_{8\,8\,8\,14}][Br^-]$, $[P_{6\ 6\ 6\ 14}][Ace]$, $[P_{6\ 6\ 6\ 14}][Cyc]$, $[P_{8\,8\,8\,14}][AOT]$ and $[P_{8\,8\,8\,8}][Cl^-]$ produced zones of inhibition with clearly distinct sections of different colours (*e.g.* Fig. 29, D) and, in such cases, the maximum and minimum distance of

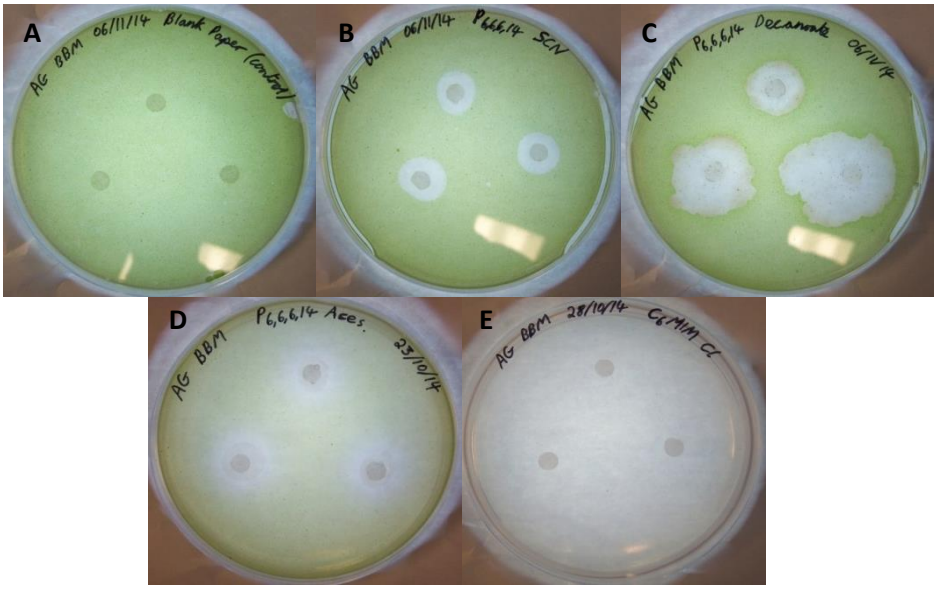

Fig. 29 - Representative Plates from the Agar Diffusion Screen. *T. minutus* cells suspended in a top agar were exposed to IL-soaked filter papers for five days, causing zones of growth inhibition. A – control with no IL on plate, B – example of regular clear inhibition zones caused by [$P_{6\,6\,6\,14}$][SCN], C – example of irregular inhibition zones caused by [$P_{6\,6\,6\,14}$][Dec], D – example of inhibition zones with distinct sections as caused by [$P_{6\,6\,6\,14}$][Ace] E – example of growth inhibition across the entire plate as caused by [C_6MIM][Cl^-].

the far edge of each section from the edge of the filter paper is given in Table 8 and Table 9, alongside the colour of the zone. This production of colour could indicate an interaction between the IL and either the filter paper or the media. The filter papers are made of cellulose, with which various ILs are known to interact (Pinkert *et al.*, 2009).

The usual triplicate dose (10 µl on each of three equidistant filter papers) of [C_2MIM][C_8SO_4] yielded large zones of growth inhibition with a small section of brown algal lawn, noticeably different from the usual green lawns (Fig. 30). A further test was conducted with a single dose of this IL (10 µl on a single, central filter paper), which yielded a green lawn with large brown spots. It is thought that this brown colour could be a result of increased fatty acid production, particularly as this is often linked with carotenoid synthesis. However, this is highly speculative, and further testing would be required with subsequent fatty acid quantification to explore this. This was considered outside the scope of the present study, given the relative toxicity of this IL. Chemically induced lipid production has been reported for other algae, using compounds structurally unrelated to [C_2MIM][C_8SO_4] (Kim *et al.*, 2013). Furthermore, macroalgal species exposed to certain imidazolium ILs have been shown to have increased unsaturated fatty acid content, and decreased saturated fatty acid content (Kumar *et al.*, 2011).

With increased incubation time (a further 5 days at low light intensity) a darker green "halo" was evident around the filter papers soaked in [$P_{8\,8\,8\,14}$][Cl^-], [$P_{6\,6\,6\,14}$][Cyc] and

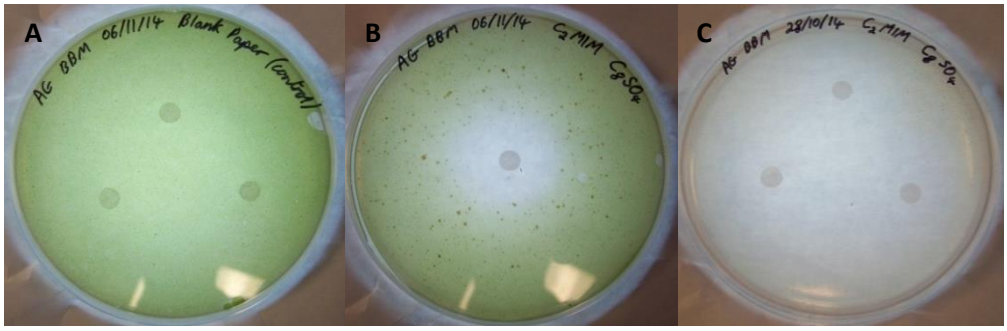

Fig. 30 - Effect of $C_2MIM\ C_8SO_4$ on Growth of *T. minutus* on Solid Media. A - Control, B - single dose of $C_2MIM\ C_8SO_4$ (10 µl on a single central filter paper), C - triple dose of $C_2MIM\ C_8SO_4$ (10 µl on each of three filter papers). With the single dose of $C_2MIM\ C_8SO_4$, brown spots are evident on the agar surface, whilst with a triplicate dose algal growth is much more inhibited, and where it is present the top agar has a brown colour.

$[P_{8\,8\,8\,14}][Br^-]$ (Fig. 31). This may suggest a higher concentration of algae in these regions, which could be a result of the water-immiscible ILs forcing the algae away from the filter paper as they spread outward.

It was apparent that some ILs formed thin films across the agar surface whilst others remained as larger globules, in some cases not even absorbing into the filter paper. This may be partly due to the different interactions of the ILs with the filter paper and/or medium, but also may be largely due to their differences in viscosity. As hypothesised, this would likely have played a significant role in the size of the inhibition zones produced by these ILs, and hence these data may not accurately reflect their toxicity in a liquid environment and should not be used to accurately rank the ILs by toxicity. Nevertheless, the purpose of this experiment was to quickly and cheaply identify highly toxic ILs that would not be carried forward into further testing. To this end, "whole plate" growth inhibition was deemed a suitable toxicity threshold, with any IL which produced smaller inhibition zones being suitable for further testing. This threshold was applied based on the assumption that any IL completely inhibiting growth on solid media would do so in the liquid environment of a

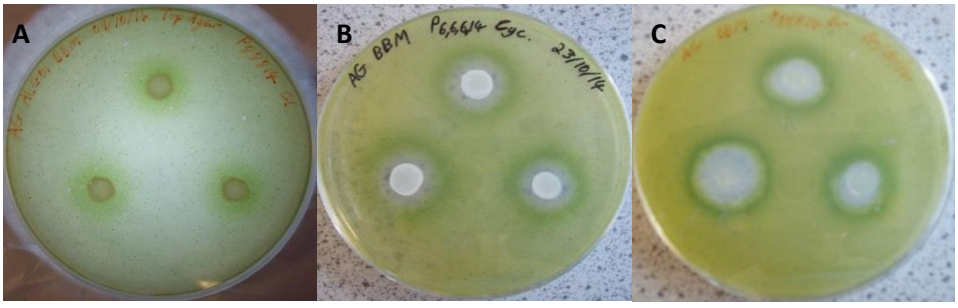

Fig. 31 - Dark Green Zones Were Apparent Around Some Inhibition Zones. A – $[P_{8\,8\,8\,14}][Cl^-]$, B - $[P_{6\ 6\ 6\ 14}][Cyc]$, C - $[P_{8\ 8\ 8\ 14}][Br^-]$. The darker green zones could indicate a higher concentration of algae as a result of the water-immiscible ILs forcing the algae away from the filter paper as they spread.

proposed milking process. It was considered undesirable to lower this threshold, since I was unaware of how the interaction of the ILs with algae on solid media compared to their interaction in liquid media. No imidazolium based ILs passed (of 14 tested), 2 out of 8 pyridinium ILs passed, 13 out of 18 ammonium ILs passed and 18 out of 19 phosphonium ILs passed. In a total of 62 ILs tested, 34 passed to further testing and 28 failed the agar diffusion screen, which represents a significant conservation of time and expense had these ILs been tested in small scale liquid culture experiments immediately.

5.2. Culture Growth in Multi-Well Plates

Various authors have demonstrated that IL toxicity towards microorganisms can be determined by assessing their effect on culture growth, itself typically determined by optical density (OD) measurements (Wood *et al.*, 2011, Cho *et al.*, 2007, Cho *et al.*, 2008). Of particular interest were the studies using multi-well plate readers (Wood *et al.*, 2011), since these required very small volumes of IL (4 µl, 2% *v/v*) and enabled high-throughput automated OD measurements. Based on such work, *T. minutus* cultures (231 ul) were established in Bioscreen 100 well plates containing various ILs (69µl, 23% *v/v*). Given that the Bioscreen is incapable of providing light for the cultures, they were incubated outside of the instrument. Their OD at 750 nm (OD_{750}) was measured every 24 hours, with the aim to determine the extent of growth inhibition (toxicity) of each IL. OD_{750} was specifically chosen as at is routinely used to measure algal growth, including by AlgaeCytes. This wavelength provides a means to measure the light scattering caused by the cells, and avoids absorption from chlorophyll and carotenoids (Chioccioli *et al.*, 2014).

Overall, results were highly variable. Initial OD_{750} readings for cultures containing certain ILs ($[C_4Pyrro][NTf_2]$, $[C_2MIM][NTf_2]$, $[P_{6\,6\,6\,14}][NTf_2]$, $[P_{6\,6\,6\,14}][Br^-]$, $[P_{8\,8\,8\,14}][Br^-]$, $[P_{8\,8\,8\,14}][Cl^-]$ and $[P_{8\,8\,8\,8}][Cl^-]$) were much higher than observed for control cultures and uninoculated BBM growth medium, indicating that the ILs themselves were either absorbing or scattering light. In an attempt to correct for this, a test was conducted in which ILs were spiked into BBM medium lacking algal cells, and into *T. minutus* cultures. The OD_{750} readings from the wells containing no cells were subtracted from OD_{750} data from wells containing algal culture, providing data corrected for IL light scatter. Results were still highly variable (Fig. 32). This could be due to the heterogeneity of certain IL phases; in particular, *bis*triflimide ($[NTf_2]$) anions formed multiple globules with varying size and position over the course of the experiment. Additionally, many ILs containing the [AOT] anion gradually formed a gel-like substance on contact with BBM media.

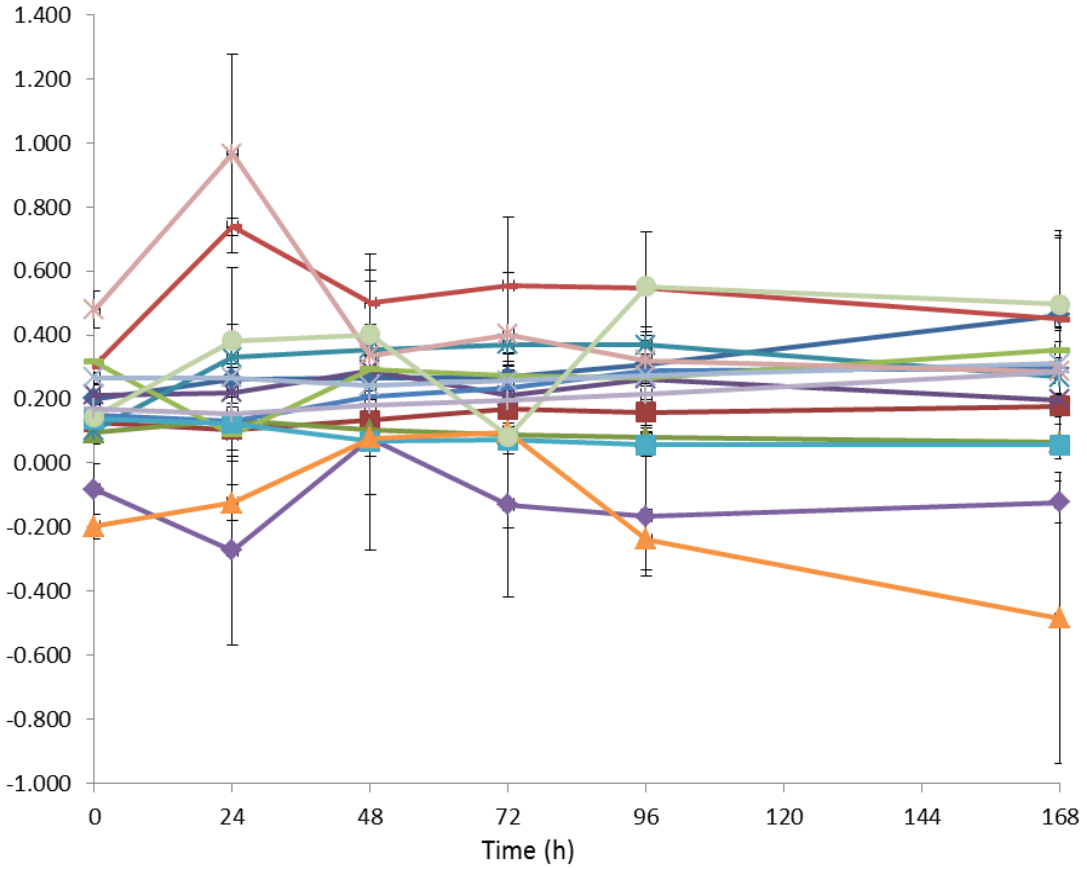

Fig. 32 - Corrected Growth of *T. minutus* in Multi-well Plates in the Presence of Various ILs. OD data was corrected for IL light scatter and absorption via subtracting the corresponding OD readings from ILs present in blank growth media. OD values given are an average of triplicate cultures, with error bars representing standard deviation. ILs were present at 23% *v/v*.
◆ control, ◆ $[N_{1\ 1\ 4\ 2\text{-}OH}][AOT]$, ■ $[C_8Py][AOT]$, ■ $[N_{1\ 2\text{-}OH\ 2\text{-}OH\ 2\text{-}OH}][CSO_4]$, ▲$[P_{4\ 4\ 4\ 6}][Cl^-]$, ▲ $[P_{8\,8\,8\,14}][Br^-]$, ● $[N_{1\ 1\ 2\ 2\text{-}O\text{-}2\text{-}O\text{-}NBn}][NTf_2]$, X $[N_{1\ 1\ 2\ 2\text{-}OH}][AOT]$, X $[P_{6\ 6\ 614}][AOT]$, X $[P_{8\ 8\ 8\ 8}][Cl^-]$, X $[N_{4\,4\,4\,4}][AOT]$, I $[P_{6\,6\,6\,14}][Dec]$, I $[P_{8\,8\,8\,14}][Cl^-]$, – $[P_{6\,6\,6\,14}][Br^-]$, – $[P_{8\,8\,8\,14}][Br^-]$.

Furthermore, the cultures were prone to evaporation during incubation, with subsequent condensation on the plate lids. To avoid this interfering with OD readings, used lids were simply exchanged with a fresh lid before each reading. However, evaporation of the water in a culture will affect the cell concentration, and therefore the OD reading. The extent of evaporation could also have varied between wells, yielding variable results. It also became apparent that algal cultures (including controls) were not homogenous in this system - despite shaking at up to 480 rpm, cells would slowly settle at the bottom of each well. This, together with evaporation, likely explains the variability apparent in the OD_{750} readings of control cultures. It was suspected the algae could be adhering to the plastic wells, but similar results were obtained when using a quartz plate. This suggested that the small, cylindrical wells were unsuitable for growth of this species.

These various issues were not encountered in the previously reported study (Wood *et al.*, 2011). This could be because they used lower concentrations of IL (2% *v/v vs.* 23% *v/v*) which were less likely to interfere with OD measurements. Additionally, they studied non-photosynthetic bacterial species which did not require incubation outside the darkness of the plate reader. Incubation within the plate reader prevents evaporation by providing an environment with a stable temperature. Whilst lower concentrations of IL could be used in the work presented here, the issues with evaporation, condensation and culture heterogeneity would remain. In conclusion, this method was deemed unsuitable for screening IL toxicity towards *T. minutus*, and development of an alternative method was necessary.

5.3. Interaction of Docusate ([AOT]) Ionic Liquids with Growth Medium

During the attempted multi-well plate toxicity screens, it was noted that some of the ILs containing the [AOT] anion formed a thick gel when mixed with the BBM growth medium at 23 % (*v/v*) IL. There was a concern that such ILs would be unsuitable for the proposed milking process, since they would be difficult to separate from the culture and the reduced mass transfer would likely reduce their extraction capability. This prompted the need to examine the miscibility and possible interactions of each [AOT] IL with the growth medium. IL (100 µl, 20% *v/v*) was added to BBM medium (400 µl), briefly vortexed, then left for 48 hours. Each of the pyridinium and pyrrolodinium - [AOT] ILs ([C_6Py][AOT], [C_8Py][AOT], [C_4Pyrro][AOT]) interacted with the medium to form a single-phase solid gel. Similar interactions of the [AOT] anion with liquid media have been reported by other authors (Wood *et al.*, 2011, Hough *et al.*, 2007). A cloudy white emulsion was formed by [$N_{1\,1\,4\,2\text{-}OH}$][AOT], [$N_{1\,1\,2\,2\text{-}OH}$][AOT] and [$P_{8\,8\,8\,14}$][AOT]. Given that these ILs did not separate into a distinct phase, they were deemed unsuitable for the proposed milking process since their separation from the growth medium would be difficult. A similar result occurred with [$N_{4\,4\,4\,4}$][AOT], but to a much lesser extent; a distinct IL phase was apparent, but the surrounding medium had turned a cloudy white. It was decided that further testing with this IL would be attempted. Interestingly, [$P_{6\,6\,6\,14}$][AOT] exhibited the desired behaviour of forming a distinct fluid phase whilst having no visual effect on the surrounding medium. This is despite its structural similarity with [$P_{8\,8\,8\,14}$][AOT], which produced a cloudy white emulsion. Given these results, it was decided that only [$P_{6\,6\,6\,14}$][AOT] and [$N_{4\,4\,4\,4}$][AOT] of the 8 [AOT] ILs that passed the agar screening method would be used in further testing. This left a total of 28 ILs to test in liquid toxicity screens.

5.4. IL Toxicity at 1% (*v/v*) in Liquid Cultures

Instead of well plates, it was proposed that *T. minutus* cultures could be grown in flasks with IL present. Samples for OD_{750} measurement could be removed from the culture *via* pipette

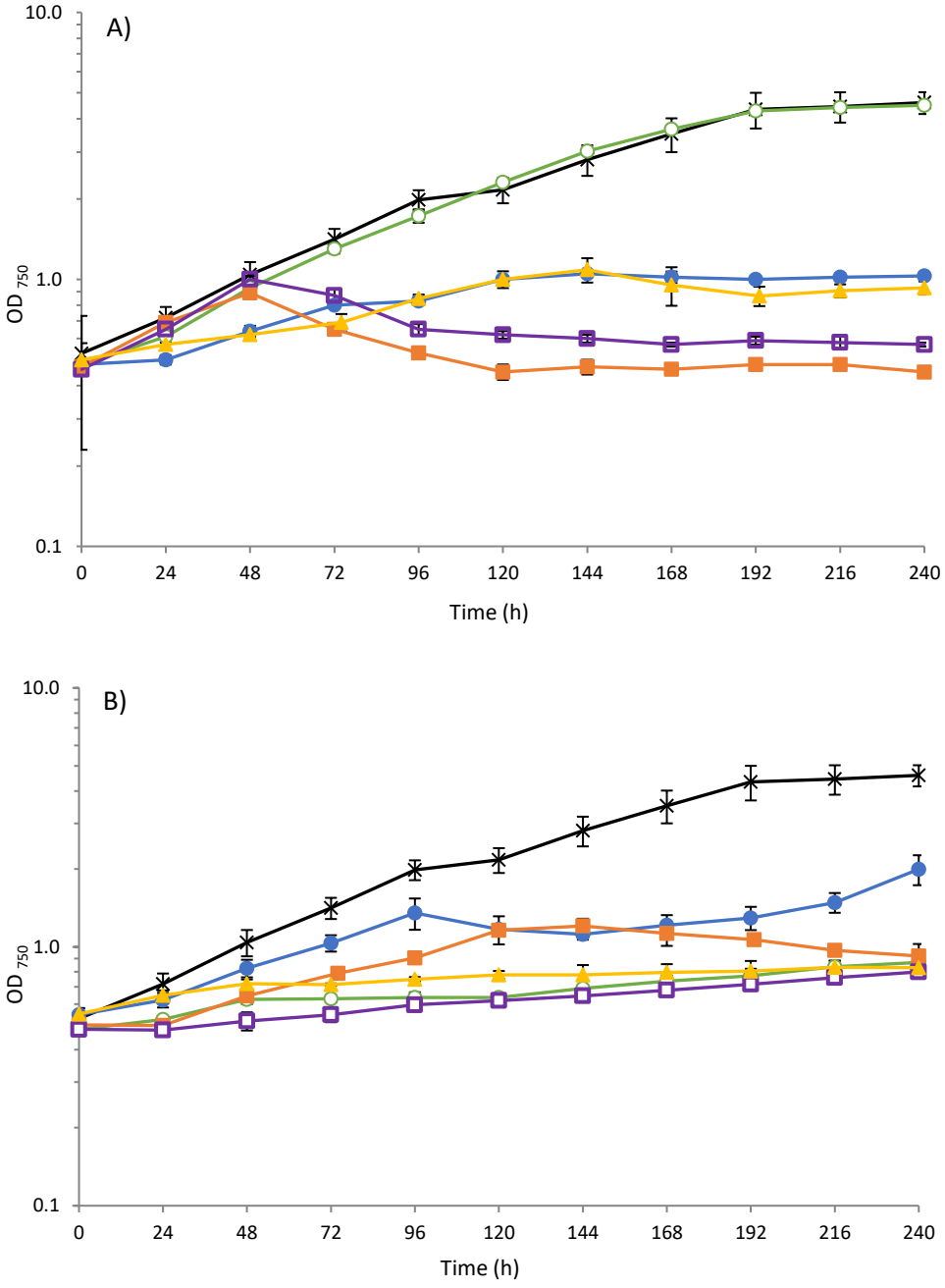

Fig. 33 - Growth of *T. minutus* cultures in the presence of various ILs. ILs were present at 1% *v/v*, with growth measured by optical density readings at 750 nm (OD_{750}). Results are presented as the mean (n = 3), with error bars representing standard deviation.
A) - Quaternary Ammonium ILs. **x** - control, ○ - $[N_{1\,1\,1\text{-Bn}\,2\text{-O-2-O-Bn}}][NTf_2]$, ● - $[N_{1\,1\,2\,2\text{-O-2-O-Bn}}][NTf_2]$, □ - $[N_{1\,1\,4\,8}][NTf_2]$, ■ - $[N_{1\,8\,8\,8}][NTf_2]$, ▲ - $[N_{1\,1\,2\,2\text{-O-2-O-1-Bn}}][NTf_2]$.
B) - Quaternary Phosphonium ILs. **x** - control, ○ - $[P_{6\,6\,6\,14}][iC_8PO_4]$, ● - $[P_{6\,6\,6\,14}][NTf_2]$, □ - Cyphos 104 (90% $[P_{6\,6\,6\,14}]$ $[iC_5PO_2]$, 10% $[P_{6\,6\,6\,14}][Cl^-]$), ■ - $[P_{4\,4\,4\,6}][Cl^-]$, ▲ - $[P_{6\,6\,6\,14}][AOT]$.

whilst avoiding removal of any water-immiscible IL, which could otherwise interfere with OD measurements. Furthermore, unlike the well-plates, the shape of Erlenmeyer flasks allows a homogenous culture to be maintained when grown with constant shaking. Unfortunately, in comparison to the proposed multi-well plate screen, this method requires larger culture and IL volumes, and more labour-intensive OD measurements. However, it provided a means to assess IL toxicity whilst utilising much smaller IL volumes than in the proposed milking process (1% *v/v vs*. 20% *v/v* IL). To minimise IL costs, 9.9 ml cultures were established in 25 ml Erlenmeyer flasks, containing just 100 µl of IL. Including triplicates, this enabled the toxicity of each IL to be tested using only 300 µl total volume of IL.

Table 10 - Maximum OD and specific growth rates (µ) of ILs which permitted *T. minutus* growth. Each IL was present at 1 % (*v/v*), with OD_{750} measurements taken every 24 h. Specific growth rates (µ) are expressed as a percentage of the average specific growth rate of control cultures (0.0116 h^{-1}, *n* = 3). Results are expressed as the arithmetic mean (*n* = 3), ± standard deviation.

Ionic Liquid	Max. OD_{750}	At time (h)	µ (% of control)
$[N_{1\,1\,1\text{-Bn}\,2\text{-O-2-O-Bn}}][NTf_2]$	4.49 ±0.03	240	99.5 ±1.3
$[P_{6\,6\,6\,14}][NTf_2]$	1.99 ±0.26	240	74.3 ±19.6
$[P_{4\,4\,4\,6}][Cl^-]$	1.20 ±0.08	144	55.1 ±2.5
$[N_{1\,1\,2\,2\text{-O-2-O-1-Bn}}][NTf_2]$	1.09 ±0.11	144	45.3 ±4.7
$[N_{1\,1\,2\,2\text{-O-2-O-Bn}}][NTf_2]$	1.05 ±0.03	144	48.5 ±1.3
$[N_{1\,1\,4\,8}][NTf_2]$	1.00 ± 0.03	48	117.6 ±6.5
$[N_{1\,8\,8\,8}][NTf_2]$	0.89 ± 0.01	48	97.2 ± 2.8
$[P_{6\,6\,6\,14}][iC_8PO_4]$	0.87 ± 0.04	240	21.3±2.8
$[P_{6\,6\,6\,14}][AOT]$	0.83 ± 0.02	240	17.1 ±3.8
Cyphos® 104 (90% $[P_{6\,6\,6\,14}][iC_5PO_2]$, 10% $[P_{6\,6\,6\,14}][Cl^-]$)	0.80 ±0.01	240	17.9 ±1.9

Of the 28 ILs which passed the agar toxicity and [AOT] miscibility screens, $[N_{1\,1\,1\text{-Bn}\,2\text{-O-2-O-Bn}}][NTf_2]$, $[N_{1\,1\,2\,2\text{-O-2-O-1-Bn}}][NTf_2]$, $[N_{1\,1\,2\,2\text{-O-2-O-Bn}}][NTf_2]$, $[P_{6\,6\,6\,14}][NTf_2]$, $[P_{6\,6\,6\,14}][iC_8PO_4]$, Cyphos® 104, $[P_{6\,6\,6\,14}][AOT]$, $[P_{4\,4\,4\,6}][Cl^-]$, $[N_{1\,1\,4\,8}][NTf_2]$ and $[N_{1\,8\,8\,8}][NTf_2]$ permitted measurable culture growth at 1% volume (Fig. 33, Table 10). The remaining ILs (Table 11) either inhibited growth completely or caused a measurable decline in OD_{750} readings over time. Many ILs that were deemed to have passed the agar screen proved to be toxic in these liquid screens. This is most likely due to increased cell contact with the IL; given that the ILs tested are immiscible with the growth medium, this more mobile and agitated liquid system generally allows greater contact between the IL and cells than in the solid medium screens. As speculated, this provides evidence that ILs that pass the agar screen can still be toxic in a liquid environment. Note that some ILs enabled growth initially but had an inhibitory effect

later. The maximum OD_{750} and time at which this was achieved is presented for each IL in Table 10. Such ILs may have the potential to be used in a short contact duration (rather than a continuous) milking process.

A cloudy white culture was produced by $[N_{4\,4\,4\,4}][AOT]$, which caused increased OD_{750} readings but, upon microscopic examination, live *T. minutus* cells could no be identified. The only IL which enabled growth akin to that of control cultures was $[N_{1\,1\,1\text{-Bn}\ 2\text{-O-2-O-Bn}}][NTf_2]$. However, this IL was particularly viscous and adhered to the flask, potentially lowering its toxicity through reduced contact with the culture. The structurally similar $[N_{1\,1\,2\ 2\text{-O-2-O-1-Bn}}][NTf_2]$ and $[N_{1\,1\,2\ 2\text{-O-2-O-Bn}}][NTf_2]$ enabled growth at a slower rate and to a lower maximal OD_{750}, achieving a plateau of around 1.1 at 144 h. Interestingly, $[N_{1\,1\,2\ 2\text{-O-2-O-NBn}}][NTf_2]$ completely prevented growth despite its structural similarities.

Table 11 - ILs which passed the agar diffusion screen, but completely inhibited growth at 1% (*v/v*) in liquid *T. minutus* cultures.

Phosphonium ILs	Ammonium ILs
$[P_{1\,4\,4\,4}][NTf_2]$	$[N_{1\,8\,8\,8}][Cl^-]$
$[P_{6\,6\,6\,14}][Sal]$	$[N_{1\,8\,8\,8}][TFA]$
$[P_{6\,6\,6\,14}][Dec]$	$[N_{1\,8\,8\,8}][Sac]$
$[P_{6\,6\,6\,14}][Sac]$	$[N_{1\,1\,2\ 2\text{-O-2-O-NBn}}][NTf_2]$
$[P_{6\,6\,6\,14}$ [Cyc]	$[N_{1\ 2\text{-OH}\ 2\text{-OH}\ 12}][NTf_2]$
$[P_{6\,6\,6\,14}][Ace]$	$[N_{4\,4\,4\,4}][AOT]$
$[P_{6\,6\,6\,14}][SCN]$	
$[P_{6\,6\,6\,14}][Br^-]$	
$[P_{8\,8\,8\,14}][Br^-]$	
$[P_{8\,8\,8\,8}][Cl^-]$	
$[P_{6\,6\,6\,14}][Cl^-]$	
$[P_{8\,8\,8\,14}][Cl^-]$	

The 2 non-toxic, non-cyclic ammonium ILs, $[N_{1\,1\,4\,8}][NTf_2]$ and $[N_{1\,8\,8\,8}][NTf_2]$, grew at comparable rates to controls for the first 48 h, but OD_{750} measurements declined thereafter. Significant cell clumping was noted beyond this time, which could explain the decreasing OD readings. However, it is unclear to what extent this affected the growth of the algae. It is possible that the IL acted in a similar manner as chemical flocculants often used to harvest algal cells. These are typically cationic species that interact with negative cell surface charges in order to cross link cells, causing flocculation. However, such flocculants are usually long polymers such as polyamines and polyacrylamides (Uduman *et al.*, 2010) that typically possess multiple positive charges per molecule, unlike these ILs. Furthermore, this does not explain why these particular ILs caused this effect and others did not. The remaining

ammonium-*bis*triflimide IL, [$N_{1\,2\text{-}OH\,2\text{-}OH\,12}$][$NTf_2$], completely inhibited growth, despite producing comparable inhibition zones in the agar screen. Notably, whilst [N_{1888}][Cl^-], [N_{1888}][TFA], [N_{1888}][Sac] and [N_{1888}][NTf_2] each passed the agar diffusion screen, only [N_{1888}][NTf_2] passed this second round of screening, suggesting comparatively lower toxicity of the [NTf_2] anion.

Of the phosphonium ILs, [P_{66614}][AOT], [P_{66614}][iC_8PO_4] and Cyphos® 104 (comprised of 90% [P_{66614}] [iC_5PO_2 and 10% [P_{66614}][Cl^-]) drastically reduced, but did not inhibit, culture growth (Fig. 33, B). More rapid growth was apparent for cultures containing [P_{66614}][NTf_2] and [P_{4446}][Cl^-], up to approximately 120 h, at which point growth slowed for cultures containing [P_{66614}][NTf_2], and OD_{750} began to slowly decline for cultures exposed to [P_{4446}][Cl^-]. The phosphonium chloride ILs with longer alkyl chains ([P_{8888}][Cl^-], [P_{66614}][Cl^-] and [P_{88814}][Cl^-]) each inhibited growth, suggesting that the toxicity of these ILs may increase with increasing alkyl chain length. Each of these ILs also produced some of the smallest inhibition zones during agar screens, again demonstrating that it is an unsuitable method for identifying non-toxic ILs. Each of the phosphonium-bromide ILs ([P_{66614}][Br^-] and [P_{88814}][Br^-]) completely inhibited growth. The most commonly tested phosphonium cation was [P_{66614}], which when paired with [Sal], [Dec], [Sac], [Cyc], [SCN], [Br^-] and [Cl^-] anions completely inhibited growth. The remaining anion partners ([NTf_2], [iC_8PO_4], [iC_5PO_2] and [AOT]) enabled growth to varying extents.

Given that relatively few ILs enabled growth to any extent, it was desirable for each to be tested in larger scale toxicity screens. However, insufficient volume of [N_{1148}][NTf2], [P_{4446}][Cl^-], [$N_{1\,1\,1\text{-}Bn\,2\text{-}O\text{-}2\text{-}O\text{-}Bn}$][$NTf_2$], [$N_{1\,1\,2\,2\text{-}O\text{-}2\text{-}O\text{-}1\text{-}Bn}$][$NTf_2$] and [$N_{1\,1\,2\,2\text{-}O\text{-}2\text{-}O\text{-}Bn}$][$NTf_2$] were available for future larger scale tests. Unfortunately, they are unavailable commercially, and their synthesis was deemed outside of the scope of this study. As such, they were not included in further testing, leaving a total of 5 IL candidates to be tested in larger scale milking experiments: [N_{1888}][NTf_2], [P_{66614}][iC_8PO_4], [P_{66614}][NTf_2], Cyphos 104 (90% [P_{66614}] [iC_5PO_2], 10% [P_{66614}][Cl^-]) and [P_{66614}][AOT].

5.5. Solvent Toxicity at 20 % (*v/v*)

Having identified ILs non-toxic at 1% (v/v), it was desirable to assess their toxicity at a larger phase ratio more applicable to the desired milking strategy. To achieve this, a photobioreactor (Photon system instrument's Multi-cultivator) was used consisting of 8

growth tubes housed within an LED-backlit, thermostatically controlled, water bath. Air is pumped into each tube and bubbles through the cultures to supply CO_2 and culture mixing.

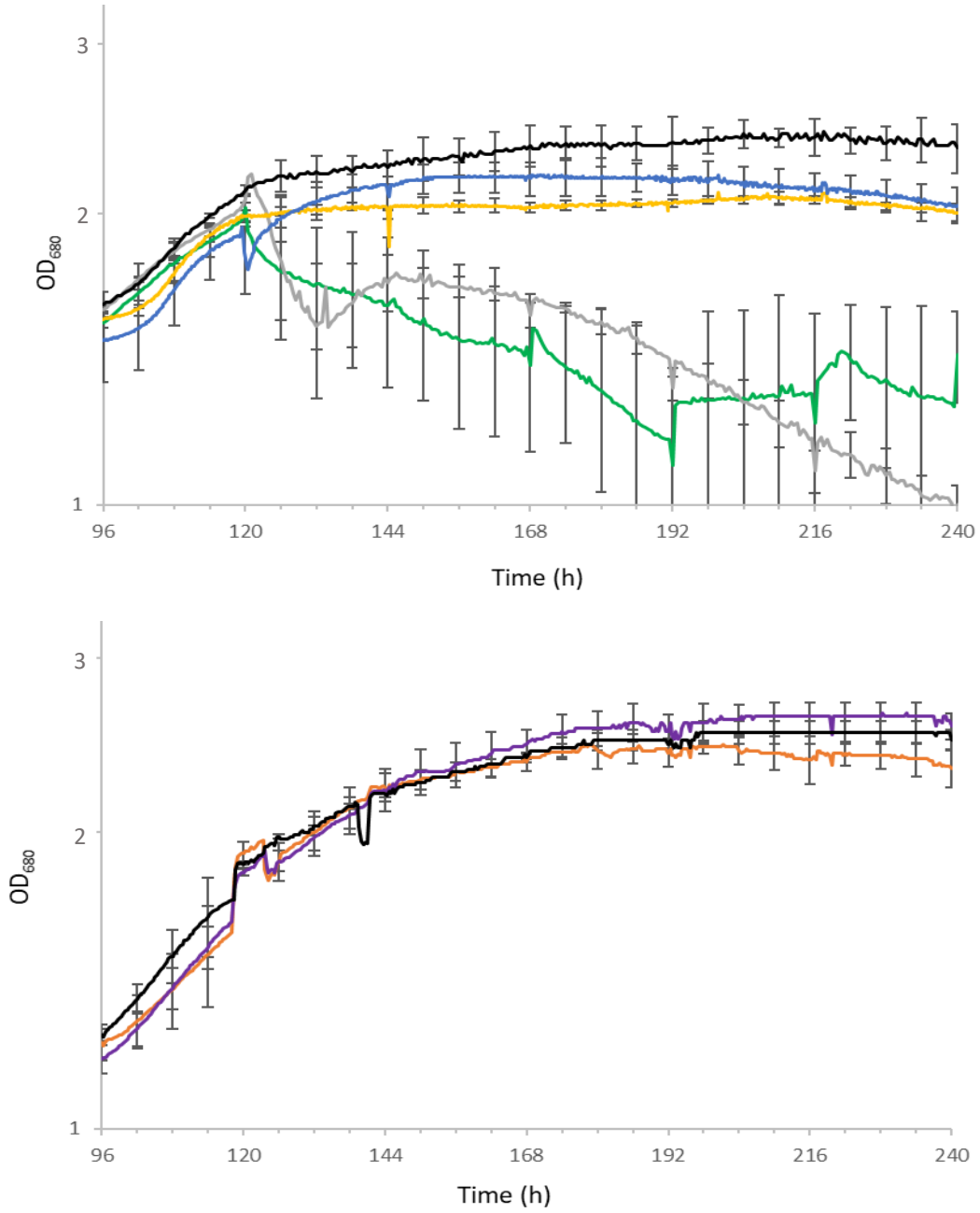

Fig. 34 - The effect of 4 ILs (top) and 2 alkanes (bottom) at 20 % (v/v) on *T. minutus* cultures. Blue - $[P_{6,6,6,14}][iC_8PO_4]$, yellow - $[P_{6,6,6,14}][AOT]$, grey - $[P_{6,6,6,14}][NTf_2]$, green - $[N_{1,8,8,8}][NTf_2]$, purple - tetradecane, orange - dodecane, black - controls. Cultures were grown in a photobioreactor at 25 ^{O}C with a constant light intensity of 200 µmol/m^2/s. After 120 h of growth solvents were added to a final phase ratio of 20% (*v/v*). Controls did not have any solvent added. OD_{680} measurements were taken every 30 mins throughout. Alkane experiments were conducted in a fume cupboard, whilst IL experiments were not. Noticeably more evaporation of cultures occurred in the fume cupboard than outside, making the data sets incomparable and hence are presented as 2 separate graphs. Data points are the mean (*n = 2* for controls, *n = 3* for all others). Error bars represent standard deviation and are only shown every 6 h for clarity. Note that the x axis begins at 96 h of growth to focus on the effect of the solvent addition.

This system is much more akin to what could be used at an industrial scale than the flask-based methods. Unfortunately, this system was unable to measure OD at 750nm, and measurements were instead taken at 680nm. AlgaeCytes have confirmed that OD_{680} measurements correlate linearly with *T. minutus* dry biomass weight and cell number, making it an appropriate means to measure cell growth.

A phase ratio of 20% (v/v) solvent was used here since previous algal milking studies have demonstrated this is effective for extracting target compounds whilst retaining cell viability (Hejazi *et al.*, 2004, Lovejoy *et al.*, 2013). Previous experiments at 1% (v/v) IL had the IL present at the onset of culture growth, based on the assumption that the algae would be more sensitive to the ILs at earlier growth stages, enabling assessment of toxicity using smaller IL volumes. However, EPA is present at the highest quantities as the culture enters stationary growth phase (Přibyl *et al.*, 2012, Cepák *et al.*, 2014). As such this growth stage is most relevant to a milking process and there is no reason for milking to begin prior to this. Hence, solvents were here added at the onset of stationary phase (after 120 h of growth). Two alkanes, dodecane (boiling point 216 °C and density 750 kg/m^3) and tetradecane (boiling point 254 °C and density 764 kg/m^3), were also tested to enable comparison of the effects of the ILs with more conventional solvents. These alkanes were chosen based on previous reports demonstrating their applicability in other algal milking processes (Hejazi *et al.*, 2002, Zhang *et al.*, 2011b)

During preliminary experiments algae were observed to settle at the bottom of each tube. This was addressed by replacing the original air pump (capacity 150 l/h) with a more powerful version (capacity 350 l/h) which provided more extensive culture mixing, preventing algae settling. Alkane experiments were conducted in a fume cupboard, whilst IL experiments were not. Noticeably more evaporation of cultures occurred in the fume cupboard than outside. Hence, the data sets are not directly comparable and are presented as 2 separate graphs (Fig. 34). In most cases the addition of solvent at 120 h caused an initial sharp decrease or increase in OD_{680} readings (Fig. 34). This is likely a result of the IL interfering with OD readings. After the addition of tetradecane or dodecane, cultures generally grew comparably to controls (Fig. 34, bottom). Dodecane arguably caused very minor cell death, as observed by a slight decrease (of 0.08) in OD_{680} over the last 48 h of incubation. On the other hand, tetradecane caused no apparent cell death, suggesting that it is less toxic than dodecane. The relative lack of toxicity of both these alkanes is further demonstrated by the culture appearance being comparable to controls over the course of the experiment (Fig. 35).

Slight culture growth continued for about 30 h after $[P_{6\,6\,6\,14}][iC_8PO_4]$ addition, although a small decrease in OD_{680} readings, indicative of slight cell death, was also observed during the last 48 h of incubation. Therefore, this IL may be best suited for use in a batch, rather than continuous, milking strategy. Average OD_{680} readings remained constant whilst $[P_{6\,6\,6\,14}][AOT]$ was present, suggesting that this IL did not cause any cell death. However, the cultures did appear to be slightly yellower in colour than the controls (Fig. 35). Such analysis is subjective, but could be indicative of an adverse effect on culture health. This could be further explored by visible and/or electron microscopy of cell morphology in future work. From a toxicity standpoint, this IL should be considered viable for continuous milking strategy. Cultures exposed to $[P_{6\,6\,6\,14}][NTf_2]$ showed continued cell death for the duration of IL exposure, and this is confirmed by the culture's loss of colour over time and complete bleaching by 240 h (Fig. 35). Whilst it is currently unknown whether this IL was able to extract

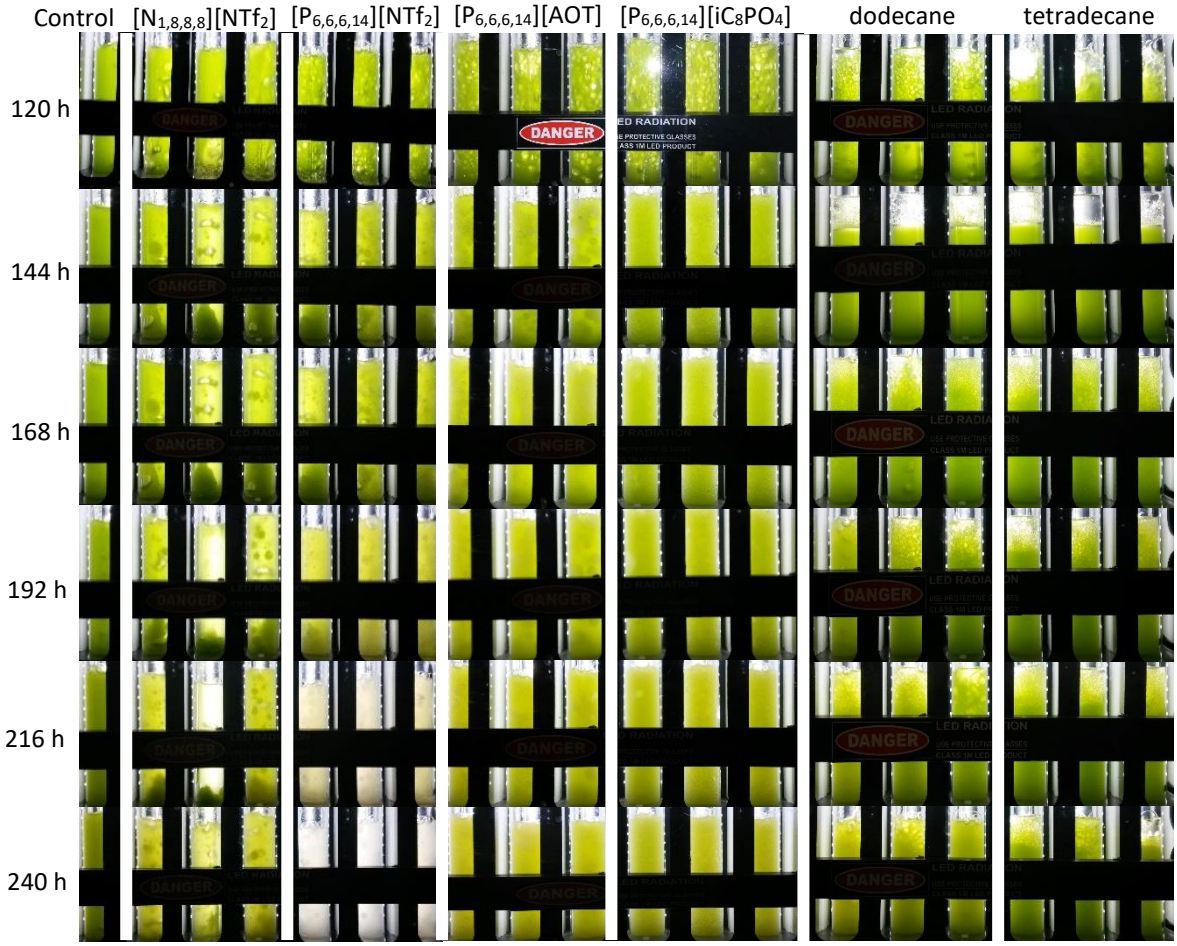

Fig. 35 - Effect of solvents on culture appearance over time. Times shown are from the onset of culture growth, with solvents added at 120 h to 20% (*v/v*). Cultures were grown in a photobioreactor at 25 ^{O}C with a constant light intensity of 200 µmol/m^2/s. Cultures containing $[P_{6,6,6,14}][NTf_2]$ exhibited bleaching over time. $[N_{1,8,8,8}][NTf_2]$ turned dark green, suggesting it was sequestering algal cells from the growth media.

EPA from these cells, its toxicity makes it unsuitable for a milking strategy. The presence of $[N_{1,8,8,8}][NTf_2]$ caused a decrease in OD_{680} over the first 72 h of contact (from 2.03 to 1.20), but caused little change thereafter. This IL turned a deep green colour over the course of the experiment (Fig. 35), suggesting that *T. minutus* cells were being sequestered in the IL phase. This would explain the decrease in OD_{680} of the growth medium, and it levelling off as the IL reaches capacity and can no longer sequester the increasing number of algal cells due to growth. This process is undesirable in a final milking strategy since maintaining maximum algal cell concentration would enable further rounds of efficient milking. For this to be realised with $[N_{1,8,8,8}][NTf_2]$, the cells must first be separated from the IL and returned to the growth medium, adding an undesirable step to the process. The health of the cells within $[N_{1,8,8,8}][NTf_2]$ is unknown, and could be examined in future work.

The extent to which $[N_{1,8,8,8}][NTf_2]$ sequestered cells appeared to be quite variable, as indicated by the differences in culture and IL colour across the replicates (Fig. 35). This explains the comparatively higher standard deviation of OD_{680} readings of cultures containing this IL. This variation could result from different extents of IL mixing within the culture. Mixing *via* bubbling air is inherently variable, and large globules of $[N_{1,8,8,8}][NTf_2]$ were observed moving around in some tubes whilst in others it largely remained at the bottom. Furthermore, the photobioreactor used here provides no means to accurately supply the same air flow rate to each tube and was subjectively assessed by eye when establishing each experiment. In conclusion, tetradecane, dodecane, $[P_{6\,6\,6\,14}][AOT]$ and $[P_{6\,6\,6\,14}][iC_8PO_4]$ showed the most promise for a milking process due to their lower toxicity. On the other hand, $[P_{6\,6\,6\,14}][NTf_2]$ caused extensive cell death and is not viable for use in a milking process. $[N_{1,8,8,8}][NTf_2]$ could be explored further, but is unlikely to be worth pursuing because it is thought to remove whole algal cells from the growth medium.

6. Results - Analysis of Eicosapentaenoic acid in Ionic Liquids

6.1. Identifying the Major Fatty Acids Present in *T. minutus*

For the development of EPA quantification methods, it was first desirable to confirm the range of fatty acids naturally present in *T. minutus*. Gas chromatography - mass spectrometry (GCMS) provides a means to do this but requires that the analytes are volatile. Thus, fatty acids extracted from lyophilised algae (using chloroform/methanol) were derivatised to fatty acid methyl esters (FAMEs). This process involves the addition of acidified methanol, followed by incubation at > 65 ^{O}C for 1 h (Laurens *et al.*, 2012). FAMEs were analysed by GCMS and identified by a >90% match with NIST 2008 FAME library spectra. The FAMEs identified (Fig. 36) were methyl dodecanoate (Me12:0), methyl tetradecanoate (Me14:0), methyl palmitate (Me16:0), methyl palmitoleate (Me16:1 ω6), methyl linoleate (Me18:2 ω6), methyl oleate (Me18:1 ω9), methyl stearate (Me18:0), methyl arachidonate (Me20:4 ω6), methyl eicosapentaenoate (Me20:5 ω3) and methyl behenate (Me22:0). DHA (22:6 ω3) was notably absent, providing an opportunity to use it as an internal standard in quantification methods. In general, most peaks were well resolved, including methyl eicosapentaenoate. Each of the fatty acids previously reported to be present in *T. minutus* (Cepák *et al.*, 2014) was identified here, with the exception of α-linolenic acid (18:3 ω3).

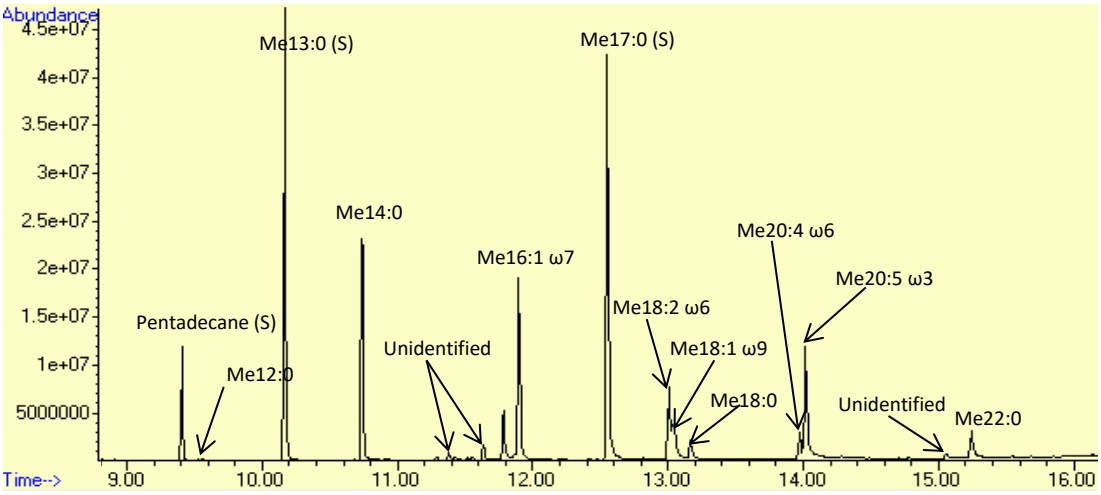

Fig. 36 - GC Chromatogram of a *T. minutus* Lipid Extract. Chloroform/methanol (2:1 *v/v*, 0.2 ml) was used to extract fatty acids from lyophilised algae biomass (10 mg). FAMES were produced by the addition of 0.6 M HCl in methanol, with 1 h incubation at 65 ^{O}C. These were analysed by GCMS equipped with an Agilent HP-5 column. Peaks were identified by a >90% match with NIST 2008 library FAME spectra. (S) denotes an artificial standard added during sample preparation. The FAMEs identified were methyl dodecanoate (Me12:0), methyl tetradecanoate (Me14:0), methyl palmitate (Me16:0), methyl palmitoleate (Me16:1 ω7), methyl linoleate (Me18:2 ω6), methyl oleate (Me18:1 ω9), methyl stearate (Me18:0), methyl arachidonate (Me20:4 ω6), methyl eicosapentaenoate (Me20:5 ω3) and methyl behenate (Me22:0).

GCMS can be used to quantify FAMEs by total ion count (TIC) or selective ion monitoring (SIM) (Tammekivi *et al.*, 2019, Dodds *et al.*, 2005, Quehenberger *et al.*, 2011). Reliable quantification requires comparison of the analyte mass spectrum with that of a radiolabelled internal standard with otherwise equivalent structure (*e.g.* deuterated EPAME). Careful consideration should be given to the ionisation method. Hard ionisation methods like electron ionisation readily fragment fatty acids at the expense of sensitivity, and *vice versa* for soft ionisation methods like electrospray ionisation (Quehenberger *et al.*, 2011). However, Flame ionisation detection (FID) is a more commonly used approach to quantify FAMEs (James and Martin, 1956, American Oil Chemist's Society, 2017) because FID has comparable sensitivity and a greater range of linearity (Dodds *et al.*, 2005) with arguably easier operation, making it a favourable method to use here.

6.2. Gas Chromatography – Flame Ionisation Detection (GC-FID)

In order to assess if ILs are capable of extracting EPA from *T. minutus* cultures, it was necessary to develop methods for quantifying fatty acid esters in ILs. However, ILs are non-volatile, which presents a problem for their analysis by GC. GC separates vapourised analytes based on their interaction with a stationary phase of an analytical column. They are carried through the column by the flow of a carrier gas, typically helium. When using a split/splitless injection port (Fig. 37), the sample is injected into a glass inlet liner which is heated to vaporise the sample (Harvey, 2011). The flow of carrier gas then introduces the sample into the column, as opposed to its direct injection. It is important that the sample has fully vaporised, since any liquid could block the column and can cause irreversible damage. This poses a problem for the analysis of non-volatile ILs. Therefore, the ILs need to be trapped before entering the column so that only the volatile FAMEs travel through the GC column. Inlet liners often contain quartz wool to help prevent non-volatiles from entering the column. Furthermore, guard columns composed of fused silica can be attached to the front of the analytical column. In this way if non-volatiles are injected, their interaction with the analytical column can be prevented. Hence, it should be possible to analyse volatile compounds dissolved in non-volatile ILs by GC whilst minimising the risk of analytical column damage. GC analysis of ILs has been reported previously (Mokhtar *et al.*, 2015, Zhang and Lee, 2010, Aguilera-Herrador *et al.*, 2008). One study utilised programmable temperature variation (PTV) injection to assist in IL retention within the liner, and suggested regular cleaning of the inlet liner should be conducted to remove non-volatiles (Mokhtar *et al.*,

2015). Another developed a novel, removable and easily cleaned cotton-packed “pre-liner” for the retention of IL, prior to introduction of volatiles into the inlet liner (Aguilera-Herrador *et al.*, 2008). Another retained IL on the tip of the injection needle within the injection port, where analytes were volatilised (Zhang and Lee, 2010). It was concluded that GC-FID analysis of fatty acid esters in ILs should be pursued.

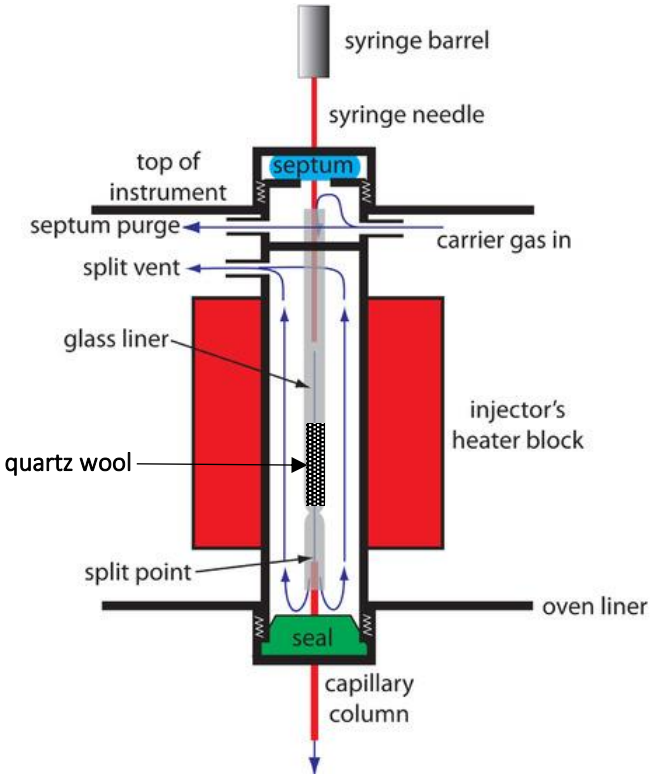

Fig. 37 - Schematic of a Split/splitless Injection Port Used With GC. Sample is loaded into a syringe needle which pierces the rubber septum. The injection port is heated to enable vaporisation of the injected sample which is then carried onto the column by the flow of the carrier gas. This gas flow can also be split to reduce the quantity of the sample loaded onto the column. Glass liners often contain quartz wool onto which the sample is injected. This increases the surface area for efficient vaporisation and helps prevent the introduction of non-volatiles. Adapted from Harvey, 2011.

An experiment was conducted with the aim of producing FAME calibration curves in $[P_{6,6,6,14}][NTf_2]$ to enable their subsequent quantification. $[P_{6,6,6,14}][NTf_2]$ was diluted 1:1 with chloroform to reduce viscosity, to which a mix of FAMEs was added at varying concentrations. These were introduced by splitless injection onto GC-FID, with a guard column in place to prevent analytical column damage. After 3 - 10 injections, the peaks in the resulting chromatograms widened significantly (Fig. 38). This is indicative of blockage of the guard column or analytical column, suspected to be caused by the IL. Peak widening could drastically reduce peak resolution and the accuracy of quantification. Indeed, removal of a few inches from the front of the guard column restored effective chromatography, presumably by removing this blockage. Furthermore, liquid could be seen in the connector

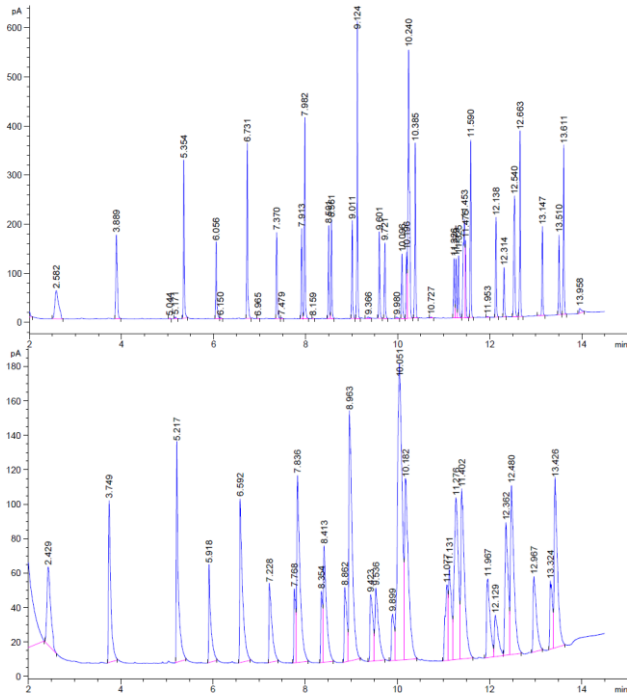

Fig. 38 - Peak Widening of FAMEs Observed After Several Injections of $[P_{6,6,6,14}][NTf_2]$ for GCFID Analysis. A mix of FAMEs including EPAME was prepared at varying concentrations in 1:1 $[P_{6,6,6,14}][NTf_2]$:chloroform to reduce viscosity. Samples were analysed by GC-FID using an HP-5 column (30 m x 320 µm x 0.25 µm) and a 10 m deactivated fused silica guard column. Initially, ideal peak separation was achieved (top), but after 3-10 injections significant peak broadening was evident (bottom). This is indicative of column blockage. Note the different y axis scales.

between the guard and analytical columns after a series of injections (Fig. 39). The frequency with which column blockage occurred could likely be reduced by regular cleaning or replacement of the inlet liner. However, this was deemed an unacceptable approach due to increased maintenance and decreased automation, when potentially working with hundreds of samples. A simple approach to avoid this would be to use a traditional volatile solvent (*e.g.* hexane) to back-extract EPA from the IL and inject the volatile extractant rather than the IL. However, this would require further method development, including determination of extraction efficiency of the fatty acid from the IL phase, potentially leading to further inaccuracies. It may also be necessary to screen other extraction solvents if a large

Fig. 39 - Liquid Visible in the Connector Removed from Between the Guard and Analytical Columns. This was presumed to be IL that was carried through the guard column by the carrier gas and deposited in the wider connector where the gas could more readily flow around it.

percentage of the EPA remains within the IL phase. Therefore, GC-FID for quantification of EPA in ILs was abandoned, and an alternative method needed to be devised. Whilst HPLC-UV is generally used infrequently for fatty acid quantification, it has been used with direct IL injection (Ge and Lee, 2013, Flieger and Czajkowska-Żelazko, 2012, Stepnowski *et al.*, 2003), making it a potential alternative.

6.3. UV-Visible spectroscopy

UV absorbance between 190 - 400 nm is often used for analyte detection after HPLC and has been used to quantify underivatized fatty acids (at 208 nm) (Guarrasi *et al.*, 2010) and esterified fatty acids (at 205 nm) (Gimenes de Souza *et al.*, 2018). The UV absorbance of underivatized fatty acids is typically lower than that of esterified fatty acids. Fatty acids largely exist as a wide variety of triglycerides within cells, so a hydrolysis step would be necessary prior to quantification of underivatized fatty acids. A personal communication with AlgaeCytes revealed that EPA ethyl ester (EPAEE) was their final commercial product, making its quantification preferable. The EPAEE derivative was used instead of EPAME in future methods. Previous work identified $[P_{6,6,6,14}][iC_8PO_4]$, $[N_{1,8,8,8}][NTf_2]$, $[P_{6,6,6,14}][NTf_2]$ and $[P_{6,6,6,14}][AOT]$ as ILs of interest for use in milking experiments. The UV absorbance spectra of EPAEE, $[P_{6,6,6,14}][iC_8PO_4]$, $[N_{1,8,8,8}][NTf_2]$ and $[P_{6,6,6,14}][NTf_2]$ were determined, to identify a suitable non-overlapping wavelength for HPLC-UV quantification. Maximum absorbance was at 190 nm for $[P_{6,6,6,14}][iC_8PO_4]$ and 191 nm for $[N_{1,8,8,8}][NTf_2]$ and $[P_{6,6,6,14}][NTf_2]$. Maximum absorption for EPAEE was at 197 nm (Fig. 40) and the molar extinction coefficient of EPAEE

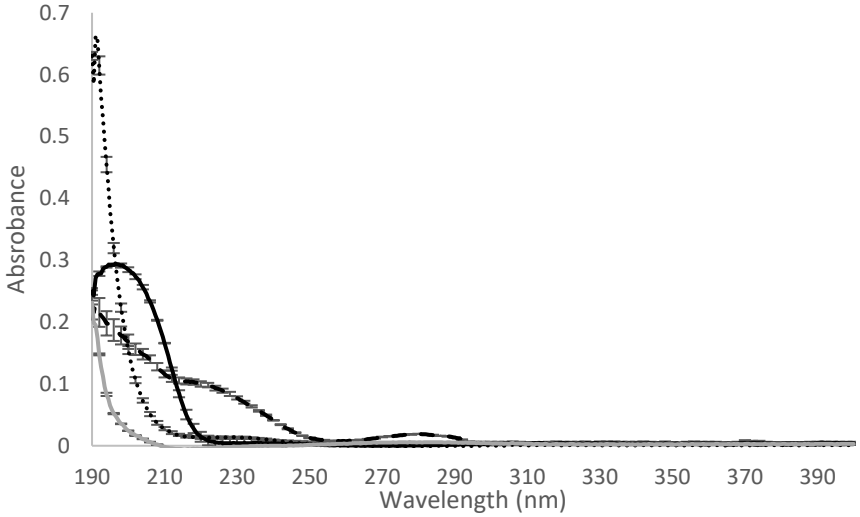

Fig. 40 - UV Spectra of EPAEE and the 4 ILs of Interest. Each analyte was dissolved in acetonitrile to varying concentrations. EPAEE (solid black, 7.6µM), $[P_{6,6,6,14}][NTf_2]$ (dotted black, 10mM), $[N_{1,8,8,8}][NTf_2]$ (Dashed black, 5mM), $[P_{6,6,6,14}][iC_8PO_4]$ (solid grey, 0.24mM). Results are the mean (n = 3), with error bars representing standard deviation.

was far greater (>200-fold) than the ILs at this wavelength (Table 12). This demonstrates that these ILs are unlikely to interfere with EPAEE quantification at 197 nm, making it a suitable detection wavelength during HPLC-UV.

Table 12 - The molar extinction coefficients at 197nm of EPAEE and the 4 ILs of interest. Values are the mean (*n* = 3), ± standard deviation.

	ε_{197nm} (L mol^{-1} cm^{-1})
EPAEE	38818 ±501
$[P_{6,6,6,14}][iC_8PO_4]$	185 ±4.4
$[N_{1,8,8,8}][NTf_2]$	37 ±3.3
$[P_{6,6,6,14}][NTf_2]$	28 ±0.7

6.4. HPLC-UV

Initial experiments were conducted to explore the effect of ILs on EPAEE quantification. Each IL was diluted 1:1 with acetonitrile to reduce viscosity and was analysed at 197 nm, with and without EPAEE present at 0.1 mg/ml. $[N_{1,8,8,8}][NTf_2]$ produced a small background peak that eluted just before EPAEE (5.74 *vs.* 5.98 mins, Fig. 41). The area of this peak did not overlap with that of EPAEE, so does not affect EPAEE quantification. Each of the ILs produced a number of minor peaks believed to be caused by contaminants. Both $[P_{6,6,6,14}][NTf_2]$ and $[P_{6,6,6,14}][iC_8PO_4]$ produced minor background peaks which did overlap with EPAEE (Fig. 41). Since the area of these peaks was much smaller than the EPAEE peak (8.8 in $[P_{6,6,6,14}][NTf_2]$ and 71.8 in $[P_{6,6,6,14}][iC_8PO_4]$ *vs.* approximately 7,500 for EPAEE) it was concluded that their area could be subtracted from the EPAEE peak during quantification.

Subsequent experiments were conducted to produce EPAEE calibration curves for use in quantification. EPAEE at concentrations ranging from 0.5 µg/ml to 100 µg/ml, was dissolved in acetonitrile and 1:1 IL:acetonitrile. These were analysed by the same HPLC-UV method, with previously suggested background peak area subtractions where necessary. Good linearity was achieved in each solvent (Fig. 42), demonstrating the applicability of this method to quantify EPAEE present in each of these ILs. The limit of quantification (LoQ) of EPAEE in each solvent was estimated using the equation:

$$LoQ = \frac{10S}{m}$$

Where S is the standard deviation of the y-intercepts and m is the slope of the calibration curve (Table 13). This is a commonly used method to estimate LoQ (Sanagi *et al.*, 2009, Chandran and Singh, 2007). $[P_{6,6,6,14}][iC_8PO_4]$ produced the highest LoQ of 3.84 µg/ml. This is

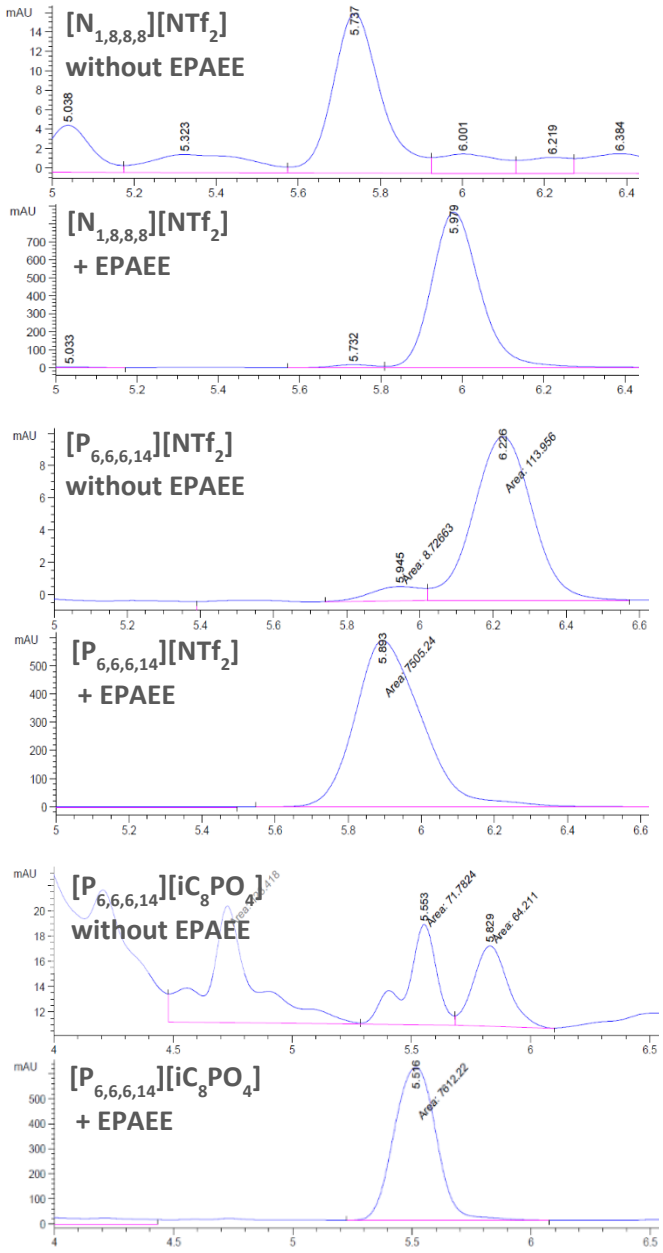

Fig. 41 - Chromatograms of $[N_{1,8,8,8}][NTf_2]$, $[P_{6,6,6,14}][NTf_2]$ and $[P_{6,6,6,14}][iC_8PO_4]$ With and Without EPAEE (0.1 mg/ml). ILs were diluted 1:1 with acetonitrile. HPLC-UV analysis was conducted with an Extend C-18 column and guard column, with an isocratic mobile phase of acetonitrile (95%), water (5%), and formic acid (0.1%). Background IL peaks overlapping with EPAEE were minimal, and were presumed to be contaminants in the ILs. Where present, it was concluded that their area could be subtracted from that of EPAEE during quantification protocols. Note the different axis scales.

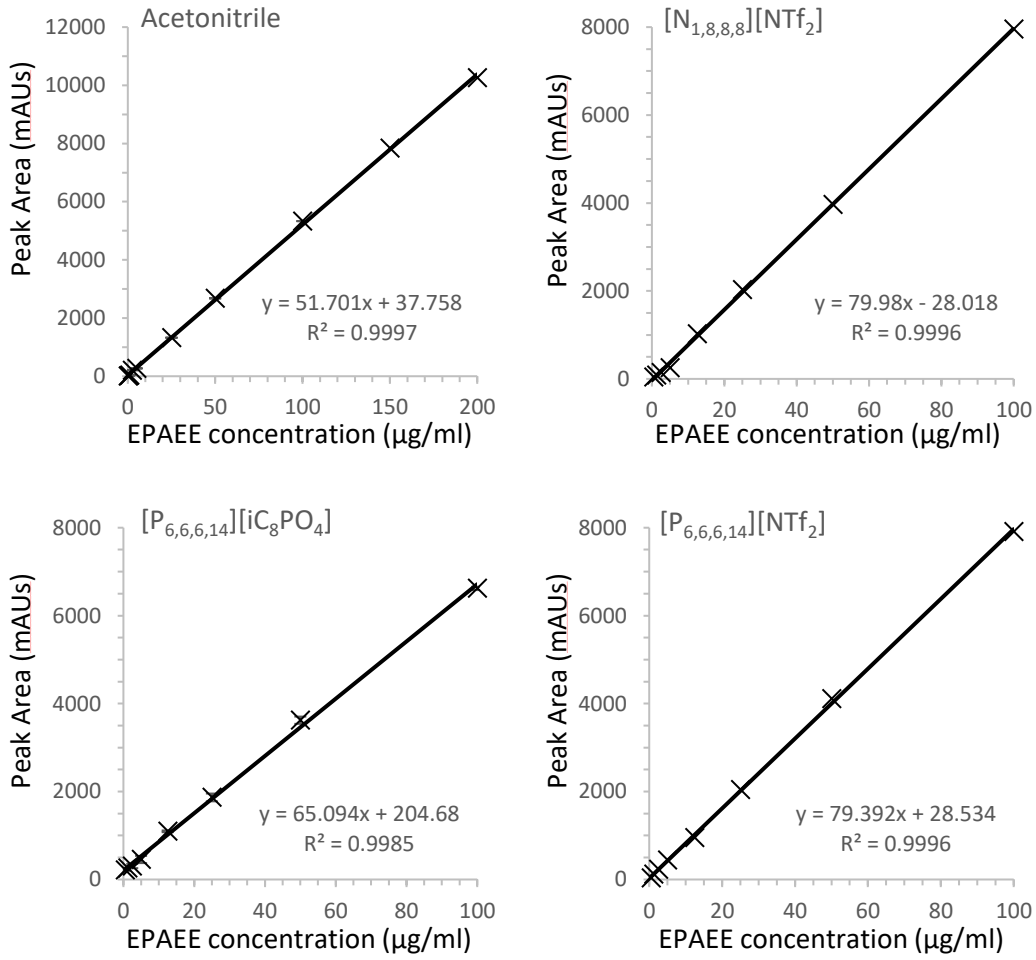

Fig. 42 - Calibration curves of EPAEE in acetonitrile, $[N_{1,8,8,8}][NTf_2]$, $[P_{6,6,6,14}][iC_8PO_4]$ and $[P_{6,6,6,14}][NTf_2]$. ILs were diluted 1:1 with acetonitrile. Analysis was conducted with an Agilent 1200 fitted with an Extend C-18 column (150 x 4.6 mm, 3.5 µm) and guard column at 30 °C, using an isocratic mobile phase of acetonitrile (95%), water (5%), and formic acid (0.1%) at a flow rate of 1 ml/min, injection volume of 10 µl and UV detection at 197nm. Note the different axis scales for acetonitrile. Data points are the mean of triplicate injections of the same sample. Error bars represent standard deviation, but in most cases are not visible.

unsurprising given this IL was shown to produce the greatest interference with EPAEE (Fig. 41). The LoQ in $[N_{1,8,8,8}][NTf_2]$ and $[P_{6,6,6,14}][NTf_2]$ was lower than in acetonitrile. Interestingly, the average EPAEE peak area at any given concentration was higher in every IL than acetonitrile (Fig. 42).

Table 13 - Summary of EPAEE Retention Time (RT) and Linearity (R^2) Achieved in Each Solvent.

Solvent	EPAEE RT (mins)	R^2	LoQ (µg/ml)
Acetonitrile	6.15	0.9997	3.13
$[P_{6,6,6,14}][iC_8PO_4]$	5.52	0.9985	3.84
$[N_{1,8,8,8}][NTf_2]$	5.98	0.9996	1.77
$[P_{6,6,6,14}][NTf_2]$	5.89	0.9996	1.91

In conclusion, this method provides accurate and reliable quantification of EPAEE in $[N_{1,8,8,8}][NTf_2]$, $[P_{6,6,6,14}][NTf_2]$ and $[P_{6,6,6,14}][iC_8PO_4]$. This enables future biphasic milking experiments using these ILs as EPA extractants. Future work requires the analysis of EPAEE calibrations in $[P_{6,6,6,14}][AOT]$, the remaining IL of interest identified in this study.

7. Results - Towards Milking *T. minutus* Using Pulsed Electric Fields

Preliminary experiments to explore the use of PEF as an EPA milking strategy were conducted utilising a commercially available electroporator (BioRad Gene Pulser Xcell). The aim was to determine whether or not PEF could permeabilise *T. minutus* cells, the duration of any permeabilization, the effect of permeabilization on cell viability and to explore the use of PEF treatments to enable or enhance EPA extraction without solvents.

7.1. Developing Methods to Determine the Extent of Cell Permeabilisation

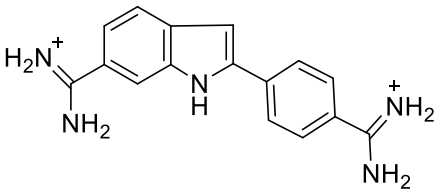

Fig. 43 - The Structure of SYTOX Green (SG). Note the positive charges. It is suspected that the application of an electric field may electrophoretically facilitate the entry of SG into cells.

The objective of these preliminary experiments was to rapidly obtain data on the extent of permeabilization of *T. minutus* cultures exposed to varying PEF treatments. A wide variety of fluorescent dyes are available for use in determining cell permeabilization (Sträuber and Müller, 2010). These dyes are membrane impermeable and exhibit greatly enhanced fluorescence upon binding with an intracellular component. The dye can only enter permeabilised cells, thus enabling measurement of cell permeabilization by fluorescence.

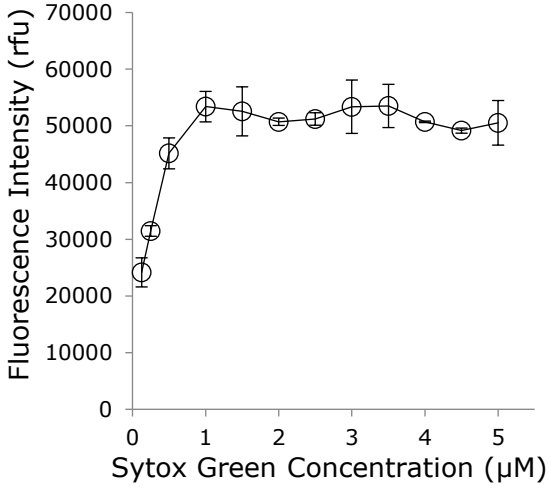

Fig. 44 - Effect of SYTOX Green Concentration on Fluorescence Intensity. Cells ($5x10^6$/ml) were heat shocked at 90 °C for 1 h. SYTOX Green was added to varying final concentrations and incubated for 1 h. The fluorescence intensity of samples was measured using a FLUOstar®® plate reader. Data points are the mean of replicates (n=3). Error bars represent standard deviation.

SYTOX Green (SG, Fig. 43) fluorescence increases 500-fold upon binding to nucleic acids (Roth *et al.*, 1997) and was chosen as a suitable dye in this study since it was readily available and it emits at 523 nm, which avoids chlorophyll *a* fluorescence emission (680-735 nm). It can be excited by frequently used Argon lasers (488 nm), and has been used successfully by other authors in microalgae viability assays (Veldhuis *et al.*, 1997, Sato *et al.*, 2004).

Preliminary experiments were conducted with the aim to determine an effective SG staining procedure. Heat shock has been used to lyse many cell types (Shehadul Islam *et al.*, 2017), and it was assumed this would also apply to *T. minutus*. Cell suspensions were heat shocked at 90 ^{O}C for 1 h and allowed to cool to room temperature. SG was then added and the cells were incubated at room temperature in the dark without shaking, varying either SG concentration, incubation time, or heat shocked cell concentration, whilst keeping the remaining variables constant (1.5 µM SYTOX Green, 1 h incubation time or 5 x 10^6 cells/ml). Fluorescence of whole cultures was measured using a FLUOstar® plate reader. When varying SG concentration from 0.125 µM to 1 µM, the fluorescence intensity of samples rapidly increased but there was little further increase at higher SG concentrations (Fig. 44). At the highest SG concentration (5 µM), the fluorescence intensity of the heat shocked cells was approximately 3.5-fold higher than a 5µM SG stained, control cell suspension which had not been heat treated (50500 rfu *vs.* 14500 rfu respectively). There was little increase in fluorescence when the SG concentration was increased beyond 1µM. Based on these data, it was concluded that a final SG concentration of 1.5 µM per 5x10^6 cells was adequate. With increasing incubation time, the fluorescence intensity of samples generally increased (Fig.

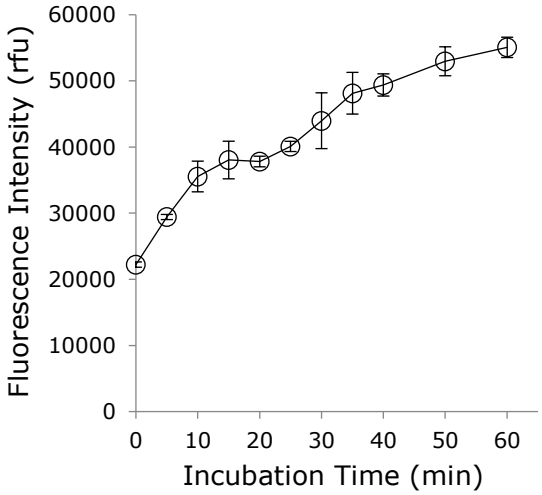

Fig. 45– Effect of Incubation Time on SYTOX Green Fluorescence Intensity. Cells (5x10^6/ml) were heat shocked at 90 ^{o}C for 1 h. SYTOX Green (1.5 µM) was added for varying durations, after which the fluorescence intensity of samples was measured using a FLUOstar® plate reader. Data points are the mean of replicates (n=3). Error bars represent standard deviation.

45). This was most notable at the shortest incubation times. A short plateau was evident between 15 and 25 min, after which fluorescence intensity increased more slowly than previously. There was little increase in mean fluorescence intensity between 50 - 60 min incubation times (52,967 rfu and 55,071 rfu, respectively). After 60 minutes of incubation, the fluorescence of heat shocked cells was approximately 3.5-fold higher than live stained control cell suspensions (55,000 rfu *vs.* 15,500 rfu, respectively). Longer staining durations were not explored since an adequate level of fluorescence was achieved after 60 mins. Furthermore, longer incubations in the dark could lead to cell death and hence false positives, particularly if the cells are in a fragile permeabilised state. As a result, an incubation time of 60 minutes was chosen for future experiments.

A linear relationship between fluorescence intensity and heat shocked cell concentration was observed (Fig. 46). Again, at a specific cell concentration ($5x10^6$ cells/ml), the heat shocked cells produced a mean fluorescence intensity approximately 3-fold higher than live stained control cell suspensions (51,000 rfu *vs.* 15,700 rfu, repectively).

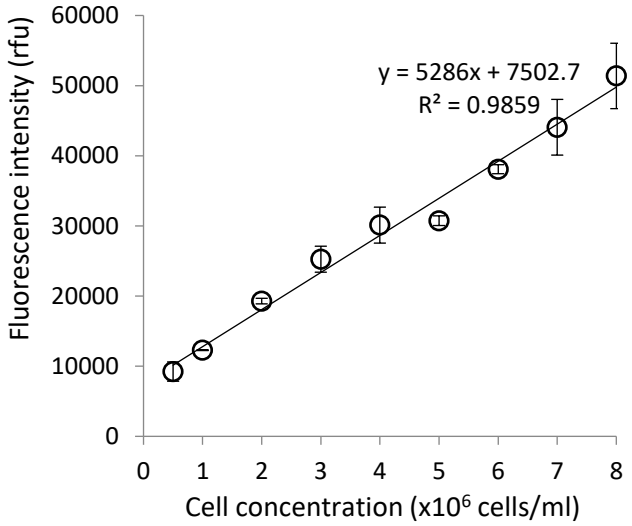

Fig. 46 - Relationship Between Fluorescence Intensity and the Concentration of Lysed Cells. Cells were heat shocked at 90°C for 1 h, after which they were incubated at varying final concentrations for 1 h with 1.5 µM SYTOX Green. The fluorescence intensity of samples was measured. Data points are the mean of replicates (n=3). Error bars represent standard deviation.

7.2. Culture Permeabilization from Varying PEF Treatments

In order to use PEF treatments to extract fatty acids, it is first necessary to understand how the extent of algae cell permeabilization changes when varying PEF conditions are used. Therefore, multiple cell suspensions containing SG were exposed to different electrical

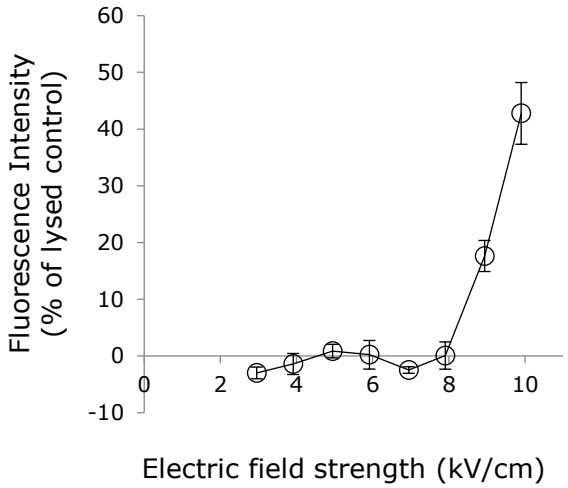

Fig. 47 - Effect of Electric Field Strength on Extent of Cell Permeabilisation. Cultures (5 x 10^6 *T. minutus* cells/ml, 300 µl) containing SYTOX Green (1.5µM) were exposed to a single 5 ms square wave pulse of varying voltage. The electrode gap distance was 2 mm. Culture fluorescence was measured 1 h after pulse delivery using a FLUOstar® plate reader. Results are presented as the mean (n = 3), with error bars representing standard deviation.

pulses varying in either their voltage, duration, or number, followed by fluorimetry to determine their extent of permeabilization as compared to a heat shocked control.

When exposed to pulses of varying voltage, no significant fluorescence was detected from cultures exposed to field strengths of 3 kV/cm to 8 kV/cm (Fig. 47). Above 8 kV/cm, there was a sharp increase in fluorescence intensity. This suggests that the permeabilization threshold for *T. minutus* is between 8 - 9 kV/cm. The highest electric field strength, 10 kV/cm, yielded fluorescence intensities equal to 43% of the mean fluorescence of heat shocked cell controls. When cultures were exposed to a field strength greater than 10 kV/cm, arcing was observed. It is unlikely that arcing at this relatively high field strength is relevant in a final milking process, since lower field strengths have been shown here to allow permeabilization of *T. minutus*. However, knowledge of this arcing threshold is useful, particularly if irreversible permeabilization were pursued as a pre-treatment to solvent extraction.

Current theory suggests that increasing pulse duration will increase the extent of permeabilisation in a given area, either through the formation of larger or more numerous pores, provided that the electric field strength applied is high enough to cause electroporation (Gabriel and Teissié, 1999). Hence, altering the duration of a pulse may provide a means to fine tune the PEF treatment to allow fatty acid extraction, whilst maintaining cell viability. Increasing pulse duration generally caused an increase in fluorescence intensity (Fig. 48). This trend was expected, given that the applied electric field strength (9 kV/cm) was greater than the permeabilization threshold determined from the

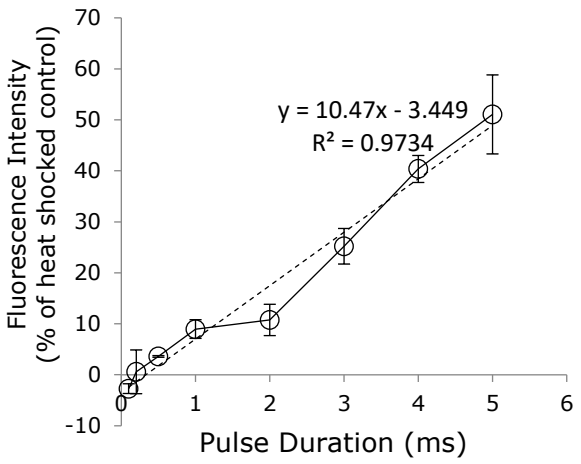

Fig. 48 - Effect of Pulse Duration on Extent of Cell Permeabilisation. Cultures (5 x 10^6 *T. minutus* cells/ml, 300µl) containing SYTOX Green (1.5µM) were exposed to a single 1.8 kV square wave pulse of varying duration. The electrode gap distance was 2 mm. Culture fluorescence was measured 1 h after pulse delivery using a FLUOstar® plate reader. Results are presented as the mean (n = 3), with error bars representing standard deviation.

previous experiment. This relationship was largely linear, however, the 2 ms pulses produced a mean fluorescence intensity almost equal to the 1 ms pulses.

Experiments exploring the effect of number of pulses were initially conducted using pulses comparable to previous experiments (9 kV/cm, 5 ms). However, arcing consistently occurred when applying more than 3 pulses at 1 min intervals, so the voltage was reduced to 8 kV/cm to avoid this. A largely linear increase in fluorescence was observed with increasing pulses, up to 6 pulses (Fig. 49). Further pulses (7 and 8) yielded little change in

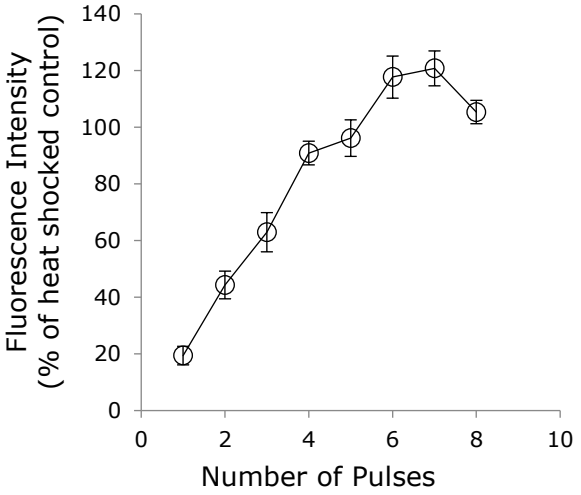

Fig. 49 - Effect of Multiple Pulses on Extent of Cell Permeabilisation. Cultures (5 x 10^6 *T. minutus* cells/ml, 300 µl) containing SYTOX Green (1.5 µM) were exposed to 1.6 kV square wave pulses with an interval of 1 min. The electrode gap distance was 2 mm. Culture fluorescence was measured 1 h after delivery of the final pulse using a FLUOstar® plate reader. Results are presented as the mean (n = 3), with error bars representing standard deviation.

fluorescence intensity. Samples exposed to 6, 7 and 8 pulses exhibited a fluorescence up to 120% of the mean fluorescence of the heat shocked cell controls. This suggested that not all heat-shocked control cells were fully stained. Alternative means of producing these controls were explored later. The cuvettes exposed to 7 or more pulses were noticeably hot to the touch, and cell permeabilization in these cases could be due to the heat as much as the PEF treatment. Unfortunately, the culture temperature cannot be accurately controlled in the electroporator used. However, a means of temperature control may be something to consider in an industrial-scale process. The higher temperatures could also explain the arcing observed when using the higher voltage; if the culture was rapidly heated to the point of boiling then arcing is likely to occur. Given these results, altering pulse duration rather than pulse number may provide a better way to fine-tune PEF treatment.

Discrepancies between the data sets are evident. During the experiment with varying pulse duration, pulses of 9 kV/cm, 5 ms duration produced 51% of the mean heat shocked cell control fluorescence. In contrast, equivalent pulses produced 18% of the mean heat shocked cell fluorescence during the experiment in which pulse voltage was varied (Table 14). When exploring the effect of multiple pulses, the application of a single 8 kV/cm, 5ms pulse yielded a mean fluorescence intensity equal to 19% of the heat shocked cell controls. In contrast, during the experiment in which pulse voltage was varied, equivalent pulses produced no significant fluorescence (Table 14). During these preliminary experiments, cells were harvested at different growth stages. Thus, potential variations in their cell membrane and/or cell wall structure could explain these differences in permeabilisation. For future experiments cells were harvested from cultures at the same growth stage (measured by OD_{750}).

Table 14 - Differences in Culture Permeabilization Across Multiple Experiments Despite Application of the Same PEF Treatment.

Experimental Variable	Pulse Conditions	Mean Fluorescence (% of heat shocked cell control)
Field Strength	9 kV/cm, 5ms	18 ±2.7
Pulse Duration	9 kV/cm, 5ms	51 ±7.7
Field Strength	8 kV/cm, 5ms	0 ±2.4
Pulse Duration	8 kV/cm, 5ms	19 ±3.3

Overall, these experiments demonstrate the capability of PEF treatments to permeabilise *T. minutus* and show that above a proposed permeabilization threshold of 8 kV/cm, the extent of permeabilization could be fine-tuned by varying either the number of

applied pulses, or their duration. However, varying pulse duration may be preferable due to the significant temperature increase noted when using multiple pulses. It is important to note that these experiments were conducted using whole culture fluorimetry, meaning that observed fluorescence could be due in part to either fragmented cells releasing nucleic acids into the media, or from permeabilization of the mutualist bacteria in the cultures. Whilst theory suggests that the larger *T. minutus* cells would be permeabilised at a lower electric field strength than smaller bacterial cells (Teissie *et al.*, 2005), it is important to consider that the applied electric field is not heterogenous, with cells nearer electrodes typically being more readily permeabilised than those further away (Wu *et al.*, 2013). Hence, smaller cells near electrodes could be more prone to permeabilisation than larger cells further away. Similarly, this method is unable to report on the extent of permeabilization of individual cells; a small number of highly permeabilised and fully stained cells could feasibly result in higher fluorescence than many, less permeabilised, cells. To explore these hypotheses, a flow cytometry method was developed in which the fluorescence of individual *T. minutus* cells could be measured specifically.

7.3. Measuring PEF-induced *T. minutus* Permeabilization by Flow Cytometry

During flow cytometry, a culture stream is flowed through a laser beam, with the stream being so fine that generally only a single cell passes through the laser beam at a time. When

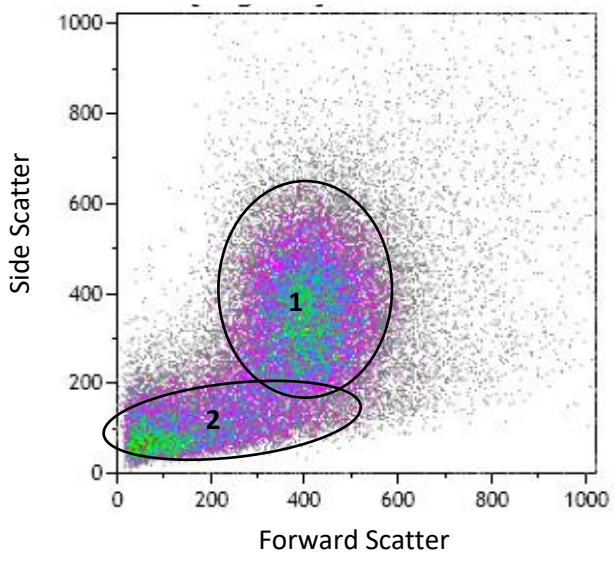

Fig. 50 - Flow Cytometry Density Plot of SYTOX Green Stained *T. minutus* Culture. The cultures contain many smaller mutualist bacteria as well as *T. minutus* cells. 2 distinct populations are circled. It is proposed that population 1 contains whole *T. minutus* cells, whilst population 2 contains bacteria and cell debris.

passing through the beam, different objects scatter light in different ways. Typically, larger cells produce higher forward scatter than smaller cells, allowing distinct cell populations to be identified. Furthermore, the fluorescence intensity of each object passing through the laser beam (termed an "event") can be measured. When analysing the cultures, two distinct populations were observed (Fig. 50). The *T. minutus* population was identified based on their higher forward scatter, whilst a second population was presumed to result from cell debris and bacteria. The identity of these cell populations was not confirmed. This could be achieved through cell sorting and subsequent microscopy of both cell populations. Further experiments only analysed events within the assumed *T. minutus* population.

Cultures were initially exposed to a single 5 ms pulse of varying amplitude (6-10 kV/cm) as in previous experiments, thereby allowing comparison of the analytical methods. PEF treated cells were categorised according to their fluorescence intensity: unstained (exhibiting equivalent fluorescence of an unstained live cell sample), fully stained (exhibiting fluorescence equivalent to a fully stained cell control), and partially stained (between these two thresholds). Due to the concerns that the heat shock method was not fully permeabilising all cells (Fig. 49), an isopropanol method was also explored; cells were separated from BBM media by centrifugation and resuspended in 70% isopropanol for 1 h, after which they were re-harvested and resuspended in fresh BBM medium. They were then stained with SG (1.5 µM) for 1 h before flow cytometry analysis.

Heat shock proved to be a more effective means of lysing cells, causing 99.8% of *T. minutus* cells to be fully stained, versus 92.6% when using the isopropanol method. However, previous results when varying number of pulses and using whole culture fluorescence measurements yielded fluorescence greater than the heat shocked control, suggesting not all cells were being lysed. Since the flow cytometry method analyses *T. minutus* cells specifically, and these were all fully stained using the heat shock method, the previous results could be explained by the bacteria present in the culture being more heat resistant than *T. minutus*. Thus, bacteria unpermeabilised by the heat shock protocol could be permeabilised by the most extreme PEF parameters. Previous studies using SG have demonstrated that the extent of lysis and resulting fluorescence fluorescence from both heat shock and isopropanol lysis methods varies with the cell type (Roth *et al.*, 1997). Based on these results, the heat shock approach was used exclusively in future experiments.

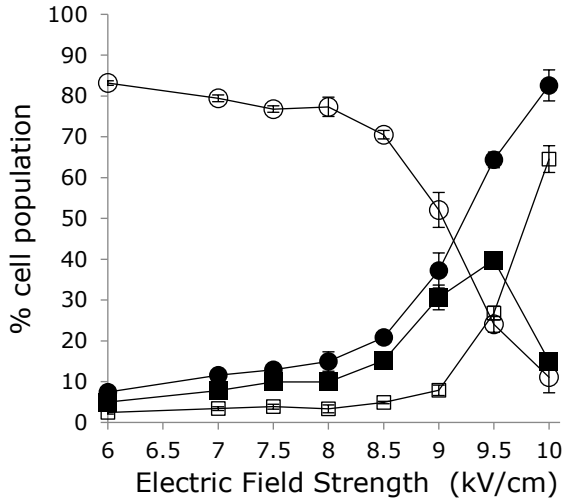

Fig. 51 - *T. minutus* Permeabilization Versus Electric Field Strength. Cell suspensions containing SYTOX Green were exposed to a single 5ms pulse of varying voltage. The fluorescence intensity of cells was measured by flow cytometry and, through comparison to fluorescence intensity of controls, were assigned to one of 3 groups: not stained (open circles), partially stained (closed squares) and fully stained (open squares). The sum of stained cells (partially and fully, closed circles) is also shown. Data points are the mean of replicates (*n*=3). Error bars represent standard deviation.

Generally, the flow cytometry method appeared to be more sensitive (Fig. 51). At 9 kV/cm around 40% of *T. minutus* cells were detected as stained (either partially or fully) by flow cytometry. In comparison, the FLUOstar® analysis of comparable cell suspensions yielded 20% of the fluorescence of the heat shocked control. This is due to the specific analysis of *T. minutus* cells during flow cytometry and demonstrates that these cells were predominantly permeabilised over the smaller bacteria, as hypothesised. Whilst trends in the results were generally comparable to those obtained using the FLUOstar® plate reader, the greater sensitivity of this method revealed a small number of stained cells between 6 kV/cm and 8 kV/cm, which were not detectable using the FLUOstar® plate reader. These data demonstrate the permeabilization threshold of *T. minutus* is below the 8 kV/cm suggested by the FLUOstar® method.

To explore this further a second cell culture was exposed to a lower range of field strengths (1 kV/cm – 7 kV/cm) (Fig. 52). This confirmed that a small percentage of cells were being permeabilised at field strengths as low as 3 kV/cm, suggesting that this is the true electropermeabilisation threshold for *T. minutus*. The relatively small extent of cell permeabilization is likely to be due to the heterogeneity of the electric field, alongside shielding effects from cells, preventing permeabilization of all cells except those nearest the electrodes. In conclusion, the specificity of flow cytometry towards *T. minutus* cells lends it greater sensitivity than that of whole culture fluorescence methods.

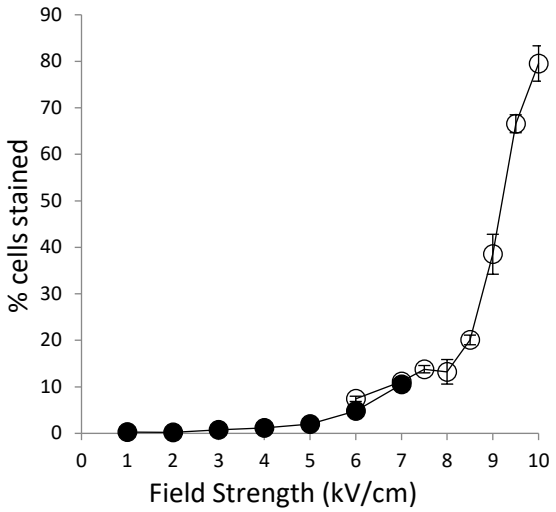

Fig. 52 – *T. minutus* Permeabilization Across a Wider Range of Electric Field Strengths. Cell suspensions containing SYTOX Green were exposed to a single 5ms pulse of varying voltage. The fluorescence intensity of *T. minutus* cells was measured by flow cytometry. Any cells exhibiting fluorescence higher those of an untreated stained control were considered permeabilised. Open circles are data collected from the initial cell population exposed to higher voltages, whilst closed circles are data from the second cell population exposed to lower voltages. Data points are the mean of replicates (n=3). Error bars represent standard deviation.

7.4. Effect of PEF Treatments on *T. minutus* Viability

A milking process requires that cells can continue to produce EPA after its extraction, which requires the cells to be metabolically active. A cell counting method was adopted to determine the effect of PEF treatments on cell reproduction as a general indicator of metabolic activity. Cell suspensions were exposed to a single 5 ms pulse after which they were used as inoculum for new cultures. After 96 hours of incubation cell counts were performed on each culture. Results were expressed as a percentage of the number of cells present in controls produced using the same inoculum, but not exposed to PEF treatment. Cultures exposed to the lowest electric field strengths (6 and 7 kV/cm), yielded cell concentrations of around 85-90% of that determined for the control cultures (Fig. 53), suggesting a reduction in cell viability. At higher field strengths the cell concentration dramatically decreased, with no apparent increase in cell concentration at all for cultures exposed to field strengths of, or greater than, 9 kV/cm. Despite this, cell counts at these highest field strengths were equivalent to controls unexposed to PEF treatment, suggesting the treatments were incapable of breaking apart cells. This apparent retention of structural integrity could perhaps be due to their cell wall, which is less likely to be affected by PEF treatment (Azencott *et al.*, 2007). However, these cells were unable to reproduce. Their viability could be explored through SG staining; if they remain permeabilised 96 h after PEF

application they can be assumed dead. It is also important to note that cells which are unable to reproduce but remain viable may be capable of continued EPA production, which could be explored by successive EPA extractions on the same nongrowing cells.

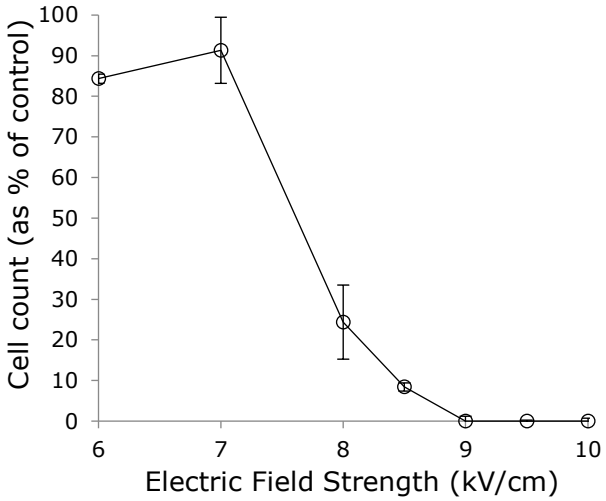

Fig. 53 - Culture Viability 96 h After PEF Treatments of Varying Voltage. Cell suspensions were exposed to a single 5 ms pulse after which they were used as inoculum for new cultures. After 96 hours of incubation cell counts were performed on each culture, and results expressed as a percentage of the mean number of cells present in triplicate controls which were not exposed to PEF treatment. Points are the mean of replicates (*n*=3), with error bars representing standard deviation.

7.5. Cell Resealing Kinetics after PEF Treatment

In order to develop a milking process, it is imperative that a significant portion of cells can continue to produce EPA after extraction. When using a PEF based milking strategy, this means that a significant number of electroporated cells must be able to reseal, and that resealed cells can continue to produce EPA. Furthermore, knowing how long the cells remain permeabilised gives an idea of the window of time available for EPA extraction. Initially, the ability of cells to reseal was explored by adding SG at different times after a pulse, with the aim of capturing resealing kinetics. If cells are reversibly permeabilised then they will reseal over time. By adding SG at different times after PEF treatment, the time taken for cells to reseal should be apparent *via* a measured decrease in fluorescence over time. PEF treatment consisting of a single 5 ms pulse with a field strength of 9 kV/cm was chosen since this had been shown previously to permeabilise *T. minutus* cells. A preliminary screening experiment utilised whole culture fluorimetry analysis due to the easy availability of the equipment. After adjusting for background fluorescence, samples electroporated in the presence of SG exhibited approximately 30% of the mean heat shocked cell control fluorescence (Fig. 54).

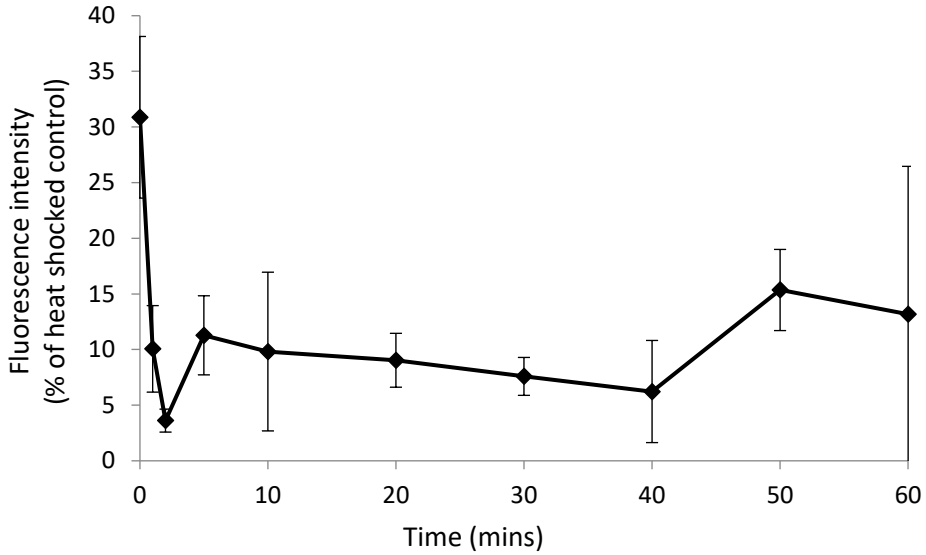

Fig. 54 - Culture Permeabilisation Over Time. Cell suspensions ($5x10^6$ cells/ml) were exposed to a single 9 kV/cm, 5 ms pulse, with SYTOX Green either present during the pulse (0 mins) or added at varying times afterwards (1 – 60 mins). Data points are the mean of replicates (*n*=3). Error bars represent standard deviation.

Each sample in which SG was added after the pulse produced around 10% of the mean fluorescence intensity of the heat shocked cell control, regardless of the time at which it was added (1 – 60 min), although these results were variable. This equates to an approximate difference of 20% between samples where SG was present during the pulse, and those samples where it was added afterwards. It was originally thought that these data suggest around 20% of cells were reversibly permeabilised, with resealing occurring in under 1 minute; presumably, approximately 10% of cells were irreversibly permeabilised. However, previous studies of resealing kinetics using similar methods (albeit with different cell types and dyes) were able to capture resealing over time, and demonstrated that full resealing took 10-30 minutes (Rols *et al.*, 1998, Neumann *et al.*, 1998). It was unexpected that *T.* minutus cells would be capable of resealing so much faster, which brought the initial interpretation of this data into question, particularly given that there was no evidence of resealing taking place over a prolonged period of time, as has been reported for other organisms (Rols et al., 1998, Neumann et al., 1998).

To determine if resealing was occurring in less than 1 minute, and to attempt to capture the kinetics of the process, the method was repeated with faster addition of SG (as early as 10 s). Samples were also analysed via flow cytometry to target T. minutus cells specifically. When exposed to the electrical pulse in the presence of SG, an average of 58% of algae cells were stained (fully or partially), compared to around 35% when SG was added after the pulse (Fig. 55). There was no significant difference in the number of cells stained

when adding SG at any time (10s - 20 min) after the pulse. In comparison, only 10% of cells in the control lacking PEF treatment were stained. Given the previous reports of cell resealing kinetics in the order of minutes, it seems highly unlikely that *T. minutus* cells were fully resealing within 10 s. Instead, it may be that SG fluorescence is affected by the application of the electric field. SYTOX Green is a cyanine mono-intercalator with positive charge (Fig. 43) which facilitates binding through interaction with the negatively charged DNA backbone (Roth *et al.*, 1997). However, the application of an electric field as in PEF treatment may facilitate entry of SG into cells by electrophoresis. In comparison, when SG is added after PEF treatment, it enters the cells by diffusion alone, meaning that it is driven exclusively by a concentration gradient. Once the gradient reaches equilibrium, a maximum intracellular SG concentration is achieved. If SG can be electrophoretically driven into cells, then a higher intracellular concentration could potentially be achieved, with increased fluorescence. This could explain the differences in fluorescence observed here. Very similar results were produced in a PEF study of *Lactobacillus plantarum* using propidium iodide dye, although the authors attributed this to rapid resealing kinetics in the order of seconds (Vaessen *et al.*, 2018). However, propidium iodide is also positively charged and could just as feasibly be electrophoretically driven into cells. This hypothesis would also explain why PEF treatments using multiple pulses yielded higher culture fluorescence than heat shocked controls (Fig. 49). In conclusion, results obtained from the addition of SG during a pulse should not be compared to those where SG is added afterwards. Hence, SG should only be added after PEF treatment in future experiments. It appears that cells exposed to a PEF treatment of a single 9 kv/cm, 5ms pulse were only irreversibly permeabilised. This is supported by the data illustrating that cells did not reproduce after such treatments, as determined by cell counts (Fig. 53). Provided SG is only added after PEF treatment, this method should still be applicable for identifying reversible cell permeabilization, and cell resealing kinetics, arising from varied (likely lower voltage) PEF treatments. Future resealing and viability studies should be conducted at lower field strengths, particularly those nearest the permeabilization threshold of 3-4 kV/cm. Unfortunately, so few cells are permeabilised at these field strengths that it could be difficult to gather accurate data. The use of a larger PEF chamber to treat larger culture volumes, combined with a rig capable of providing a more homogenous electric field could alleviate this problem.

7.6. PEF Assisted EPA Extraction

With methods to determine the extent of *T. minutus* permeabilization successfully developed, it was desirable to explore the extent to which such permeabilization led to EPA extraction. Ultimately the aim was to extract EPA with or without solvents, with no need to concentrate or dry the cell culture.

In a study where EPA production from *T. minutus* was optimised, up to 26mg EPA was extracted per gram of biomass (Cepák *et al.*, 2014). This equates to just 3.6 µg of EPA from the $1.5x10^6$ cells used in previous PEF experiments (300µl of $5x10^6$ cells/ml). To improve analytical accuracy, a number of cell samples were PEF-treated in parallel and the samples were pooled for analysis of the EPA. Thus, 50 cuvettes, each containing 300µl of *T. minutus* culture were exposed to a single 9 kV/cm, 5ms pulse and pooled to yield 15 ml of PEF treated culture. To further ensure detectable quantities of EPA in these initial experiments, the cells were concentrated by centrifugation and the supernatant discarded. Wet biomass was extracted for 60 mins using heptane, EPA was transesterified into EPAEE and then EPAEE was quantified by HPLC-UV. The same procedures were conducted on cells which were not exposed to PEF treatment.

Interestingly, 14.9 mg of EPA was extracted per g of PEF treated biomass versus 16.4 mg of EPA per g of untreated biomass. This could be due to PEF-treated cells releasing EPA into the medium, which would then be discarded in the supernatant. To test this an extraction was conducted on the supernatant with subsequent derivatisation, but no EPAEE was detected. However, PUFAs are largely insoluble in water and, depending on their concentration, will either form an emulsion or a separate phase. It was hypothesised that lipids, including EPA, could be left stuck to the plastic sides of the electroporation cuvette after pouring out the culture for pooling. To test this, 3 µg of EPAEE was added to BBM medium (lacking cells) and exposed to the same PEF treatment. This was then poured out and the cuvette sides rinsed with heptane. This heptane was transferred to the PEF treated media for further extraction. More than 4 times the quantity of EPAEE was recovered by using a single heptane wash (Fig. 56), proving that a majority of EPAEE remains in the cuvette after media transfer. Recovery of EPAEE from washed samples varied greatly and could likely be improved with multiple, and/or longer, washes. Emulsified oil droplets typically have a surface charge, either by possessing an inherent charge or by adsorbing ions present in the solution. This causes the droplets to repel each other, making it difficult for them to form a separate phase. In electrocoagulation, the application of an electric field can neutralise these charges by the production of counterions from a sacrificial anode, thus removing a barrier to the aggregation of emulsified oil droplets (An *et al.*, 2017). This could explain the difference

in EPA extracted from PEF treated and untreated biomass: if EPA is present in a separate layer in PEF treated media due to electrocoagulation, then more could stick to the plastic cuvette when pouring out the media when compared to an emulsion (as in untreated media). This could be tested by quantifying EPAEE in heptane washes and media separately, in both PEF treated and untreated conditions.

Given the effect of the heptane wash, further extractions were conducted directly in the cuvettes, without cell centrifugation, by adding heptane after PEF treatment and shaking by hand for 15 s. This was conducted on PEF treated and untreated cell cultures, and EPAEE-spiked BBM media. Only 43% of the EPAEE was recovered from the spiked media, indicating that a longer extraction is necessary. Neither of the heptane extractions (conducted on PEF treated and untreated cultures) contained detectable EPAEE. This suggests that either PEF treatment did not extract EPA from cells, or it did so at undetectable levels. This could be explored further by performing extractions on concentrated wet biomass as in previous experiments. However, one objective of this project was to extract EPA without the need to concentrate biomass beforehand, to attempt to reduce overall process costs. Extractions could be carried out on pooled PEF treated biomass. However, since only 300µl aliquots could be PEF treated at a time, the duration between PEF treatment and extraction would vary greatly across the aliquots by the time enough culture had been pooled. Alternatively, the cells could be extracted with heptane directly within the electroporation cuvettes and

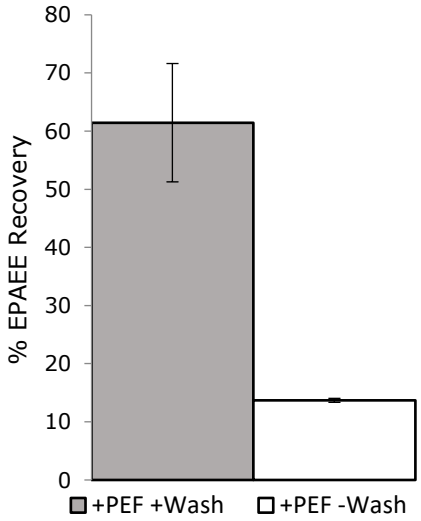

Fig. 56 - EPAEE Recovered from PEF Treated BBM Media With and Without a Single Heptane Wash. BBM media was spiked with 3 µg of EPAEE. This was exposed to a single 9 kV/cm, 5 ms pulse. After transfer of the culture, cuvettes were washed once with heptane (+Wash) or not (-wash). Heptane washes were transferred to the media for further extraction, whilst those samples that did not receive a wash received fresh heptane for extraction. EPAEE was quantified by HPLC-UV. Results are the mean (*n* = 3), with error bars representing standard deviation.

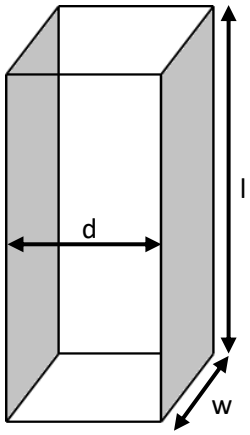

Fig. 57 - Schematic of a Parallel Plate Electrode System. Electrodes are coloured grey, d – electrode gap distance, w – chamber width, l – chamber length. To maintain a given electric field strength at a specific voltage, d must remain the same. Therefore, the chamber volume can only be increased through increasing its length or width.

the extracts pooled for derivatization and analysis. However, this method of extraction is unsuitable because vigorous shaking of sensitive permeabilised cells could cause their lysis, inflating the quantity of EPA extracted and preventing cell recovery. Furthermore, no magnetic stirring bars small enough to provide gentler agitation within the cuvette are available. Hence, it was desirable to design a larger glass electroporation chamber, which can be effectively washed with solvent.

7.7. Design and Construction of an Alternative PEF Chamber

Previous results using the commercially available electroporator (BioRad Gene Pulser Xcell) identified three key aspects of the rig which hinder its use in proficiently researching a PEF based milking process: (i) the culture volumes used are very small, (ii) it uses plastic cuvettes to which fatty acids can readily adhere, (iii) it produces a heterogenous electric field, making it difficult to attain optimum PEF conditions. Therefore, a new PEF treatment chamber was designed to overcome each of these obstacles. Conventional electroporation chambers typically utilise parallel plate electrodes (Fig. 57), as found in electroporation cuvettes. These are not ideal for scale-up to larger treatment volumes, since, in order to maintain the desired electric field strength of a pulse, either the distance between electrodes (d) must be kept constant, or the applied voltage must be increased alongside the electrode gap distance. Increasing the volume of a parallel plate chamber whilst retaining electrode gap distance requires the length (l) and/or width (w) to be increased (Fig. 57). However, drastic increases in size with a comparatively small electrode gap distance decrease the structural integrity of the chamber and greatly enhance the area of electrode plate required, which should be a

consideration for minimising costs for a commercial process. Increasing the applied voltage increases the power consumption, which could become undesirably high for a commercial process. Furthermore, for the sake of convenience and to minimise costs, it was desirable to use an electroporation chamber compatible with the previously used Bio-Rad pulse generator. This can produce a maximum pulse of 3000 V, thus limiting the maximum electrode gap distance.

These issues are elegantly circumvented by utilising an array of needle electrodes, such as in the design by Zhao et. al. (Zhao *et al.*, 2016, Wu *et al.*, 2013). Based on this work, a new treatment chamber was designed and constructed in-house for use in conjunction with the available Bio-Rad pulse generator. The chamber design consists of 37 electrodes housed in a glass chamber with an inlet for pumping in cell culture and a burette tap outlet, and utilises the same connection to the pulse generator as the commercial cuvette apparatus. The printed circuit board (PCB) for the device has separate tracks on each side - one track connects anodes, and another connects cathodes (Fig. 58). Stainless steel acupuncture needles (Physique, UK) were used as the electrodes, with a slightly larger diameter than their holes in the PCB (0.35 mm vs 0.3 mm) to minimise their movement whilst soldering. To help keep the electrodes parallel they were fed through two PCBs before soldering them to only one of the PCBs (Fig. 59 A). The second PCB acted as a guide and was

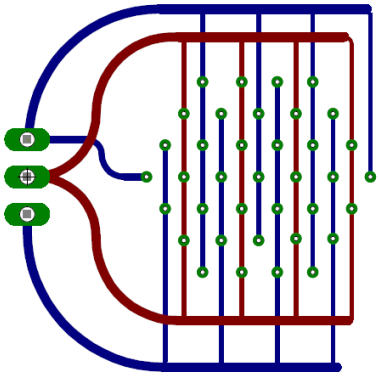

Fig. 58 - Printed Circuit Board (PCB) Design for the Custom PEF Rig. The PCB is double sided, with one track (blue or red) on either side. The tracks are 0.254 mm wide, with blue being positive and red negative. Green denotes pads for soldering, with white centres for electrode holes. Holes centres are 2.54mm apart from their neighbours in any direction, and 0.3 mm in diameter, fitted with 0.35mm diameter electrodes (yielding an edge-to-edge electrode gap distance of 2.19mm).

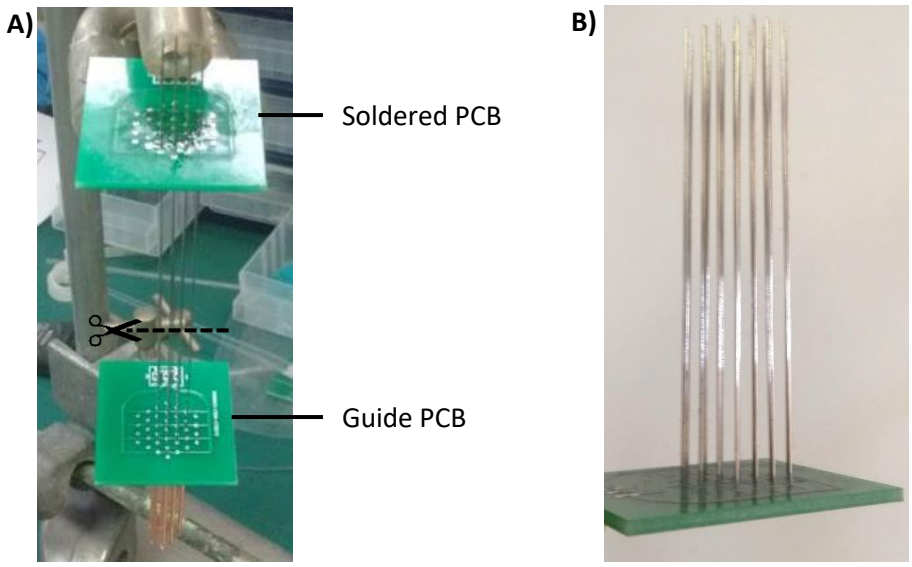

Fig. 59 - Soldering Electrodes to the PCB. A) Electrodes were fed through 2 PCBs, with one acting as a guide to keep the electrodes parallel. After all electrodes had been soldered to the base PCB they were cut to the desired length, removing the guide PCB and yielding B).

later removed when the electrodes were cut to the desired length (60 mm). Despite this, it should be noted that the electrodes are not precisely parallel (Fig. 59 B). This could likely be avoided in future designs by using less flexible (thicker) electrodes.

The glassware to house the electrodes was blown in-house and consists of a cylinder with a side arm approximately one third of the way down through which doses of culture could be pumped, and a tapered bottom end with a burette tap to allow culture removal after PEF treatment (Fig. 60). The tap allows the PEF treatment to be conducted on culture batches, or continuously if the tap is left open or removed. The circuit board could be placed atop the cylinder with attached electrodes inside the glass housing, and could be sealed using an aquatic-safe and electrically inert silicone (added *via* the side arm inlet). Assuming a final silicone depth of 10 mm would leave 55 mm of height inside the chamber to be filled with cell culture. Thus, the total chamber volume (excluding the volume of the electrodes within the chamber, the inlet side arm, and proposed silicone) is 13.8 ml. However, approximately 5.8 ml of culture between the edge electrodes and glassware would not be PEF treated, leaving an effective volume treated of approximately 8 ml. This ratio was deemed acceptable for the present proof-of-concept study given that the extra room allows for easier overall manufacture. However, this could be improved upon in future designs by more tightly

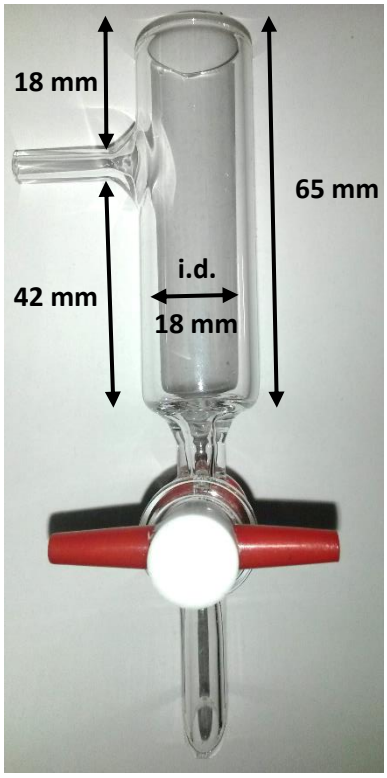

Fig. 60 - Glassware for the Electroporation Chamber. The glassware was blown in-house to the specified dimensions. The side arm provides an inlet for pumping in culture, which can be removed *via* the burette tap. The electrodes sit inside the glassware, sealed at the top of the glass cylinder using silicone. i.d. = internal diameter.

housing the electrodes within the glassware, or even utilising an outer cylindrical electrode. To ensure safe use of the device, a housing box (30 cm wide x 30 cm deep x 50 cm high) of 4 mm thick Perspex with an aluminium frame was constructed, to which it could be wired. The PEF chamber is accessed through a door in the box which breaks the circuit to the chamber upon opening. An emergency stop was also included.

In comparison to the design by Zhao et. al., the main differences here are the increased electrode gap distance (2.19mm vs 0.2mm), and the lack of electrode polarity switching. The increased electrode gap distance greatly reduces the likelihood of unintentional short circuiting between the electrodes, which could arise at the pad of the electrode when soldering them to the PCB, or further from their base if the electrodes touch due to not being entirely parallel. This electrode gap distance is similar to that used in the cuvette-based electroporation system (2.19 mm vs 2 mm), from which preliminary permeabilization data had already been gathered, providing a reliable starting point for experiments using this new chamber. A larger gap distance also increases the volume of culture that can be treated relative to the total volume of electrodes. Therefore, it was desirable to convert the continuous process of Zhao *et al.*, to a batch process delivering doses

of culture, which could be removed *via* burette tap after PEF treatment. The process can then be repeated as many times as desired. Previous work has suggested that cell survival is lowest at the cathodes (due to localised pH changes arising from the creation of OH^- ions during water electrolysis), with application of multiple pulses greatly exacerbating this (Wu *et al.*, 2013). To avoid this, the design by Zhao *et al.* included a system where the polarity of the electrodes was swapped after each pulse. This was deemed unnecessary in the design here since PEF treatments using multiple pulses would generally be avoided in this system, due to the previous results demonstrating their increased heat generation and tendency for arcing. Furthermore, unlike the pulse generator used by Zhao *et al.*, the in-house pulse generator is incapable of producing more than 2 high voltage sequential pulses automatically, so pulses must be delivered manually. However, if the application of multiple pulses was desired, cell survival could likely be increased through mixing the treated culture between each pulse by removing it from the chamber and pumping it back in.

This design offers numerous advantages to the previously used cuvette system: a much larger volume of culture can be treated with each pulse (13.8 ml vs 300 µl), the burette tap allows easier sample pooling and rapid post-treatment contact with a solvent of choice, the chamber is easily flushed of any algal oil by pumping through a solvent, and is comprised of glass, which is generally more inert than the plastic of the cuvettes and less likely to adsorb oil droplets. Finally, the use of an electrode array, as opposed to parallel plate electrodes, yields a more homogenous electric field (Zhao *et al.*, 2016), and a greater area in which this field is at a critical “sweet spot” for the desired cell permeabilization. Unfortunately, construction of this chamber was not finished, but experiments should be conducted with it in future work.

8. Discussion and Future Work

8.1. Small Scale Ionic Liquid Toxicity

IL toxicity was initially tested by agar diffusion and 1% (*v/v*) liquid toxicity screens. In these experiments, the *bis*triflimide ([NTf_2]) anion was generally less toxic than other anions. However, published data highlight its apparent toxicity towards other species of algae (Stolte *et al.*, 2007, Pretti *et al.*, 2009). Generally, it has been shown that increasing the lipophilicity of an IL usually increases its toxicity (Stolte *et al.*, 2007, Pham *et al.*, 2008, Latala *et al.*, 2009). As a result, the mechanism of non-specific IL toxicity is largely proposed to occur *via* cell membrane disruption through insertion of lipophilic moieties (Sena *et al.*, 2010). However, Wood *et al.* reported that quaternary ammonium ILs paired with the *bis*triflimide anion showed the opposite trend, becoming less toxic towards *E. coli* with increasing alkyl chain length (Wood *et al.*, 2011). Such a result was also apparent here for *T. minutus*. Whilst Wood *et al.* did not test the toxicity of quaternary phosphonium *bis*triflimide ILs, results presented here suggest that this trend may also be true for these ILs. *Bis*triflimide anions contain electronegative oxygen and fluorine atoms capable of forming dipole interactions with the hydrogen atoms of long alkyl chains, such as those found within the phospholipid membrane, and the cations of some ILs studied here. It is proposed that these interactions can result in the alkyl chains of the cation wrapping around the *bis*triflimide anion, helping prevent insertion of the IL into the cell membrane.

Overall, imidazolium ILs proved to be very toxic towards *T. minutus*, and this has been reported for other algal species (Stolte *et al.*, 2007, Pretti *et al.*, 2009). It is generally suggested that increasing aromaticity of an IL increases its toxicity. For example, Stolte and co-workers report EC_{50} values of imidazolium and pyridinium halide ILs an order of magnitude lower (*i.e.* more toxic) than corresponding piperidinium and pyrrolidinium ILs, and 2 orders of magnitude lower than corresponding quaternary ammonium ILs, toward *Scenedesmus vacuolatus* (Stolte *et al.*, 2007). However, other studies have demonstrated that shorter alkyl chain imidazolium ILs are less toxic than other cationic structures (*e.g.* quaternary phosphonium ILs) with comparatively longer alkyl chains (Wells and Coombe, 2006). This is not apparent in the data presented here; in the agar diffusion screen, imidazolium ILs with short alkyl chains (*e.g.* [C_4MIM][AOT]) completely inhibited growth, whereas comparable quaternary ILs with much longer alkyl chains (*e.g.* [$P_{6\,6\,6\,14}$][AOT]) did not, and, in some cases, even allowed growth when present in liquid media. This could indicate that the core structures of imidazolium ILs are particularly toxic to *T. minutus*. Furthermore, despite containing aromatic rings, [$N_{1\,1\,1\text{-Bn}\,2\text{-O-}2\text{-OBn}}$][$NTf_2$], [$N_{1\,1\,2\,2\text{-O-}2\text{-O-Bn}}$][$NTf_2$],

and [$N_{1\ 1\ 2\ 2\text{-}O\text{-}2\text{-}O\text{-}1\text{-}Bn}$][$NTf_2$] showed little growth inhibition, even when compared to linear quaternary ammonium ILs.

In the biphasic milking process proposed in this project, solvent would be added at the end of the exponential growth phase; this is when EPA levels are maximal and has the additional benefit of reducing the time for which the culture is exposed to the solvent. However, to monitor the effect of ILs on algal growth they were here added during the lag phase, before growth started. Whilst this situation is not directly comparable to the proposed milking process, it was considered that any IL inhibiting algal growth would also likely cause cell death in established cultures. Furthermore, cells are likely to be more sensitive during early growth stages, potentially lowering the concentration of IL required to see an effect in such experiments. That said, it was not expected that the majority of ILs tested in shake flask experiments would completely inhibit growth, especially considering the low quantity of IL present (1% *v/v*), and this could in part be attributed to the presence of ILs during early growth stages. It is thought that the cell walls of *T. minutus* may be thicker or more chemically resistant by stationary phase of growth compared to lag or exponential growth phases (personal communication, AlgaeCytes). Hence, addition of ILs at these later stages of growth may help alleviate their toxicity due to the presence of a more robust physical barrier to the cell membrane.

8.2. Large Scale Solvent Toxicity

The photobioreactor used in this study provided a viable means to assess solvent toxicity at 20% (v/v). However, aspects of this system, particularly with air flow, make it undesirable for use in a final milking strategy. Firstly, this system pumped air through the cultures, which could increase the extent of oxidation of fatty acids, potentially decreasing overall EPA productivity. This could be alleviated by using pure CO_2 instead, with the added benefit of further increasing growth rates, and possibly increasing lipid production (Singh and Singh, 2014). Furthermore, a means to accurately control the rate of airflow through each tube is necessary to ensure the same growth rate and extent of solvent mixing. The extent of solvent mass transfer and the available surface area of solvent is likely to greatly affect the quantity of EPA that can be extracted. Lower viscosity solvents, such as tetradecane and dodecane, have the advantage of being more readily dispersed into multiple micelles throughout the culture than higher viscosity solvents such as the ILs used here. However, the extent of extraction is dependent on many factors, and needs to be experimentally determined for each solvent in future work.

Interestingly, the results at 20% (*v/v*) showed that $[P_{6\,6\,6\,14}][AOT]$ and $[P_{6\,6\,6\,14}][iC_8PO_4]$ were less toxic than $[P_{6\,6\,6\,14}][NTf_2]$, whereas the opposite was true at 1% (*v/v*). This demonstrates that the volume of the IL and the stage of growth at which it is added have noticeable effects on their toxicity. This makes it particularly desirable to test the final IL of interest, Cyphos 104 (90% $[P_{6\,6\,6\,14}]$ $[iC_5PO_2]$, 10% $[P_{6\,6\,6\,14}][Cl^-]$) by this method in future work. Similarly, the synthesis of $[N_{1\,1\,4\,8}][NTf2]$, $[P_{4\,4\,4\,6}][Cl^-]$, $[N_{1\ 1\ 1\text{-}Bn\ 2\text{-}O\text{-}2\text{-}O\text{-}Bn}][NTf_2]$, $[N_{1\ 1\ 2\ 2\text{-}O\text{-}2\text{-}O\text{-}1\text{-}Bn}][NTf_2]$ and $[N_{1\,1\,2\,2\text{-}O\text{-}2\text{-}O\text{-}Bn}][NTf_2]$ should be considered for future work, since these ILs passed the low volume toxicity screens but insufficient volumes were available for larger scale tests. Furthermore, it may desirable to test the toxicity of ILs that passed the agar screen using 1% (*v/v*) IL added at the onset of stationary phase as opposed to the lag phase. This may identify more IL candidates. Having discovered some biocompatible IL milking candidates, structurally analogous ILs could be synthesised or procured for further testing. In this way a deeper understanding of structure-toxicity relationships could be gained, and a greater range of IL candidates discovered.

Tetradecane and dodecane were largely non-toxic and this has been reported for other algal species (Hejazi *et al.*, 2004, Frenz *et al.*, 1989b). In fact, it has been reported that *Nannochloropsis* sp. appear to grow faster in the presence of these solvents (Zhang *et al.*, 2011b). Based on these data, it would be desirable to screen further conventional solvents in future work. Polyunsaturated alkenes could be of particular interest; their ability to form π - π interactions with polyunsaturated fatty acids could increase their selectivity for these substances over other hydrophobic compounds. However, this could also result in more difficult product separation after extractions.

8.3. Quantification of Eicosapentaenoic Acid in Ionic Liquids

Methods for quantification of fatty acids in conventional extractants (*e.g.* alkanes) are readily available in the literature (Laurens *et al.*, 2012, Monteiro *et al.*, 2008). However, such methods for ILs were unavailable and so were developed here. In order to accurately quantify the EPA present in each IL, especially $[N_{1,8,8,8}][NTf_2]$ which was believed to sequester *T. minutus* cells, it would first be necessary to separate the biomass to avoid any further extraction during the transesterification process. This could likely be performed by centrifugation. Samples will require subsequent esterification of EPA to EPAEE for quantification. A method for transesterification, identified in the literature (Laurens *et al.*, 2012), was used here for hexane and heptane extractions. However, the ILs of interest are miscible with the acidified ethanol used in this process. Injection of HCl, present in this

IL/ethanol/HCl solution, should be avoided since it is corrosive to stainless steel, potentially causing appreciable damage to the HPLC system. Thus, an additional sample drying step would be necessary to evaporate the ethanol and HCl whilst retaining the IL and EPAEE.

DHA, given its natural absence in *T. minutus* and structural similarity to EPA, could be added to every sample as an internal standard to measure transesterification efficiency and any loss of sample during the drying process. Whilst unnatural fatty acids (with an odd number of carbon atoms) could be purchased from chemical suppliers for this purpose, they are typically saturated or mono- and trans- unsaturated (*e.g.* elaidic acid, 18:1 ω9). This structural difference is particularly important when considering fatty acid oxidation. Generally, the more double bonds present in a fatty acid, the more prone it is to photooxidation and autooxidation (Shahidi and Zhong, 2010). These adverse reactions are likely to occur to some extent during the extraction, drying, and derivatisation processes. Using DHA as an internal standard could allow the extent of any such reactions to be quantified, and a percentage loss of the internal standard could be justifiably applied to EPA. To achieve this, DHAEE calibration curves would need to be produced in each of the ILs of interest. Furthermore, it may be desirable to produce calibrations for every fatty acid identified in *T. minutus*, since their quantification could provide useful information on extractant specificity for EPA over other fatty acids. These quantification methods can be applied to samples taken during biphasic extractions using the most promising solvents identified in this work (tetradecane, dodecane, $[P_{6\,6\,6\,14}][AOT]$ and $[P_{6\,6\,6\,14}][iC_8PO_4]$). This could be combined with the toxicity data already gathered to determine the viability of each of the solvents in a biphasic milking strategy.

EPA extraction experiments could be conducted using the same apparatus (multicultivator) as the large-scale toxicity experiments (section 4.4.4), utilising 64 ml of culture and 16 ml of IL added at the onset of stationary phase (120 h). Every 24 h for 5 days a 1 ml IL sample could be taken. Sampling in this way would provide valuable data regarding the required contact duration for maximum EPA extraction. Samples should be taken after temporarily turning off the airflow to the culture for 5-10 minutes, allowing the IL phase to fully agglutinate and removing large air bubbles, thereby enabling accurate removal of the specified IL volume. IL samples can then be centrifuged to isolate any biomass, and an 800 µl IL aliquot removed. At this stage, the IL sample could be stored under N_2 at -80 ^oC. However, it would be preferable to immediately conduct transesterficiation and subsequent quantification. A known quantity of DHA (dissolved in ethanol) should be added to the sample, followed by 800 µl of acidifed ethanol (0.6 M HCl). The sample should be mixed, and

capped after brief exposure to N_2 so as to remove excess O_2. Transesterification can then be conducted at 65 ^{O}C for 1 h, after which samples should be fully dried in a vacuum oven or under N_2 to remove ethanol and HCl. An 800 µl aliquot of acetonitrile can then be added to reduce viscosity for HPLC analysis, enabling quantification of both EPAEE and DHAEE. The volumes given should be adequate; 64 ml of *T. minutus* culture in stationary phase should contain approximately 3 mg of EPA (Cepák *et al.*, 2014). The highest LoQ for EPAEE in an IL candidate ($[P_{6\,6\,6\,14}][iC_8PO_4]$) was 3.84 µg/ml. Given that the final sample is diluted 1:1 in acetonitrile, twice this concentration (7.68 µg/ml) would be necessary for quantification to be possible. This equates to 122.9 µg of EPA in the total IL volume (16 ml), meaning that the IL needs to extract only 4% of the total EPA in the culture for it to be quantifiable. This is assuming 100% transesterification efficiency, which is admittedly unlikely. However, any IL unable to extract significantly higher quantities of EPA than this could justifiably be deemed unsuitable for a milking strategy. Finally, culture samples could be taken simultaneously from a control culture without IL present, and the exact EPA content in the sample (and therefore the whole culture) determined using the methods outlined in section 4.8 and GC-FID quantification (Laurens *et al.*, 2012). This provides a reliable means to demonstrate how much EPA was available for extraction at a given time.

8.4. Proposed means to Recover EPA from ILs, and recycle ILs

Various methods being researched for product recovery and IL recycling were discussed in section 2.6.8. Of these, it is proposed that molecular distillation and liquid/liquid back extraction would be most applicable to the separation of EPA esters from ILs at present. This is because alternative technologies (*e.g.* membrane filtration, adsorption) are in comparative infancy when regarding their specific application towards the separation of fatty acid esters from ILs. Liquid/liquid extraction and molecular distillation are more proven methods, enabling easier immediate research. That said, alternative technologies should continue to be considered as they develop. Liquid/liquid extraction requires a solvent which is immiscible with the IL, and in which the EPA esters are soluble. Simple miscibility studies of the IL candidates with solvents commonly used to extract fatty acids (*e.g.* hexane, chloroform) should be conducted. Then, if an immiscible solvent is identified, the extent to which they can recover EPA AGs from the IL can be explored using ILs dosed with algal oil containing a predetermined, known quantity of EPA. The quantity of solvent, number of extractions, extent of mixing and temperature are all potential variables that could be explored to determine the most efficient method. After extraction of EPA AGs, other

impurities may remain in the IL. The potential for other immiscible solvents to further purify the IL can likewise be explored. Molecular distillation has been used to purify PUFAs from complex oils (Zhang *et al.*, 2013b), and should be applicable in their extraction from an IL. Experiments could be conducted under varying parameters (*e.g.* temperature, pressure, feed rate and roller speed) to determine the best conditions for EPAEE recovery from an IL. This approach can also be used to determine the best conditions to remove further volatile impurities remaining in the IL. Finally, non-volatile impurities could then be removed by liquid/liquid extraction.

Ultimately, the recyclability of an IL should be tested through repeated cycles of EPA extraction from a culture and IL purification. The extent to which the efficiency of EPA extraction from an algal culture is affected by any remaining impurities in the IL should be explored, as well as how much, if any, IL is lost throughout repeated processes. This data can be used to infer how many extraction-purification cycles a given IL can be utilised for, and how much fresh IL needs to be supplied per milking cycle. Understanding the limits of an ILs life cycle in a prolonged milking process in this manner is key to determining if that IL is cost effective in such a process.

8.5. Proposed Methods for Biphasic System Milking at a Pilot Commercial Scale

The multicultivator apparatus used in the 20% (*v/v*) toxicity screens is fit for toxicity and initial extraction experiments, but aspects of its design make it inappropriate for pilot scale experiments aimed at determining the commercial viability of biphasic milking. A design for a more appropriate photobioreactor for this purpose is presented in Fig. 61. The multicultivator system necessitates batch extractions whereas an ideal rig would enable continuous milking. To enable this, the proposed photobioreactor would utilise a chemostat system whereby fresh media is added and used culture removed to maintain a culture in stationary phase. Whilst temperature and light intensity could be controlled in the multicultivator apparatus, there was no means to automatically control culture pH nor accurately control air flow rate, both of which would be desirable in a commercial rig. In the proposed rig design (Fig. 61) temperature, pH, and OD sensors would enable culture conditions to be monitored and kept steady; temperature can be controlled via a heating/cooling water coil, OD by culture removal and media addition, and pH by buffer addition.

There is also no significant means to mix the extraction solvent with the culture using the mutlicultivator instrument, besides the mixing provided by airflow into the culture.

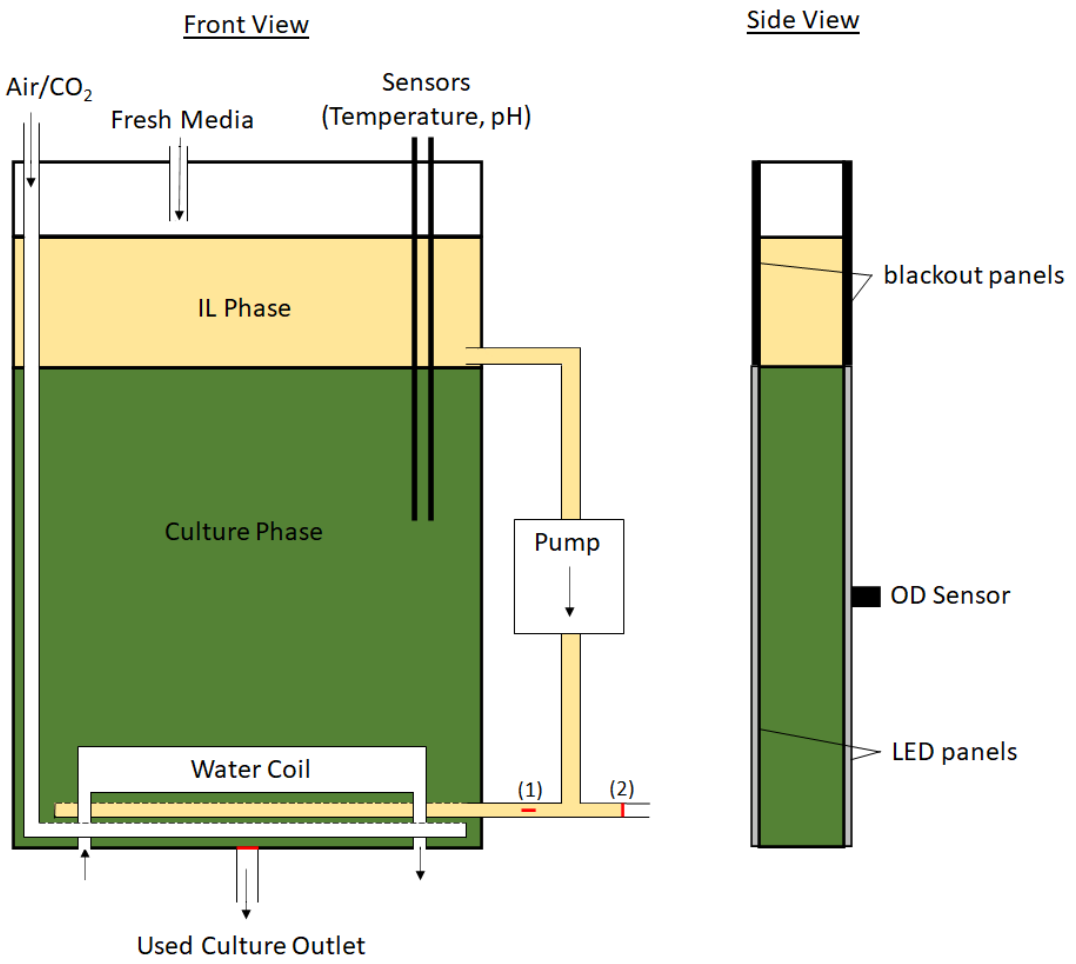

Fig. 61 - Schematic design of a continuous biphasic milking system. A chemostat system is proposed, with various sensors (temperature, pH, OD) included to monitor the culture conditions and keep them steady. Air (potentially enriched with CO_2) is sparged into the bottom of the culture. A similar technique should be utilised for the IL, enabling maximum contact with the culture. Taps (red lines) enable the IL flow to be redirected; tap (1) controls flow into the culture, while tap (2) enables IL removal for subsequent EPA extraction. Lighting is provided by LED panels.

Notably, this method provided greater mixing of solvents denser than the culture (since they sit below the culture and are somewhat carried into it by rising air bubbles), than those less dense than the culture. More efficient mixing of the solvent and culture would enable a greater surface area of solvent to be in contact with the culture, potentially increasing mass transfer and extraction efficiency. This, and the effect this has on solvent toxicity, should be explored in a rig capable of better mixing. The proposed rig (Fig. 61) addresses this by pumping solvents from their phase directly into the culture phase, through a meshed material to provide fine globules - akin to gas sparging. Clearly the viscosity of the solvent (particularly ILs, which are typically far more viscous than alkanes) will play a role in the efficacy of this process, and some experimentation would be required to determine the smallest solvent globule size that can be produced cost effectively. Note that it would not be

ideal to increase the temperature of the IL in order to reduce its viscosity, since this will cause unwanted heating of the algal culture. The most successful solvents identified so far (dodecane, tetradecane, $[P_{6\,6\,6\,14}][iC_8PO_4]$ and $[P_{6\,6\,6\,14}][AOT]$) were all less dense than the culture, and the rig design reflects this. If appropriate solvents are identified which are denser than the culture, then the rig design can be adapted to pump the solvent to the top of the culture. In the proposed design the IL pump can easily be switched off to provide culture "rest periods" as needed, and brief pauses of the IL and air pump can be utilised to minimise interference with OD readings. IL can be removed by a tap for subsequent EPA extraction and replaced with fresh (recycled) IL as needed.

The proposed photobioreactor (Fig. 61) is panel shaped (*i.e.* of comparatively smaller depth than height and width) to enable sufficient penetration of the light provided by front and back LED panels. These panels are specifically located to provide adequate culture lighting while avoiding lighting of the IL phase to minimise photooxidation of extracted PUFAs. While single IL and air lines are shown in the schematic, multiple lines could be incorporated to achieve desired mass transfer. It is thought that these will provide sufficient culture mixing to maintain a homogenous culture. However, if this is not the case then alternative means of mixing could be provided. Impellers are conventionally used in cylindrical chemostats to mix cultures. However, this is unlikely to provide efficient mixing in the panel-shaped proposed photobioreactor. Instead, a system where the culture is pumped around the panel could be more efficient. A rig of this design containing a total volume of around a few litres should be appropriate for experiments aimed at determining commercial viability of a milking process. However, a commercially operating rig would likely require volumes of hundreds or thousands of litres. This may best be achieved using multiple identical panel reactors, as opposed to a single large reactor. This would enable individual reactors to be taken out of commission for repairs and cleaning while others remain in use for continued milking. Larger scale systems require larger quantities of IL. Fortunately bulk quantities (>1 kg) of $[P_{6\,6\,6\,14}][iC_8PO_4]$ and $[P_{6\,6\,6\,14}][AOT]$ are available commercially from Iolitec.

8.6. Pulsed Electric Fields

Flow cytometry analysis proved to be more sensitive than the FLUOstar® plate reader and should be used in future work with the newly designed PEF chamber. However, the identity of the two cell populations observed by flow cytometry (Fig. 50) should be confirmed *via* cell sorting and subsequent microscopy in future work. Flow cytometry could

also be used to explore *T. minutus* fragmentation; a decrease in the number of events within the proposed *T. minutus* population (gate 2, Fig. 50), alongside an increase in events in the bacteria and cell debris population (gate 1, Fig. 50), would be indicative of this.

EPA, both as a free fatty acid and when esterified to glycerol (as it is usually found within cells), is far smaller than the proteins and DNA shown to be transported during electroporation. However, triglycerides of EPA and other fatty acids are stored along with pigments (which can serve as anti-oxidant protectants), into a hydrophobic lipid body up to 2 µm in diameter (Přibyl *et al.*, 2012). It is unclear at present whether pores large enough to enable whole lipid bodies to exit a cell can be reversibly produced in *T. minutus* membranes by PEF treatment. However, it should be noted that the size of the lipid bodies varies during culture growth, meaning that it is important to explore the ability of PEF treatments to extract EPA at different growth stages. The concentration at which surfactants begin to form micelles is known as the critical micelle concentration and is estimated to be between 60 - 100 µM for EPA (Ouellet *et al.*, 2009). It may be plausible to extract TAGs when they are present at these low concentrations before their agglutination into a lipid body. The effect of PEF treatments on the *T. minutus* cell wall, and what can traverse it, is unknown. One study demonstrated that the cell wall of *Chlamydomonas reinhardtii* posed a significant barrier to entry of Bovine Serum Albumin (66 kDa, estimated molecular radius 3.5 nm), but not to Calcein (623 Da, estimated molecular radius 0.6 nm) (Azencott *et al.*, 2007). Clearly, more needs to be known about the effect of the *T. minutus* cell wall in PEF based extractions. *T. minutus* cells lacking walls would be a valuable tool for exploring this and could potentially be produced *via* enzyme treatments or mutations.

The low water solubility of triglycerides also provides a significant barrier to their diffusion out of an electroporated cell and into the culture medium. Through gentle agitation (*e.g.* bubbling air) lipid bodies could potentially be disrupted into smaller micelles more capable of exiting the cell through the pores created by PEF treatment. In such a scenario, the lower density lipids could reach sufficient concentrations to form a separate phase to the culture medium, allowing easy removal. Subsequent PEF treatments could even be used to encourage their aggregation by electrocoagulation (An *et al.*, 2017). Alternatively, a solvent in which EPA is more soluble could be added to the medium, and cell contact with this could encourage the release of EPA. For this to work as a milking process the solvent must be biocompatible. Hence, the ability of the biocompatible solvents identified in this work (tetradecane, dodecane, $[P_{6\,6\,6\,14}][AOT]$ and $[P_{6\,6\,6\,14}][iC_8PO_4]$) to extract EPA from PEF treated

cells, and their effect on the viability of electropermeabilised cells, should be explored in future work.

8.7. Proposed Studies Using the Needle Array Rig

Unfortunately, construction of the new PEF chamber containing an array of needle electrodes was not finished. However, it should be used in future experiments. Firstly, it should be examined if pumping the culture at a desired speed through the rig, without PEF treatment, influences cell viability or permeabilization. This experiment could easily be conducted by pumping culture through the rig, then staining cells with SYTOX Green with subsequent flow cytometry analysis. Ideally no permeabilization would occur as a result of passing the culture through the rig without PEF treatment, but if that is not the case then this experiment provides a baseline level of permeabilization to take into account when conducting later experiments utilising PEF treatments. Then, a series of experiments should be conducted to confirm the extent of permeabilization and cell viability under varying PEF parameters. These could again be conducted using SYTOX green staining (after PEF treatment) and flow cytometry analysis to determine extent of permeabilisation, and culture growth to determine cell viability, as in the studies using the commercial cuvette-based rig. It would be interesting to see what differences arise due to the more homogenous electric field provided by the electrode array design. If ideal conditions are identified in which cells can be permeabilised without substantial loss in viability, then these conditions can be explored to determine if they enhance EPA extraction when using the biocompatible solvents identified here. This can be done by treating the culture in the PEF chamber, then immediately transferring it to a vial containing a solvent and providing gentle mixing, followed by removal of an aliquot of solvent on which to conduct transesterification and EPAEE quantification. The effect of solvent-culture contact time on extraction and cell viability should also be studied. Additionally, after a culture has been treated with PEF and removed from the chamber, the chamber could be washed with hexane. To determine if any TAGs were released form cells with PEF treatment alone (*i.e.* without solvent), EPAEE could be quantified in this hexane wash.

8.8. Proposed Pilot and Commercial Scale PEF Rig Designs

It is thought that IL exposure to PEF will cause degradation of ILs. Due to the high cost of ILs this should be avoided at all costs. However, it may be possible to avoid PEF induced degradation of the IL while treating the culture simply by exploiting their phase separation,

as illustrated in Fig. 62. In this rig design the electrodes do not extend into the IL phase, such that theoretically it is not exposed to a substantial electric field. However, it is unclear if this principle will work, and should be explored experimentally, potentially using a needle array rig modified to provide space for the IL. PEF treatments could then be conducted on the culture while phase-separated IL is present but not in contact with the electrodes, followed by NMR analysis of the IL to determine if any degradation products are present. Alkane solvents will not be prone to this issue since they are uncharged (and they are cheaper to replace should degradation occur). However, safety implications should also be considered

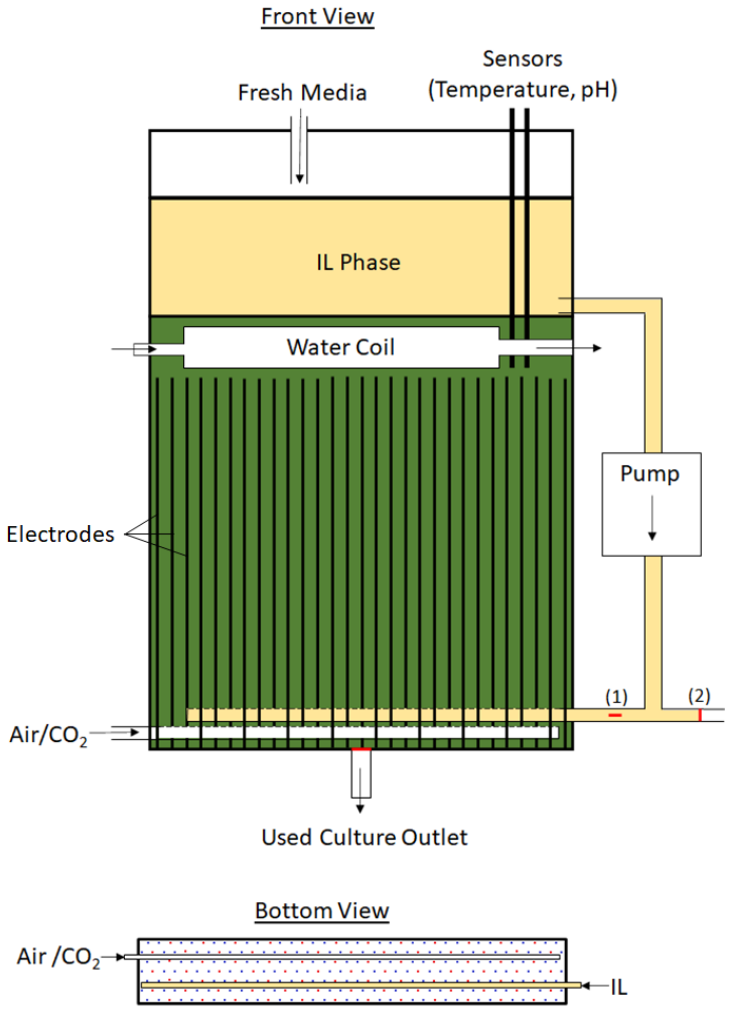

Fig. 62 - Schematic of a PEF and IL Milking Rig Consisting of a Single Chamber. In this design the IL remains in the reactor while the culture is treated with PEF. However, the electrodes do not extend into the IL phase, thereby hopefully avoiding exposure of the IL to PEF, which are thought to degrade the IL. IL is only pumped into the culture phase after PEF treatment. The needle electrode array should be arranged to minimise untreated culture volume and obstruction with other components (bottom view). Red dots represent cathodes, and blue dots represent anodes. As with previous designs light is provided to the culture phase only, by front and back LED panels, and the culture is maintained in stationary phase using chemostat principles.

with any solvent; arcing between the electrodes could occur and may be far more hazardous in the presence of such solvents.

Should this approach be viable then it enables the development of a combined PEF and solvent milking rig consisting of a single chamber (Fig. 62). In this system, the culture can be chemostatically maintained, and be PEF treated at desired intervals. After PEF treatment the IL can be pumped through the culture for a desired time. The IL pump can then be turned off to allow culture recovery and full IL phase separation before subsequent rounds of PEF treatment and IL exposure. The electrodes are arranged to minimise the volume of culture that is not between electrodes (*e.g.* between an electrode and the chamber edge), thereby maximising PEF treatment efficiency. The gas and IL supply lines could fit between rows of electrodes, but the water coil used for temperature control will be too large and must instead be isolated from the electrodes, leaving some culture volume untreated by each pulse. Electrodes could be individually removable through the bottom of the reactor for easy replacement and cleaning. As in the previous (IL only) design (Fig. 61), the culture phase can be lit by front and back LED panels while lighting of the IL phase is specifically avoided. If such a system is deemed unsuitable due to degradation of the solvent or safety concerns, then the IL would need to be added only after PEF treatment, and fully removed prior to subsequent PEF treatments. This could potentially be achieved by pumping the IL in and out.

Alternatively, a dual chamber design could be pursued (Fig. 63) whereby culture is chemostatically maintained and PEF treated in one chamber, then transferred to another for IL extraction, then back for culture recovery, and the whole process iterated. This system has the advantage of ensuring the extraction solvent is not present during PEF treatment, and enables extraction to be conducted entirely in the dark, with the solvent remaining in the dark throughout the process. This reduces the likelihood of PUFA photooxidation occurring. Furthermore, if the required solvent-culture contact time is sufficiently short, aeration of the chamber may also be unnecessary, further reducing PUFA oxidation potential. However, this design relies upon PEF treated cells remaining permeabilised for sufficient duration to allow their transfer to a second chamber and subsequent extraction.

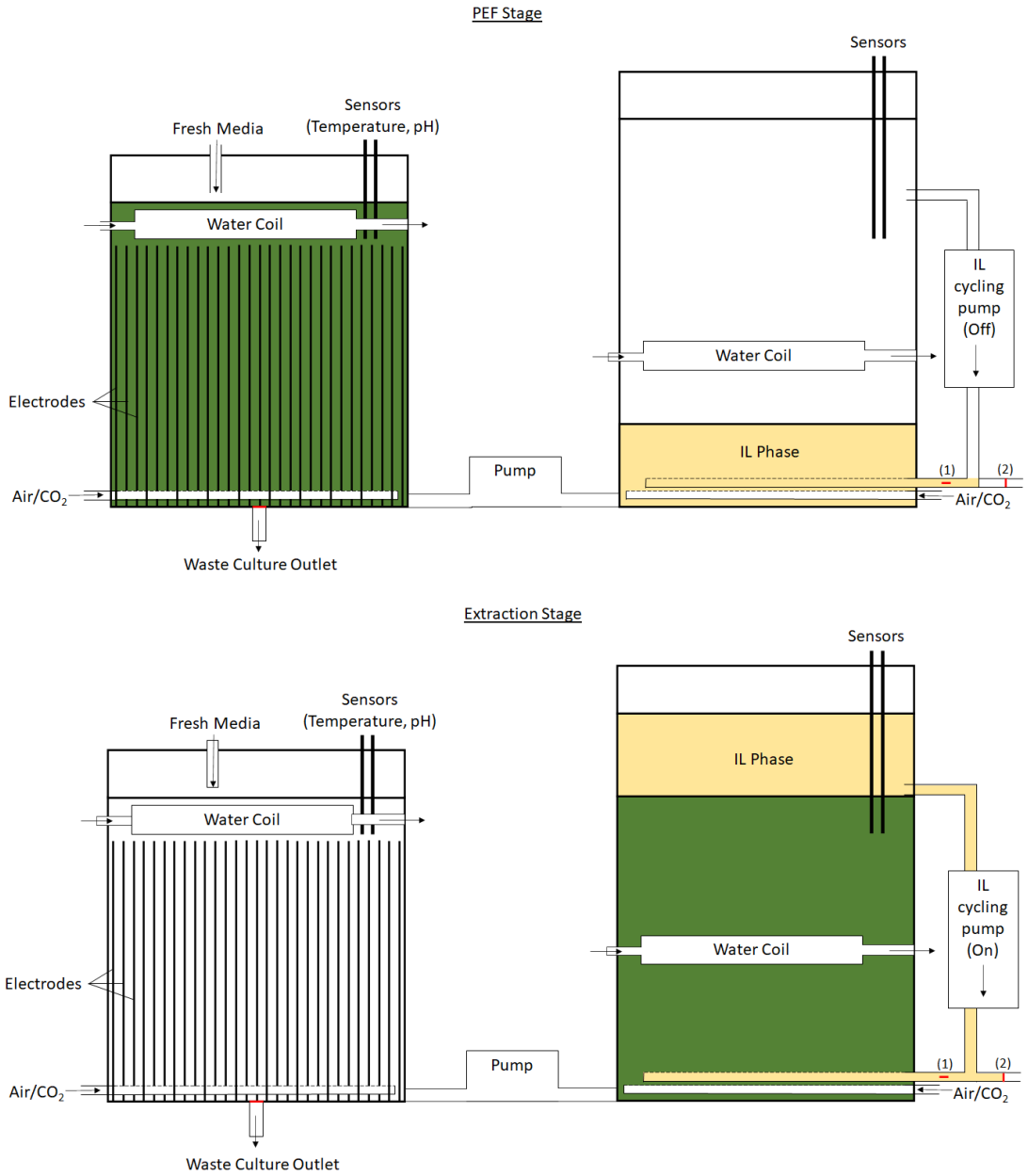

Fig. 63 Schematic of a PEF and IL Milking rig Consisting of two Chambers. In this design the IL is separated from the PEF apparatus to prevent its electrodegradation. Culture is chemostatically maintained in the first chamber, where it is PEF treated. After treatment, the culture is pumped into a second chamber containing the IL, where the IL is cycled through the culture for extraction. After extraction and full phase separation, the culture is pumped back into the initial chamber. Depending on the IL-culture contact time desired, the second chamber could be unlit and without an air supply, drastically reducing the likelihood of PUFA oxidation within the IL.

9. Conclusions

Top agar and small-scale liquid screens were successfully used in a tiered approach to identify ILs non-toxic to *T. minutus* that could potentially be used in a milking strategy. These methods enabled the analysis of 62 ILs at a fraction of the time and cost that would be required to test them all at a greater scale. Subsequent higher volume experiments identified two ILs biocompatible with *T. minutus*, $[P_{6\,6\,6\,14}][AOT]$ and $[P_{6\,6\,6\,14}][iC_8PO_4]$, alongside tetradecane and dodecane. Having identified these ILs, analogous structures could be synthesised to increase the scope of solvents available for this strategy. The identification of these biocompatible solvents is a significant step towards a biphasic system for milking fatty acids from *T. minutus*. The ability of these solvents to extract EPA from cells can be explored in future work using the HPLC-UV method presented here to quantify EPA in ILs.

The ability of PEF treatments to permeabilise *T. minutus* cells was successfully demonstrated using the SYTOX Green stain and flow cytometry analysis. The threshold for permeabilization of *T. minutus* was found to be approximately 3 kV/cm. A method for determining the extent of cell viability after PEF treatments, using cell counts of recovering cultures, has also been successfully demonstrated. EPA extraction *via* PEF could not be demonstrated due to the small culture treatment volumes of the commercially available electroporator. However, a larger treatment chamber was designed to enable further exploration of PEF for milking fatty acids from *T. minutus*, using the methods that have been outlined here.

The results presented here represent a significant step forwards in developing a process for milking EPA from *T. minutus*. In order to fully realise this process, future work should focus on quantifying the EPA extracted by the biocompatible solvents identified here, both on PEF-treated and untreated cultures.

10. Bibliography

AFI, L., METZGER, P., LARGEAU, C., CONNAN, J., BERKALOFF, C. & ROUSSEAU, B. 1996. Bacterial degradation of green microalgae: incubation of *Chlorella emersonii* and *Chlorella vulgaris* with *Pseudomonas oleovorans* and *Flavobacterium aquatile*. *Org. Geochem.,* 25**,** 117-130.

AGHAPOUR AKTIJ, S., ZIREHPOUR, A., MOLLAHOSSEINI, A., TAHERZADEH, M. J., TIRAFERRI, A. & RAHIMPOUR, A. 2020. Feasibility of membrane processes for the recovery and purification of bio-based volatile fatty acids: A comprehensive review. *J. Ind. Eng. Chem.,* 81**,** 24-40.

AGUILERA-HERRADOR, E., LUCENA, R., CARDENAS, S. & VALCARCEL, M. 2008. Direct coupling of ionic liquid based single-drop microextraction and GC/MS. *Anal. Chem.,* 80**,** 793-800.

AHMAD, N., MICHOUX, F., LÖSSL, A. G. & NIXON, P. J. 2016. Challenges and perspectives in commercializing plastid transformation technology. *J. Exp. Bot.,* 67**,** 5945-5960.

ALFALAVAL. 2015. *Algae Harvesting* [Online]. Available: https://www.alfalaval.com/products/separation/centrifugal-separators/separators/ [Accessed 30/10/21].

AMERICAN OIL CHEMIST'S SOCIETY 2017. Fatty Acid Composition of Marine Oils by GLC. *Official methods and recommended practices of the AOCS,* Official Method Ce 1b-89.

AN, C., HUANG, G., YAO, Y. & ZHAO, S. 2017. Emerging usage of electrocoagulation technology for oil removal from wastewater: A review. *Sci. Total Environ.,* 579**,** 537-556.

ANNÉ, J., VRANCKEN, K., VAN MELLAERT, L., VAN IMPE, J. & BERNAERTS, K. 2014. Protein secretion biotechnology in Gram-positive bacteria with special emphasis on *Streptomyces lividans*. *BBA - Mol. Cell Res.,* 1843**,** 1750-1761.

ARCHER, D. G. & WANG, P. 1990. The Dielectric Constant of Water and Debye-Hückel Limiting Law Slopes. *J. Phys. Chem. Ref. Data,* 19**,** 371-411.

AUTEN, R. L. & DAVIS, J. M. 2009. Oxygen Toxicity and Reactive Oxygen Species: The Devil Is in the Details. *Pediatr. Res.,* 66**,** 121-127.

AZENCOTT, H. R., PETER, G. F. & PRAUSNITZ, M. R. 2007. Influence of the Cell Wall on Intracellular Delivery to Algal Cells by Electroporation and Sonication. *Ultrasound Med. Biol.,* 33**,** 1805-1817.

BACELLAR, I. O. L. & BAPTISTA, M. S. 2019. Mechanisms of Photosensitized Lipid Oxidation and Membrane Permeabilization. *ACS Omega,* 4**,** 21636-21646.

BASF. 2021. *BASIL™—BASF's Processes Based on Ionic Liquids* [Online]. Available: https://www.sigmaaldrich.com/GB/en/technical-documents/technical-article/chemistry-and-synthesis/reaction-design-and-optimization/basil-basf-s-processes [Accessed 12/11/21].

BATEMAN, J. M. & PURTON, S. 2000. Tools for chloroplast transformation in *Chlamydomonas*: expression vectors and a new dominant selectable marker. *MGG,* 263**,** 404-410.

BENEDETTO, A. 2017. Room-temperature ionic liquids meet bio-membranes: the state-of-the-art. *Biophys. Rev.,* 9**,** 309-320.

BENEDETTO, A., BINGHAM, R. J. & BALLONE, P. 2015. Structure and dynamics of POPC bilayers in water solutions of room temperature ionic liquids. *J. Chem. Phys.,* 142.

BENEDETTO, A., HEINRICH, F., GONZALEZ, M. A., FRAGNETO, G., WATKINS, E. & BALLONE, P. 2014. Structure and Stability of Phospholipid Bilayers Hydrated by a Room-Temperature Ionic Liquid/Water Solution: A Neutron Reflectometry Study. *J. Phys. Chem. B,* 118**,** 12192-12206.

BINGHAM, R. J. & BALLONE, P. 2012. Computational Study of Room-Temperature Ionic Liquids Interacting with a POPC Phospholipid Bilayer. *J. Phys. Chem. B,* 116**,** 11205-11216.

BJORNSSON, W. J., MACDOUGALL, K. M., MELANSON, J. E., O'LEARY, S. J. B. & MCGINN, P. J. 2012. Pilot-scale supercritical carbon dioxide extractions for the recovery of triacylglycerols from microalgae: a practical tool for algal biofuels research. *J. Appl. Phycol.,* 24**,** 547-555.

BLANCHARD, L. A., HANCU, D., BECKMAN, E. J. & BRENNECKE, J. F. 1999. Green processing using ionic liquids and CO_2. *Nature,* 399**,** 28-29.

BOER, K., MOHEIMANI, N., BOROWITZKA, M. & BAHRI, P. 2012. Extraction and conversion pathways for microalgae to biodiesel: a review focused on energy consumption. *J. Appl. Phycol.,* 24**,** 1681-1698.

BOGORAD, L. 2000. Engineering chloroplasts: an alternative site for foreign genes, proteins, reactions and products. *Trends Biotechnol.,* 18**,** 257-263.

BRAUN, E. & AACH, H. G. 1975. Enzymatic degradation of the cell wall of *Chlorella spp. Planta,* 126**,** 181-185.

CEPÁK, V., PŘIBYL, P., KOHOUTKOVÁ, J. & KAŠTÁNEK, P. 2014. Optimization of cultivation conditions for fatty acid composition and EPA production in the eustigmatophycean microalga *Trachydiscus minutus*. *J. Appl. Phycol.,* 26**,** 181-190.

CHANDRAN, S. & SINGH, R. S. 2007. Comparison of various international guidelines for analytical method validation. *Pharmazie,* 62**,** 4-14.

CHANG, D. C. & REESE, T. S. 1990. Changes in membrane structure induced by electroporation as revealed by rapid-freezing electron microscopy. *Biophys. J.,* 58**,** 1-12.

CHEN, B., MCCLEMENTS, D. J. & DECKER, E. A. 2011. Minor components in food oils: a critical review of their roles on lipid oxidation chemistry in bulk oils and emulsions. *Crit. Rev. Food Sci.,* 51**,** 901-916.

CHEN, C.-Y., BAI, M.-D. & CHANG, J.-S. 2013. Improving microalgal oil collecting efficiency by pretreating the microalgal cell wall with destructive bacteria. *Biochem. Eng. J.,* 81**,** 170-176.

CHEN, G. 2004. Electrochemical technologies in wastewater treatment. *Sep. Purif. Technol.,* 38**,** 11-41.

CHENG, C.-H., DU, T.-B., PI, H.-C., JANG, S.-M., LIN, Y.-H. & LEE, H.-T. 2011. Comparative study of lipid extraction from microalgae by organic solvent and supercritical CO_2. *Bioresour. Technol.,* 102**,** 10151-10153.

CHENG, J. 2016. Lipid oxidation in meat. *Nutr. Food Sci.,* 6**,** 494.

CHENG, P., JI, B., GAO, L., ZHANG, W., WANG, J. & LIU, T. 2013. The growth, lipid and hydrocarbon production of *Botryococcus braunii* with attached cultivation. *Bioresour. Technol.,* 138**,** 95-100.

CHENG, Q., DAY, A., DOWSON-DAY, M., SHEN, G. F. & DIXON, R. 2005. The *Klebsiella pneumoniae* nitrogenase Fe protein gene (nifH) functionally substitutes for the chlL gene in *Chlamydomonas reinhardtii*. *Biochem. Biophys. Res. Commun.,* 329**,** 966-975.

CHENG, Y. S., LABAVITCH, J. M. & VANDERGHEYNST, J. S. 2015. Elevated CO_2 concentration impacts cell wall polysaccharide composition of green microalgae of the genus *Chlorella*. *Lett. Appl. Microbiol.,* 60**,** 1-7.

CHEW, G., BOGGS, T., DYKES, H. W. & DOHERTY, S. 2013. *Method and Apparatus for Iterative Lysis and Extraction of Algae*. Patent Number: US20130072701 A1.

CHEW, G., REICH, A., DYKES, H. W. & DI SALVO, R. 2011. *Method and Apparatus for Processing Algae*. Patent Number: US20110192792 A1.

CHIOCCIOLI, M., HANKAMER, B. & ROSS, I. L. 2014. Flow cytometry pulse width data enables rapid and sensitive estimation of biomass dry weight in the microalgae *Chlamydomonas reinhardtii* and *Chlorella vulgaris*. *PLoS One,* 9**,** e97269.

CHO, C.-W., PHAM, T. P. T., JEON, Y.-C., VIJAYARAGHAVAN, K., CHOE, W.-S. & YUN, Y.-S. 2007. Toxicity of imidazolium salt with anion bromide to a phytoplankton *Selenastrum capricornutum*: Effect of alkyl-chain length. *Chemosphere,* 69**,** 1003-1007.

CHO, C.-W., PHUONG THUY PHAM, T., JEON, Y.-C. & YUN, Y.-S. 2008. Influence of anions on the toxic effects of ionic liquids to a phytoplankton *Selenastrum capricornutum*. *Green Chem.,* 10**,** 67-72.

CHOI, S.-A., OH, Y.-K., JEONG, M.-J., KIM, S. W., LEE, J.-S. & PARK, J.-Y. 2014. Effects of ionic liquid mixtures on lipid extraction from *Chlorella vulgaris*. *Renewable Energy,* 65**,** 169-174.

CHOUDHURY, A. R., WINTERTON, N., STEINER, A., COOPER, A. I. & JOHNSON, K. A. 2005. In situ Crystallization of Low-Melting Ionic Liquids. *J. Am. Chem. Soc.,* 127**,** 16792-16793.

CIUDAD, G., RUBILAR, O., AZÓCAR, L., TORO, C., CEA, M., TORRES, Á., RIBERA, A. & NAVIA, R. 2014. Performance of an enzymatic extract in *Botrycoccus braunii* cell wall disruption. *J. Biosci. Bioeng.,* 117**,** 75-80.

CORNMELL, R. J., WINDER, C. L., SCHULER, S., GOODACRE, R. & STEPHENS, G. 2008. Using a biphasic ionic liquid/water reaction system to improve oxygenase-catalysed biotransformation with whole cells. *Green Chem.,* 10**,** 685-691.

CRAMPON, C., MOUAHID, A., TOUDJI, S.-A. A., LÉPINE, O. & BADENS, E. 2013. Influence of pretreatment on supercritical CO_2 extraction from *Nannochloropsis oculata*. *J. Supercrit. Fluid.,* 79**,** 337-344.

DAI, Y.-M., CHEN, K.-T. & CHEN, C.-C. 2014. Study of the microwave lipid extraction from microalgae for biodiesel production. *Chem. Eng. J.,* 250**,** 267-273.

DASILVA, G., PAZOS, M., GARCÍA-EGIDO, E., GALLARDO, J. M., RODRÍGUEZ, I., CELA, R. & MEDINA, I. 2015. Healthy effect of different proportions of marine ω-3 PUFAs EPA and DHA supplementation in Wistar rats: Lipidomic biomarkers of oxidative stress and inflammation. *J. Nutr. Biochem.,* 26**,** 1385-1392.

DE TOMMASI, E., GIELIS, J. & ROGATO, A. 2017. Diatom Frustule Morphogenesis and Function: a Multidisciplinary Survey. *Mar. Genomics,* 35**,** 1-18.

DI SALVO, R., REICH, A. & TEIXEIRA, R. 2012. *Method and apparatus using an active ionic liquid for algae biofuel harvest and extraction*. Patent Number: US8303818 B2.

DIAMOND, L. W. & AKINFIEV, N. N. 2003. Solubility of CO_2 in water from −1.5 to 100 °C and from 0.1 to 100 MPa: evaluation of literature data and thermodynamic modelling. *Fluid Phase Equilib.,* 208**,** 265-290.

DODDS, E. D., MCCOY, M. R., REA, L. D. & KENNISH, J. M. 2005. Gas chromatographic quantification of fatty acid methyl esters: Flame ionization detection vs. Electron impact mass spectrometry. *Lipids,* 40**,** 419-428.

DOMÍNGUEZ, R., PATEIRO, M., GAGAOUA, M., BARBA, F. J., ZHANG, W. & LORENZO, J. M. 2019. A Comprehensive Review on Lipid Oxidation in Meat and Meat Products. *Antioxidants,* 8**,** 429.

DORON, L., SEGAL, N. A. & SHAPIRA, M. 2016. Transgene Expression in Microalgae-From Tools to Applications. *Front Plant Sci,* 7**,** 505-505.

EARLE, M. J., ESPERANÇA, J. M. S. S., GILEA, M. A., CANONGIA LOPES, J. N., REBELO, L. P. N., MAGEE, J. W., SEDDON, K. R. & WIDEGREN, J. A. 2006. The distillation and volatility of ionic liquids. *Nature,* 439**,** 831-834.

ECKELBERRY, N. 2013. *Systems and methods for harvesting and dewatering algae*. Patent Number: WO2013116357 A1. PCT/US2013/023878.

ECONOMOU, C., WANNATHONG, T., SZAUB, J. & PURTON, S. 2014. A simple, low-cost method for chloroplast transformation of the green alga *Chlamydomonas reinhardtii*. *Methods Mol. Biol.,* 1132**,** 401-411.

EING, C., GOETTEL, M., STRAESSNER, R., GUSBETH, C. & FREY, W. 2013. Pulsed Electric Field Treatment of Microalgae; Benefits for Microalgae Biomass Processing. *IEEE T. Plasma Sci.,* 41**,** 2901-2907.

EROGLU, E. & MELIS, A. 2010. Extracellular terpenoid hydrocarbon extraction and quantitation from the green microalgae *Botryococcus braunii*. *Bioresour. Technol.,* 101**,** 2359-2366.

ESCOFFRE, J.-M., PORTET, T., WASUNGU, L., TEISSIÉ, J., DEAN, D. & ROLS, M.-P. 2008. What is (Still not) Known of the Mechanism by Which Electroporation Mediates Gene Transfer and Expression in Cells and Tissues. *Mol. Biotechnol.,* 41**,** 286-295.

EVANS, K. O. 2006. Room-temperature ionic liquid cations act as short-chain surfactants and disintegrate a phospholipid bilayer. *Colloids Surf. Physicochem. Eng. Aspects,* 274**,** 11-17.

FLIEGER, J. & CZAJKOWSKA-ŻELAZKO, A. 2012. Identification of ionic liquid components by RP-HPLC with diode array detector using chaotropic effect and perturbation technique. *J. Sep. Sci.,* 35**,** 248-255.

FOOTE, C. S. 1991. Definition of Type I and Type II Photosensitized Oxidation. *Photochem. Photobiol.,* 54**,** 659.

FRENZ, J., LARGEAU, C. & CASADEVALL, E. 1989a. Hydrocarbon recovery by extraction with a biocompatible solvent from free and immobilized cultures of *Botryococcus braunii*. *Enzyme Microb.Tech.,* 11**,** 717-724.

FRENZ, J., LARGEAU, C., CASADEVALL, E., KOLLERUP, F. & DAUGULIS, A. J. 1989b. Hydrocarbon recovery and biocompatibility of solvents for extraction from cultures of *Botryococcus braunii*. *Biotechnol. Bioeng.,* 34**,** 755-762.

FUJITA, K., KOBAYASHI, D., NAKAMURA, N. & OHNO, H. 2013. Direct dissolution of wet and saliferous marine microalgae by polar ionic liquids without heating. *Enzyme Microb. Technol.,* 52**,** 199-202.

GABRIEL, B. & TEISSIÉ, J. 1999. Time Courses of Mammalian Cell Electropermeabilization Observed by Millisecond Imaging of Membrane Property Changes during the Pulse. *Biophys. J.,* 76**,** 2158-2165.

GAL, N., MALFERARRI, D., KOLUSHEVA, S., GALLETTI, P., TAGLIAVINI, E. & JELINEK, R. 2012. Membrane interactions of ionic liquids: Possible determinants for biological activity and toxicity. *Biochim. Biophys. Acta,* 1818**,** 2967-2974.

GAN, L., CHEN, S. & JENSEN, G. J. 2008. Molecular organization of Gram-negative peptidoglycan. *P. Natl. Acad. Sci. USA,* 105**,** 18953-18957.

GAO, B., YANG, J., LEI, X., XIA, S., LI, A. & ZHANG, C. 2016. Characterization of cell structural change, growth, lipid accumulation, and pigment profile of a novel oleaginous microalga, *Vischeria stellata* (Eustigmatophyceae), cultured with different initial nitrate supplies. *J. Appl. Phycol.,* 28**,** 821-830.

GAO, S., YANG, J., TIAN, J., MA, F., TU, G. & DU, M. 2010. Electro-coagulation–flotation process for algae removal. *J. Hazard. Mater.,* 177**,** 336-343.

GARRISON, A. & HUIGENS, R. 2016. Eradicating Bacterial Biofilms with Natural Products and Their Inspired Analogues that Operate Through Unique Mechanisms. *Curr. Top. Med. Chem.,* 17**,** PMID: 27966398.

GE, D. & LEE, H. K. 2013. Ionic liquid based dispersive liquid-liquid microextraction coupled with micro-solid phase extraction of antidepressant drugs from environmental water samples. *J. Chromatogr. A,* 1317**,** 217-222.

GECIOVA, J., BURY, D. & JELEN, P. 2002. Methods for disruption of microbial cells for potential use in the dairy industry—a review. *Int. Dairy J.,* 12**,** 541-553.

GEHL, J. 2003. Electroporation: theory and methods, perspectives for drug delivery, gene therapy and research. *Acta Physiol. Scand.,* 177**,** 437-447.

GERDE, J. A., MONTALBO-LOMBOY, M., YAO, L., GREWELL, D. & WANG, T. 2012. Evaluation of microalgae cell disruption by ultrasonic treatment. *Bioresour. Technol.,* 125**,** 175-181.

GERKEN, H., DONOHOE, B. & KNOSHAUG, E. 2013. Enzymatic cell wall degradation of *Chlorella vulgaris* and other microalgae for biofuels production. *Planta,* 237**,** 239-253.

GIBSON, B., WILSON, D. J., FEIL, E. & EYRE-WALKER, A. 2018. The distribution of bacterial doubling times in the wild. *P. Natl. Acad. Sci. Biol.,* 285**,** 20180789.

GIGOVA, L., IVANOVA, N., GACHEVA, G., ANDREEVA, R. & FURNADZHIEVA, S. 2012. Response of *Trachydiscus minutus* (Xanthophyceae) to Temperature and Light. *J. Phycol.,* 48**,** 85-93.

GIMENES DE SOUZA, C., TORRES DE ARAÚJO, M., CAVALCANTE DOS SANTOS, R., FRANÇA DE ANDRADE, D., VASCONCELLO DA SILVA, B. & D'AVILA, L. A. 2018. Analysis and Quantitation of Fatty Acid Methyl Esters in Biodiesel by High-Performance Liquid Chromatography. *Energy Fuels,* 32**,** 11547-11554.

GOETTEL, M., EING, C., GUSBETH, C., STRAESSNER, R. & FREY, W. 2013. Pulsed electric field assisted extraction of intracellular valuables from microalgae. *Algal Res.,* 2**,** 401-408.

GORDON, C. M., MULDOON, M. J., WAGNER, M., HILGERS, C., DAVIS JR, J. H. & WASSERSCHEID, P. 2007. *Ionic Liquids in Synthesis (2nd Edition).* Synthesis and Purification, Pages: 7-55. Wiley-VCH Verlag GmbH & Co. KGaA, Weinheim

GRAF, R., ANZALI, S., BUENGER, J., PFLUECKER, F. & DRILLER, H. 2008. The multifunctional role of ectoine as a natural cell protectant. *Clin. Dermatol.,* 26**,** 326-333.

GRANDVIEWRESEARCH. 2020. *Omega 3 Market Size, Share & Trends Analysis Report By Type (EPA, DHA, ALA), By Source (Marine Source, Plant Source), By Application, By Region, And Segment Forecasts, 2020 - 2027* [Online]. Available: https://www.grandviewresearch.com/industry-analysis/omega-3-market [Accessed 09/07/2020 2020].

GREENLY, J. M. & TESTER, J. W. 2015. Ultrasonic cavitation for disruption of microalgae. *Bioresour. Technol.,* 184**,** 276-279.

GRIMI, N., DUBOIS, A., MARCHAL, L., JUBEAU, S., LEBOVKA, N. I. & VOROBIEV, E. 2014. Selective extraction from microalgae *Nannochloropsis sp.* using different methods of cell disruption. *Bioresour. Technol.,* 153**,** 254-259.

GUARRASI, V., MANGIONE, M. R., SANFRATELLO, V., MARTORANA, V. & BULONE, D. 2010. Quantification of underivatized fatty acids from vegetable oils by HPLC with UV detection. *J. Chromatogr. Sci.,* 48**,** 663-668.

GUDE, V., PATIL, P., MARTINEZ-GUERRA, E., DENG, S. & NIRMALAKHANDAN, N. 2013. Microwave energy potential for biodiesel production. *Sustain. Chem. Process.,* 1**,** 5.

GUTIÉRREZ, C. L., GIMPEL, J., ESCOBAR, C., MARSHALL, S. H. & HENRÍQUEZ, V. 2012. Chloroplast genetic tool for the green microalgae *Haematococcus pluvialis*. *J. Phycol.,* 48**,** 976-983.

GUTOWSKI, K. E., BROKER, G. A., WILLAUER, H. D., HUDDLESTON, J. G., SWATLOSKI, R. P., HOLBREY, J. D. & ROGERS, R. D. 2003. Controlling the Aqueous Miscibility of Ionic Liquids: Aqueous Biphasic Systems of Water-Miscible Ionic Liquids and Water-Structuring Salts for Recycle, Metathesis, and Separations. *JACS,* 125**,** 6632-6633.

HADRICH, B., AKREMI, I., DAMMAK, M., BARKALLAH, M., FENDRI, I. & ABDELKAFI, S. 2018. Optimization of lipids' ultrasonic extraction and production from *Chlorella sp.* using response-surface methodology. *Lipids Health Dis.,* 17**,** 87-87.

HARVEY, D. 2011. Analytical chemistry 2.0--an open-access digital textbook. *Anal. Bioanal. Chem.,* 399**,** 149-152.

HAYHURST, E. J., KAILAS, L., HOBBS, J. K. & FOSTER, S. J. 2008. Cell wall peptidoglycan architecture in *Bacillus subtilis*. *Proc. Natl. Acad. Sci. USA,* 105**,** 14603-14608.

HEASMAN, M., DIEMAR, J., O'CONNOR, W., SUSHAMES, T. & FOULKES, L. 2000. Development of extended shelf-life microalgae concentrate diets harvested by centrifugation for bivalve molluscs – a summary. *Aquac. Res.,* 31**,** 637-659.

HEATLEY, N. G. 1944. A method for the assay of penicillin. *Biochem. J.,* 38**,** 61-65.

HEJAZI, M. A., DE LAMARLIERE, C., ROCHA, J. M., VERMUE, M., TRAMPER, J. & WIJFFELS, R. H. 2002. Selective extraction of carotenoids from the microalga *Dunaliella salina* with retention of viability. *Biotechnol. Bioeng.,* 79**,** 29-36.

HEJAZI, M. A., HOLWERDA, E. & WIJFFELS, R. H. 2004. Milking microalga *Dunaliella salina* for beta-carotene production in two-phase bioreactors. *Biotechnol. Bioeng.,* 85**,** 475-481.

HENSLEE, B. E., MORSS, A., HU, X., LAFYATIS, G. P. & JAMES LEE, L. 2014. Cell-cell proximity effects in multi-cell electroporation. *Biomicrofluidics,* 8**,** 052002.

HERBERT, D., ELSWORTH, R. & TELLING, R. C. 1956. The Continuous Culture of Bacteria; a Theoretical and Experimental Study. *Microbiology,* 14**,** 601-622.

HERRERO, M., CIFUENTES, A. & IBAÑEZ, E. 2006. Sub- and supercritical fluid extraction of functional ingredients from different natural sources: Plants, food-by-products, algae and microalgae: A review. *Food Chem.,* 98**,** 136-148.

HIBINO, M., ITOH, H. & KINOSITA, K. 1993. Time courses of cell electroporation as revealed by submicrosecond imaging of transmembrane potential. *Biophys. J.,* 64**,** 1789-1800.

HILLEN, L. W., POLLARD, G., WAKE, L. V. & WHITE, N. 1982. Hydrocracking of the oils of *Botryococcus braunii* to transport fuels. *Biotechnol. Bioeng.,* 24**,** 193-205.

HORNER, R. A. 2002. *A Taxonomic Guide to Some Common Marine Phytoplankton* Pages: 161-162. Biopress, Bristol

HOU, X.-D., LIU, Q.-P., SMITH, T. J., LI, N. & ZONG, M.-H. 2013. Evaluation of Toxicity and Biodegradability of Cholinium Amino Acids Ionic Liquids. *PLoS One,* 8**,** e59145.

HOUGH, W. L., SMIGLAK, M., RODRIGUEZ, H., SWATLOSKI, R. P., SPEAR, S. K., DALY, D. T., PERNAK, J., GRISEL, J. E., CARLISS, R. D., SOUTULLO, M. D., DAVIS, J. J. H. & ROGERS, R. D. 2007. The third evolution of ionic liquids: active pharmaceutical ingredients. *New J. Chem.,* 31**,** 1429-1436.

HU, Q., SOMMERFELD, M., JARVIS, E., GHIRARDI, M., POSEWITZ, M., SEIBERT, M. & DARZINS, A. 2008. Microalgal triacylglycerols as feedstocks for biofuel production: perspectives and advances. *The Plant Journal,* 54**,** 621-639.

HUANG, K. C., MUKHOPADHYAY, R., WEN, B., GITAI, Z. & WINGREEN, N. S. 2008. Cell shape and cell-wall organization in Gram-negative bacteria. *Proc. Natl. Acad. Sci. USA,* 105**,** 19282-19287.

JAHOUACH-RABAI, W., TRABELSI, M., VAN HOED, V., ADAMS, A., VERHÉ, R., DE KIMPE, N. & FRIKHA, M. H. 2008. Influence of bleaching by ultrasound on fatty acids and minor compounds of olive oil. Qualitative and quantitative analysis of volatile compounds (by SPME coupled to GC/MS). *Ultrason. Sonochem.,* 15**,** 590-597.

JAMES, A. T. & MARTIN, A. J. P. 1956. Gas–liquid chromatography: the separation and identification of the methyl esters of saturated and unsaturated acids from formic acid to octadecanoic acid. *Biochem. J.,* 63**,** 144-152.

JEONG, S., HA, S. H., HAN, S.-H., LIM, M.-C., KIM, S. M., KIM, Y.-R., KOO, Y.-M., SO, J.-S. & JEON, T.-J. 2012. Elucidation of molecular interactions between lipid membranes and ionic liquids using model cell membranes. *Soft Matter,* 8**,** 5501-5506.

JIN, B., DUAN, P., XU, Y., WANG, F. & FAN, Y. 2013. Co-liquefaction of micro- and macroalgae in subcritical water. *Bioresour. Technol.,* 149**,** 103-110.

JING, B., LAN, N., QIU, J. & ZHU, Y. 2016. Interaction of Ionic Liquids with a Lipid Bilayer: A Biophysical Study of Ionic Liquid Cytotoxicity. *J. Phys. Chem. B,* 120**,** 2781-2789.

KILULYA, K. F., MSAGATI, T. A. M. & MAMBA, B. B. 2014. Ionic Liquid-Based Extraction of Fatty Acids from Blue-Green Algal Cells Enhanced by Direct Transesterification and Determination Using GC × GC-TOFMS. *Chromatographia,* 77**,** 479-486.

KIM, S., KIM, H., KO, D., YAMAOKA, Y., OTSURU, M., KAWAI-YAMADA, M., ISHIKAWA, T., OH, H.-M., NISHIDA, I., LI-BEISSON, Y. & LEE, Y. 2013. Rapid Induction of Lipid Droplets in *Chlamydomonas reinhardtii* and *Chlorella vulgaris* by Brefeldin A. *PLoS One,* 8**,** e81978.

KIM, Y.-H., CHOI, Y.-K., PARK, J., LEE, S., YANG, Y.-H., KIM, H. J., PARK, T.-J., HWAN KIM, Y. & LEE, S. H. 2012. Ionic liquid-mediated extraction of lipids from algal biomass. *Bioresour. Technol.,* 109**,** 312-315.

KINDLE, K. L., RICHARDS, K. L. & STERN, D. B. 1991. Engineering the chloroplast genome: techniques and capabilities for chloroplast transformation in *Chlamydomonas reinhardtii*. *Proc. Natl. Acad. Sci. USA,* 88**,** 1721-1725.

KLEINEGRIS, D. M., VAN ES, M. A., JANSSEN, M., BRANDENBURG, W. A. & WIJFFELS, R. H. 2011. Phase toxicity of dodecane on the microalga *Dunaliella salina*. *J. Appl. Phycol.,* 23**,** 949-958.

KOÇ, A., WHEELER, L. J., MATHEWS, C. K. & MERRILL, G. F. 2004. Hydroxyurea Arrests DNA Replication by a Mechanism That Preserves Basal dNTP Pools. *J. Biol. Chem.,* 279**,** 223-230.

KOL, M. A., DE KRUIJFF, B. & DE KROON, A. I. P. M. 2002. Phospholipid flip-flop in biogenic membranes: what is needed to connect opposite sides. *Semin. Cell Dev. Biol.,* 13**,** 163-170.

KÖNIG, A., STEPANSKI, M., KUSZLIK, A., KEIL, P. & WELLER, C. 2008. Ultra-purification of ionic liquids by melt crystallization. *Chem. Eng. Res. Des.,* 86**,** 775-780.

KONTRO, I., SVEDSTRÖM, K., DUŠA, F., AHVENAINEN, P., RUOKONEN, S.-K., WITOS, J. & WIEDMER, S. K. 2016. Effects of phosphonium-based ionic liquids on phospholipid membranes studied by small-angle X-ray scattering. *Chem. Phys. Lipids,* 201**,** 59-66.

KOTNIK, T. & MIKLAVCIC, D. 2000. Analytical description of transmembrane voltage induced by electric fields on spheroidal cells. *Biophys. J.,* 79**,** 670-679.

KRÖCKEL, J. & KRAGL, U. 2003. Nanofiltration for the Separation of Nonvolatile Products from Solutions Containing Ionic Liquids. *Chem. Eng. Technol.,* 26**,** 1166-1168.

KUCMANOVÁ, A. & GERULOVÁ, K. 2019. Microalgae Harvesting: A Review. *Research Papers Faculty of Materials Science and Technology Slovak University of Technology,* 27**,** 129-143.

KULACKI, K. J. & LAMBERTI, G. A. 2008. Toxicity of imidazolium ionic liquids to freshwater algae. *Green Chem.,* 10**,** 104-110.

KUMAR, M., TRIVEDI, N., REDDY, C. R. K. & JHA, B. 2011. Toxic Effects of Imidazolium Ionic Liquids on the Green Seaweed *Ulva lactuca*: Oxidative Stress and DNA Damage. *Chem. Res. Toxicol.,* 24**,** 1882-1890.

LADIKOS, D. & LOUGOVOIS, V. 1990. Lipid oxidation in muscle foods: A review. *Food Chem.,* 35**,** 295-314.

LANDELS, A., BEACHAM, T. A., EVANS, C. T., CARNOVALE, G., RAIKOVA, S., COLE, I. S., GODDARD, P., CHUCK, C. & ALLEN, M. J. 2019. Improving electrocoagulation floatation for harvesting microalgae. *Algal Res.,* 39**,** 101446.

LANE, K., DERBYSHIRE, E., LI, W. & BRENNAN, C. 2013. Bioavailability and Potential Uses of Vegetarian Sources of Omega-3 Fatty Acids: A Review of the Literature. *Crit. Rev. Food Sci.,* 54**,** 572-579.

LANG, O., WISNIEWSKI, T. & LUTZ, M. 2013. *Short Path Distillation of Ionic Liquids*. Patent Number: WO171060.

LATALA, A., NEDZI, M. & STEPNOWSKI, P. 2009. Toxicity of imidazolium and pyridinium based ionic liquids towards algae. *Chlorella vulgaris*, *Oocystis submarina* (green algae) and *Cyclotella meneghiniana*, *Skeletonema marinoi* (diatoms). *Green Chem.,* 11**,** 580-588.

LATALA, A., NEDZI, M. & STEPNOWSKI, P. 2010. Toxicity of imidazolium ionic liquids towards algae. Influence of salinity variations. *Green Chem.,* 12**,** 60-64.

LATAŁA, A., STEPNOWSKI, P., NĘDZI, M. & MROZIK, W. 2005. Marine toxicity assessment of imidazolium ionic liquids: Acute effects on the Baltic algae *Oocystis submarina* and *Cyclotella meneghiniana*. *Aquat. Toxicol.,* 73**,** 91-98.

LAURENS, L. L., QUINN, M., VAN WYCHEN, S., TEMPLETON, D. & WOLFRUM, E. 2012. Accurate and reliable quantification of total microalgal fuel potential as fatty acid methyl esters by in situ transesterification. *Anal. Bioanal. Chem.,* 403**,** 167-178.

LAVIE, C. J., MILANI, R. V., MEHRA, M. R. & VENTURA, H. O. 2009. Omega-3 Polyunsaturated Fatty Acids and Cardiovascular Diseases. *J. Am. Coll. Cardiol.,* 54**,** 585-594.

LEE, A. K., LEWIS, D. M. & ASHMAN, P. J. 2009. Microbial flocculation, a potentially low-cost harvesting technique for marine microalgae for the production of biodiesel. *J. Appl. Phycol.,* 21**,** 559-567.

LEE, H., KIM, S. M. & JEON, T. J. 2015. Effects of imidazolium-based ionic liquids on the stability and dynamics of gramicidin A and lipid bilayers at different salt concentrations. *J. Mol. Graph. Model.,* 61**,** 53-60.

LEE, J.-Y., YOO, C., JUN, S.-Y., AHN, C.-Y. & OH, H.-M. 2010. Comparison of several methods for effective lipid extraction from microalgae. *Bioresour. Technol.,* 101**,** 75-77.

LEMUS, J., PALOMAR, J., HERAS, F., GILARRANZ, M. A. & RODRIGUEZ, J. J. 2012. Developing criteria for the recovery of ionic liquids from aqueous phase by adsorption with activated carbon. *Sep. Purif. Technol.,* 97**,** 11-19.

LEÓN, R., FERNANDES, P., PINHEIRO, H. M. & CABRAL, J. M. S. 1998. Whole-cell biocatalysis in organic media. *Enzyme Microb. Technol.,* 23**,** 483-500.

LI, N., ZHANG, Y., MENG, H., LI, S., WANG, S., XIAO, Z., CHANG, P., ZHANG, X., LI, Q., GUO, L., IGARASHI, Y. & LUO, F. 2019. Characterization of Fatty Acid Exporters involved in fatty acid transport for oil accumulation in the green alga *Chlamydomonas reinhardtii*. *Biotechnol. Biofuels,* 12**,** PMID: 30651755.

LOU, W.-Y., ZONG, M.-H. & SMITH, T. J. 2006. Use of ionic liquids to improve whole-cell biocatalytic asymmetric reduction of acetyltrimethylsilane for efficient synthesis of enantiopure (*S*)-1-trimethylsilylethanol. *Green Chem.,* 8**,** 147-155.

LOVEJOY, K., DAVIS, L., MCCLELLAN, L., LILLO, A., WELSH, J., SCHMIDT, E., SANDERS, C., LOU, A., FOX, D., KOPPISCH, A. & SESTO, R. 2013. Evaluation of ionic liquids on phototrophic microbes and their use in biofuel extraction and isolation. *J. Appl. Phycol.,* 25**,** 973-981.

MAASE, M. 2005. *Distillation of Ionic Liquids*. Patent Number: WO068404.

MANN, J. E. & MYERS, J. 1968. On Pigments, Growth, and Photosynthesis of *Phaeodactylum tricornutum*. *J. Phycol.,* 4**,** 349-355.

MARCHAND, D. & RONTANI, J.-F. 2001. Characterisation of photo-oxidation and autoxidation products of phytoplanktonic monounsaturated fatty acids in marine particulate matter and recent sediments. *Org. Geochem.,* 32**,** 287-304.

MARKIEWICZ, M., JUNGNICKEL, C. & ARP, H. P. H. 2013. Ionic Liquid Assisted Dissolution of Dissolved Organic Matter and PAHs from Soil Below the Critical Micelle Concentration. *Environ. Sci. Technol.,* 47**,** 6951-6958.

MASON, T. J., LORIMER, J. P., BATES, D. M. & ZHAO, Y. 1994. Dosimetry in sonochemistry: the use of aqueous terephthalate ion as a fluorescence monitor. *Ultrason. Sonochem.,* 1**,** S91-S95.

MATZKE, M., STOLTE, S., BOSCHEN, A. & FILSER, J. 2008. Mixture effects and predictability of combination effects of imidazolium based ionic liquids as well as imidazolium based

ionic liquids and cadmium on terrestrial plants (*Triticum aestivum*) and limnic green algae (*Scenedesmus vacuolatus*). *Green Chem.,* 10**,** 784-792.
MENDES, R. L., NOBRE, B. P., CARDOSO, M. T., PEREIRA, A. P. & PALAVRA, A. F. 2003. Supercritical carbon dioxide extraction of compounds with pharmaceutical importance from microalgae. *Inorg. Chim. Acta,* 356**,** 328-334.
MENG, X., SHANG, H., ZHENG, Y. & ZHANG, Z. 2013. Free fatty acid secretion by an engineered strain of *Escherichia coli*. *Biotechnol. Lett.,* 35**,** 2099-2103.
METZGER, P. & LARGEAU, C. 2005. *Botryococcus braunii*: a rich source for hydrocarbons and related ether lipids. *Appl. Microbiol. Biotechnol.,* 66**,** 486-496.
MILLEDGE, J. & HEAVEN, S. 2013. A review of the harvesting of micro-algae for biofuel production. *Rev. Environ. Sci. Bio.,* 12**,** 165-178.
MIN, B. & AHN, D. U. 2005. Mechanism of lipid peroxidation in meat and meat products -A review. *Food Sci. Biotechnol.,* 14**,** 152-163.
MITCHELL, M. J., JENSEN, O. E., CLIFFE, K. A. & MAROTO-VALER, M. M. 2010. A model of carbon dioxide dissolution and mineral carbonation kinetics. *P. Roy. Soc. A-Math. Phy.,* 466**,** 1265-1290.
MOHEIMANI, N., CORD-RUWISCH, R., RAES, E. & BOROWITZKA, M. 2013. Non-destructive oil extraction from *Botryococcus braunii* (Chlorophyta). *J. Appl. Phycol.,* 25**,** 1653-1661.
MOHEIMANI, N., MATSUURA, H., WATANABE, M. & BOROWITZKA, M. 2014. Non-destructive hydrocarbon extraction from *Botryococcus braunii* BOT-22 (race B). *J. Appl. Phycol.,* 26**,** 1453-1463.
MOKHTAR, S. U., CHIN, S. T., VIJAYARAGHAVAN, R., MACFARLANE, D. R., DRUMMER, O. H. & MARRIOTT, P. J. 2015. Direct ionic liquid extractant injection for volatile chemical analysis – a gas chromatography sampling technique. *Green Chem.,* 17**,** 573-581.
MOLINA GRIMA, E., BELARBI, E. H., ACIÉN FERNÁNDEZ, F. G., ROBLES MEDINA, A. & CHISTI, Y. 2003. Recovery of microalgal biomass and metabolites: process options and economics. *Biotechnol. Adv.,* 20**,** 491-515.
MONTEIRO, M. R., AMBROZIN, A. R. P., LIÃO, L. M. & FERREIRA, A. G. 2008. Critical review on analytical methods for biodiesel characterization. *Talanta,* 77**,** 593-605.
MOPSIK, F. I. 1967. Dielectric Constant of Hexane as a Function of Temperature, Pressure, and Density. *J. Res. Natl. Bur. Stand. Sec. A,* 71A**,** 287-292.
MOVAHED, S. & LI, D. 2012. Electrokinetic transport through the nanopores in cell membrane during electroporation. *J. Colloid Interface Sci.,* 369**,** 442-452.
MUBARAK, M., SHAIJA, A. & SUCHITHRA, T. V. 2016. Ultrasonication: An effective pre-treatment method for extracting lipid from *Salvinia molesta* for biodiesel production. *Resource-Efficient Technol.,* 2**,** 126-132.
MÜHLROTH, A., LI, K., RØKKE, G., WINGE, P., OLSEN, Y., HOHMANN-MARRIOTT, M. F., VADSTEIN, O. & BONES, A. M. 2013. Pathways of lipid metabolism in marine algae, co-expression network, bottlenecks and candidate genes for enhanced production of EPA and DHA in species of Chromista. *Mar. Drugs,* 11**,** 4662-4697.
N. JEAN, C. B., J.P. SIMORRE. 2014. *Peptidoglycan molecular Structure* [Online]. Glycopedia.eu. Available: https://glycopedia.eu/e-chapters/the-structure-of-bacterial-cell/article/peptidoglycan-molecular-structure [Accessed 2020].
NEUMANN, E., TOENSING, K., KAKORIN, S., BUDDE, P. & FREY, J. 1998. Mechanism of Electroporative Dye Uptake by Mouse B Cells. *Biophys. J.,* 74**,** 98-108.
NEWMAN, S. M., HARRIS, E. H., JOHNSON, A. M., BOYNTON, J. E. & GILLHAM, N. W. 1992. Nonrandom distribution of chloroplast recombination events in *Chlamydomonas reinhardtii*: evidence for a hotspot and an adjacent cold region. *Genetics,* 132**,** 413-429.

ORIGINOIL. 2014a. *Electro Water Separation* [Online]. Available: https://www.originclear.com/technologies/electro-water-separation#ews [Accessed 2021].

ORIGINOIL. 2014b. *OriginOil Announces Breakthrough Process for Live Algae Oil Extraction* [Online]. Available: https://www.originclear.com/company-news/originoil-announces-breakthrough-process-for-live-algae-oil-extraction [Accessed 2021].

OUELLET, M., EMOND, V., CHEN, C. T., JULIEN, C., BOURASSET, F., ODDO, S., LAFERLA, F., BAZINET, R. P. & CALON, F. 2009. Diffusion of docosahexaenoic and eicosapentaenoic acids through the blood–brain barrier: An in situ cerebral perfusion study. *Neurochem. Int.,* 55**,** 476-482.

PALOMAR, J., LEMUS, J., GILARRANZ, M. A. & RODRIGUEZ, J. J. 2009. Adsorption of ionic liquids from aqueous effluents by activated carbon. *Carbon,* 47**,** 1846-1856.

PANIKASHVILI, D., SAVALDI-GOLDSTEIN, S., MANDEL, T., YIFHAR, T., FRANKE, R. B., HOFER, R., SCHREIBER, L., CHORY, J. & AHARONI, A. 2007. The *Arabidopsis* DESPERADO/AtWBC11 transporter is required for cutin and wax secretion. *Plant Physiol.,* 145**,** 1345-1360.

PATIL, P., REDDY, H., MUPPANENI, T., PONNUSAMY, S., SUN, Y., DAILEY, P., COOKE, P., PATIL, U. & DENG, S. 2013. Optimization of microwave-enhanced methanolysis of algal biomass to biodiesel under temperature controlled conditions. *Bioresour. Technol.,* 137**,** 278-285.

PATIL, P. D., REDDY, H., MUPPANENI, T., MANNARSWAMY, A., SCHUAB, T., HOLGUIN, F. O., LAMMERS, P., NIRMALAKHANDAN, N., COOKE, P. & DENG, S. 2012. Power dissipation in microwave-enhanced *in situ* transesterification of algal biomass to biodiesel. *Green Chem.,* 14**,** 809-818.

PEET, M. & STOKES, C. 2005. Omega-3 fatty acids in the treatment of psychiatric disorders. *Drugs,* 65**,** 1051-1059.

PEKARSKY, A., SPADIUT, O., RAJAMANICKAM, V. & WURM, D. J. 2019. A fast and simple approach to optimize the unit operation high pressure homogenization - a case study for a soluble therapeutic protein in *E. coli*. *Prep. Biochem. Biotechnol.,* 49**,** 74-81.

PERNAK, J., WASIŃSKI, K., PRACZYK, T., NAWROT, J., CIENIECKA-ROSŁONKIEWICZ, A., WALKIEWICZ, F. & MATERNA, K. 2012. Sweet ionic liquids-cyclamates: Synthesis, properties, and application as feeding deterrents. *Sci. China Chem.,* 55**,** 1532-1541.

PFLASTER, E. L., SCHWABE, M. J., BECKER, J., WILKINSON, M. S., PARMER, A., CLEMENTE, T. E., CAHOON, E. B. & RIEKHOF, W. R. 2014. A High-Throughput Fatty Acid Profiling Screen Reveals Novel Variations in Fatty Acid Biosynthesis in *Chlamydomonas reinhardtii* and Related Algae. *Eukaryot. Cell,* 13**,** 1431-1438.

PFRUENDER, H., JONES, R. & WEUSTER-BOTZ, D. 2006. Water immiscible ionic liquids as solvents for whole cell biocatalysis. *J. Biotechnol.,* 124**,** 182-190.

PHAM, T. P. T., CHO, C.-W., MIN, J. & YUN, Y.-S. 2008. Alkyl-chain length effects of imidazolium and pyridinium ionic liquids on photosynthetic response of *Pseudokirchneriella subcapitata*. *J. Biosci. Bioeng.,* 105**,** 425-428.

PIGHIN, J. A., ZHENG, H., BALAKSHIN, L. J., GOODMAN, I. P., WESTERN, T. L., JETTER, R., KUNST, L. & SAMUELS, A. L. 2004. Plant cuticular lipid export requires an ABC transporter. *Science,* 306**,** 702-704.

PINKERT, A., MARSH, K. N., PANG, S. & STAIGER, M. P. 2009. Ionic Liquids and Their Interaction with Cellulose. *Chem. Rev.,* 109**,** 6712-6728.

PLECHKOVA, N. V. & SEDDON, K. R. 2008. Applications of ionic liquids in the chemical industry. *Chem. Soc. Rev.,* 37**,** 123-150.

POPKO, J. 2016. *Encyclopedia of Lipidomics* Pages: 1-7. Springer Netherlands, Dordrecht

POPPER, Z. A., RALET, M.-C. & DOMOZYCH, D. S. 2014. Plant and algal cell walls: diversity and functionality. *Ann. Bot.,* 114**,** 1043-1048.

PRABAKARAN, P. & RAVINDRAN, A. D. 2011. A comparative study on effective cell disruption methods for lipid extraction from microalgae. *Lett. Appl. Microbiol.,* 53**,** 150-154.

PRATT, A. J. & MACRAE, I. J. 2009. The RNA-induced silencing complex: a versatile gene-silencing machine. *J. Biol. Chem.,* 284**,** 17897-17901.

PRETTI, C., CHIAPPE, C., BALDETTI, I., BRUNINI, S., MONNI, G. & INTORRE, L. 2009. Acute toxicity of ionic liquids for three freshwater organisms: *Pseudokirchneriella subcapitata*, *Daphnia magna* and *Danio rerio*. *Ecotoxicol. Environ. Saf.,* 72**,** 1170-1176.

PŘIBYL, P., ELIÁŠ, M., CEPÁK, V., LUKAVSKÝ, J. & KAŠTÁNEK, P. 2012. Zoosporogenesis, Morphology, Ultrastructure, Pigment Composition, and Phylogenetic Position of *Trachydiscus minutus* (Eustigmatophyceae, Heterokontophyta). *J. Phycol.,* 48**,** 231-242.

PUCIHAR, G., KOTNIK, T., KANDUŠER, M. & MIKLAVČIČ, D. 2001. The influence of medium conductivity on electropermeabilization and survival of cells in vitro. *Bioelectrochemistry,* 54**,** 107-115.

QI, X., LI, L., TAN, T., CHEN, W. & SMITH, R. L. 2013. Adsorption of 1-Butyl-3-Methylimidazolium Chloride Ionic Liquid by Functional Carbon Microspheres from Hydrothermal Carbonization of Cellulose. *Environ. Sci. Technol.,* 47**,** 2792-2798.

QUEHENBERGER, O., ARMANDO, A. M. & DENNIS, E. A. 2011. High sensitivity quantitative lipidomics analysis of fatty acids in biological samples by gas chromatography-mass spectrometry. *Biochim. Biophys. Acta,* 1811**,** 648-656.

RADAKOVITS, R., JINKERSON, R. E., DARZINS, A. & POSEWITZ, M. C. 2010. Genetic Engineering of Algae for Enhanced Biofuel Production. *Eukaryot. Cell,* 9**,** 486-501.

REBROS, M., GUNARATNE, H. Q. N., FERGUSON, J., SEDDON, K. R. & STEPHENS, G. 2009. A high throughput screen to test the biocompatibility of water-miscible ionic liquids. *Green Chem.,* 11**,** 402-408.

REDDY, H. K., MUPPANENI, T., SUN, Y., LI, Y., PONNUSAMY, S., PATIL, P. D., DAILEY, P., SCHAUB, T., HOLGUIN, F. O., DUNGAN, B., COOKE, P., LAMMERS, P., VOORHIES, W., LU, X. & DENG, S. 2014. Subcritical water extraction of lipids from wet algae for biodiesel production. *Fuel,* 133**,** 73-81.

REEP, P. & GREEN, M. 2012. *Procedure for extracting lipids from algae without cell sacrifice*. Patent Number: WO/2012/021831. US patent application.

RELLER, L. B., WEINSTEIN, M., JORGENSEN, J. H. & FERRARO, M. J. 2009. Antimicrobial Susceptibility Testing: A Review of General Principles and Contemporary Practices. *Clin. Infect. Dis.,* 49**,** 1749-1755.

REMACLE, C., CLINE, S., BOUTAFFALA, L., GABILLY, S., LAROSA, V., BARBIERI, M. R., COOSEMANS, N. & HAMEL, P. P. 2009. The ARG9 gene encodes the plastid-resident *N*-acetyl ornithine aminotransferase in the green alga *Chlamydomonas reinhardtii*. *Eukaryot. Cell,* 8**,** 1460-1463.

RIESZ, P., BERDAHL, D. & CHRISTMAN, C. L. 1985. Free radical generation by ultrasound in aqueous and nonaqueous solutions. *Environ. Health Perspect.,* 64**,** 233-252.

RIESZ, P. & KONDO, T. 1992. Free radical formation induced by ultrasound and its biological implications. *Free Radical Biol. Med.,* 13**,** 247-270.

ROGERS, R. D. & SEDDON, K. R. 2003. Ionic Liquids--Solvents of the Future? *Science,* 302**,** 792-793.

ROLS, M.-P., DELTEIL, C., GOLZIO, M. & TEISSIÉ, J. 1998. Control by ATP and ADP of voltage-induced mammalian-cell-membrane permeabilization, gene transfer and resulting expression. *Eur. J. Biochem.,* 254**,** 382-388.

ROLS, M. P. & TEISSIE, J. 1992. Experimental evidence for the involvement of the cytoskeleton in mammalian cell electropermeabilization. *Biochim. Biophys. Acta,* 1111**,** 45-50.

ROSSI, P. C., PRAMPARO MDEL, C., GAICH, M. C., GROSSO, N. R. & NEPOTE, V. 2011. Optimization of molecular distillation to concentrate ethyl esters of eicosapentaenoic (20:5 *ω*-3) and docosahexaenoic acids (22:6 *ω*-3) using simplified phenomenological modeling. *J. Sci. Food Agric.,* 91**,** 1452-1458.

ROTH, B. L., POOT, M., YUE, S. T. & MILLARD, P. J. 1997. Bacterial viability and antibiotic susceptibility testing with SYTOX green nucleic acid stain. *Appl. Environ. Microbiol.,* 63**,** 2421-2431.

SAFI, D. C., RODRIGUEZ, L., MULDER, W. J., ENGELEN-SMIT, N., SPEKKING, W., BROEK, L., OLIVIERI, G. & SIJTSMA, L. 2017. Energy consumption and water-soluble protein release by cell wall disruption of *Nannochloropsis gaditana*. *Bioresour. Technol.,* 239**,** 204-210.

SAMEK, O., JONÁŠ, A., PILÁT, Z., ZEMÁNEK, P., NEDBAL, L., TŘÍSKA, J., KOTAS, P. & TRTÍLEK, M. 2010. Raman microspectroscopy of individual algal cells: sensing unsaturation of storage lipids *in vivo*. *Sensors (Basel),* 10**,** 8635-8651.

SAMORÌ, C., MALFERRARI, D., VALBONESI, P., MONTECAVALLI, A., MORETTI, F., GALLETTI, P., SARTOR, G., TAGLIAVINI, E., FABBRI, E. & PASTERIS, A. 2010a. Introduction of oxygenated side chain into imidazolium ionic liquids: Evaluation of the effects at different biological organization levels. *Ecotoxicol. Environ. Saf.,* 73**,** 1456-1464.

SAMORÌ, C., TORRI, C., SAMORÌ, G., FABBRI, D., GALLETTI, P., GUERRINI, F., PISTOCCHI, R. & TAGLIAVINI, E. 2010b. Extraction of hydrocarbons from microalga *Botryococcus braunii* with switchable solvents. *Bioresour. Technol.,* 101**,** 3274-3279.

SANAGI, M. M., LING, S. L., NASIR, Z., HERMAWAN, D., IBRAHIM, W. A. & ABU NAIM, A. 2009. Comparison of signal-to-noise, blank determination, and linear regression methods for the estimation of detection and quantification limits for volatile organic compounds by gas chromatography. *J. AOAC Int.,* 92**,** 1833-1838.

SANTANA, A., JESUS, S., LARRAYOZ, M. A. & FILHO, R. M. 2012. Supercritical Carbon Dioxide Extraction of Algal Lipids for the Biodiesel Production. *Procedia Engineer.,* 42**,** 1755-1761.

SATO, M., MURATA, Y., MIZUSAWA, M., IWAHASHI, H. & OKA, S. 2004. A simple and rapid dual-fluorescence viability assay for microalgae. *Microbiol. Cult. Collect.,* 20**,** 53-59.

SAUER, T. & GALINSKI, E. A. 1998. Bacterial milking: A novel bioprocess for production of compatible solutes. *Biotechnol. Bioeng.,* 57**,** 306-313.

SCHOLZ, M. J., WEISS, T. L., JINKERSON, R. E., JING, J., ROTH, R., GOODENOUGH, U., POSEWITZ, M. C. & GERKEN, H. G. 2014. Ultrastructure and composition of the *Nannochloropsis gaditana* cell wall. *Eukaryot. Cell,* 13**,** 1450-1464.

SCHRODA, M. 2006. RNA silencing in *Chlamydomonas*: mechanisms and tools. *Curr. Genet.,* 49**,** 69-84.

SCHWAN, H. P. 1957. *Advances in Biological and Medical Physics, Volume 5* Electrical Properties of Tissue and Cell Suspensions, Pages: 147-209. Academic Press Inc., New York

SCHWISTER, K. & DEUTICKE, B. 1985. Formation and properties of aqueous leaks induced in human erythrocytes by electrical breakdown. *Biochim. Biophys. Acta,* 816**,** 332-348.

SCRIMGEOUR, C. 2005. *Bailey's Industrial Oil and Fat Products* Chemistry of Fatty Acids, Pages: 1-27. John Wiley & Sons, Hoboken, USA

SEDDON, K. R., STARK, A. & TORRES, M.-J. 2000. Influence of chloride, water, and organic solvents on the physical properties of ionic liquids. *Pure Appl. Chem.,* 72**,** 2275-2287.

SENA, D. W., KULACKI, K. J., CHALONER, D. T. & LAMBERTI, G. A. 2010. The role of the cell wall in the toxicity of ionic liquids to the alga *Chlamydomonas reinhardtii*. *Green Chem.,* 12**,** 1066-1071.

SHAHIDI, F. & ZHONG, Y. 2010. Lipid oxidation and improving the oxidative stability. *Chem. Soc. Rev.,* 39**,** 4067-4079.

SHANG, T., LIU, L., ZHOU, J., ZHANG, M., HU, Q., FANG, M., WU, Y., YAO, P. & GONG, Z. 2017. Protective effects of various ratios of DHA/EPA supplementation on high-fat diet-induced liver damage in mice. *Lipids Health Dis.,* 16**,** 65-65.

SHEHADUL ISLAM, M., ARYASOMAYAJULA, A. & SELVAGANAPATHY, P. R. 2017. A Review on Macroscale and Microscale Cell Lysis Methods. *Micromachines,* 8**,** 83.

SIDDIQUI, A., WEI, Z., BOEHM, M. & AHMAD, N. 2020. Engineering microalgae through chloroplast transformation to produce high-value industrial products. *Biotechnol. Appl. Biochem.,* 67**,** 30-40.

SINGH, S. P. & SINGH, P. 2014. Effect of CO_2 concentration on algal growth: A review. *Renew. Sust. Energ. Rev.,* 38**,** 172-179.

SKLAVOUNOS, E., HELMINEN, J. K. J., KYLLÖNEN, L., KILPELÄINEN, I. & KING, A. W. T. 2016. *Encyclopedia of Inorganic and Bioinorganic Chemistry* Ionic Liquids: Recycling, Pages: 1-16. John Wiley & Sons, Hoboken, USA

SMITH, H. L. & WALTMAN, P. 1995. *The Theory of the Chemostat: Dynamics of Microbial Competition* The Simple Chemostat, Pages: 1-20. Cambridge University Press, Cambridge

SODEINDE, O. A. & KINDLE, K. L. 1993. Homologous recombination in the nuclear genome of *Chlamydomonas reinhardtii*. *Proc. Natl. Acad. Sci. USA,* 90**,** 9199-9203.

SOLAESA Á, G., SANZ, M. T., FALKEBORG, M., BELTRÁN, S. & GUO, Z. 2016. Production and concentration of monoacylglycerols rich in omega-3 polyunsaturated fatty acids by enzymatic glycerolysis and molecular distillation. *Food Chem.,* 190**,** 960-967.

STARK, A., BEHREND, P., BRAUN, O., MÜLLER, A., RANKE, J., ONDRUSCHKA, B. & JASTORFF, B. 2008. Purity specification methods for ionic liquids. *Green Chem.,* 10**,** 1152-1161.

STEPHENS, G. & LICENCE, P. 2011. Ioinic Liquids: Toxic or Not? *Chimica Oggi,* 29.

STEPNOWSKI, P., MÜLLER, A., BEHREND, P., RANKE, J., HOFFMANN, J. & JASTORFF, B. 2003. Reversed-phase liquid chromatographic method for the determination of selected room-temperature ionic liquid cations. *J. Chromatogr. A,* 993**,** 173-178.

STOLTE, S., MATZKE, M., ARNING, J., BOSCHEN, A., PITNER, W.-R., WELZ-BIERMANN, U., JASTORFF, B. & RANKE, J. 2007. Effects of different head groups and functionalised side chains on the aquatic toxicity of ionic liquids. *Green Chem.,* 9**,** 1170-1179.

STRANSKA-ZACHARIASOVA, M., KASTANEK, P., DZUMAN, Z., RUBERT, J., GODULA, M. & HAJSLOVA, J. 2016. Bioprospecting of microalgae: Proper extraction followed by high performance liquid chromatographic–high resolution mass spectrometric fingerprinting as key tools for successful metabolom characterization. *J. Chromatogr. B,* 1015-1016**,** 22-33.

STRÄUBER, H. & MÜLLER, S. 2010. Viability states of bacteria—Specific mechanisms of selected probes. *Cytometry A,* 77A**,** 623-634.

SUKARNI, SUDJITO, HAMIDI, N., YANUHAR, U. & WARDANA, I. N. G. 2014. Potential and properties of marine microalgae *Nannochloropsis oculata* as biomass fuel feedstock. *Int. J. Energ. Environ. Engineer.,* 5**,** 279-290.

SUKENIK, A. & SHELEF, G. 1984. Algal autoflocculation—verification and proposed mechanism. *Biotechnol. Bioeng.,* 26**,** 142-147.

SUMMERS, S. R., SPRENGER, K. G., PFAENDTNER, J., MARCHANT, J., SUMMERS, M. F. & KAAR, J. L. 2017. Mechanism of Competitive Inhibition and Destabilization of *Acidothermus cellulolyticus* Endoglucanase 1 by Ionic Liquids. *J. Phys. Chem. B,* 121**,** 10793-10803.

SUN, J., LIU, H., YANG, W., CHEN, S. & FU, S. 2017. Molecular Mechanisms Underlying Inhibitory Binding of Alkylimidazolium Ionic Liquids to Laccase. *Molecules,* 22**,** 1353.

SUTTANGKAKUL, A., SIRIKHACHORNKIT, A., JUNTAWONG, P., PUANGTAME, W., CHOMTONG, T., SRIFA, S., SATHITNAITHAM, S., DUMRONGTHAWATCHAI, W., JARIYACHAWALID, K. & VUTTIPONGCHAIKIJ, S. 2019. Evaluation of strategies for

improving the transgene expression in an oleaginous microalga *Scenedesmus acutus*. *BMC Biotechnol.,* 19.

TAMMEKIVI, E., VAHUR, S., KEKIŠEV, O., VAN DER WERF, I. D., TOOM, L., HERODES, K. & LEITO, I. 2019. Comparison of derivatization methods for the quantitative gas chromatographic analysis of oils. *Anal. Methods,* 11**,** 3514-3522.

TEISSIE, J., GOLZIO, M. & ROLS, M. P. 2005. Mechanisms of cell membrane electropermeabilization: A minireview of our present (lack of ?) knowledge. *Biochim. Biophys. Acta,* 1724**,** 270-280.

TEISSIÉ, J. & ROLS, M. P. 1993. An experimental evaluation of the critical potential difference inducing cell membrane electropermeabilization. *Biophys. J.,* 65**,** 409-413.

TEIXEIRA, R. E. 2012. Energy-efficient extraction of fuel and chemical feedstocks from algae. *Green Chem.,* 14**,** 419-427.

TO, T. Q., PROCTER, K., SIMMONS, B. A., SUBASHCHANDRABOSE, S. & ATKIN, R. 2018. Low cost ionic liquid–water mixtures for effective extraction of carbohydrate and lipid from algae. *Faraday Discuss.,* 206**,** 93-112.

TOOR, S. S., REDDY, H., DENG, S., HOFFMANN, J., SPANGSMARK, D., MADSEN, L. B., HOLM-NIELSEN, J. B. & ROSENDAHL, L. A. 2013. Hydrothermal liquefaction of *Spirulina* and *Nannochloropsis salina* under subcritical and supercritical water conditions. *Bioresour. Technol.,* 131**,** 413-419.

TORTORA, G. J., FUNKE, B. R. & CASE, C. L. 2019. *Microbiology: an introduction 13th Edition.* Microbial Growth, Pages: 177-204. Pearson, Essex

UDUMAN, N., QI, Y., DANQUAH, M. K., FORDE, G. M. & HOADLEY, A. 2010. Dewatering of microalgal cultures: A major bottleneck to algae-based fuels. *J. Renew. Sustain. Ener.,* 2**,** 012701.

VAESSEN, E. M. J., DEN BESTEN, H. M. W., PATRA, T., VAN MOSSEVELDE, N. T. M., BOOM, R. M. & SCHUTYSER, M. A. I. 2018. Pulsed electric field for increasing intracellular trehalose content in *Lactobacillus plantarum* WCFS1. *Innov. Food Sci. Emerg. Technol.,* 47**,** 256-261.

VECCHIO, S., CAMPANELLA, L., NUCCILLI, A. & TOMASSETTI, M. 2008. Kinetic study of thermal breakdown of triglycerides contained in extra-virgin olive oil. *J. Therm. Anal. Calorim.,* 91**,** 51-56.

VELDHUIS, M. J. W., CUCCI, T. L. & SIERACKI, M. E. 1997. Cellular DNA content of marine phytoplankton using two new fluorochromes: Taxonomic and ecological implications. *J. Phycol.,* 33**,** 527-541.

VENTURA, S. P. M., DE BARROS, R. L. F., SINTRA, T., SOARES, C. M. F., LIMA, Á. S. & COUTINHO, J. A. P. 2012. Simple screening method to identify toxic/non-toxic ionic liquids: Agar diffusion test adaptation. *Ecotoxicol. Environ. Saf.,* 83**,** 55-62.

VENTURA, S. P. M., E SILVA, F. A., GONÇALVES, A. M. M., PEREIRA, J. L., GONÇALVES, F. & COUTINHO, J. A. P. 2014. Ecotoxicity analysis of cholinium-based ionic liquids to *Vibrio fischeri* marine bacteria. *Ecotoxicol. Environ. Saf.,* 102**,** 48-54.

VERSTEEGH, G. J. M. & BLOKKER, P. 2004. Resistant macromolecules of extant and fossil microalgae. *Phycol. Res.,* 52**,** 325-339.

WATANABE, T., ANDO, K., DAIDOJI, H., OTAKI, Y., SUGAWARA, S., MATSUI, M., IKENO, E., HIRONO, O., MIYAWAKI, H., YASHIRO, Y., NISHIYAMA, S., ARIMOTO, T., TAKAHASHI, H., SHISHIDO, T., MIYASHITA, T., MIYAMOTO, T. & KUBOTA, I. 2017. A randomized controlled trial of eicosapentaenoic acid in patients with coronary heart disease on statins. *J. Cardiol.,* 70**,** 537-544.

WEISS, T. L., ROTH, R., GOODSON, C., VITHA, S., BLACK, I., AZADI, P., RUSCH, J., HOLZENBURG, A., DEVARENNE, T. P. & GOODENOUGH, U. 2012. Colony Organization in the Green Alga *Botryococcus braunii* (Race B) Is Specified by a Complex Extracellular Matrix. *Eukaryot. Cell,* 11**,** 1424-1440.

WELLS, A. S. & COOMBE, V. T. 2006. On the Freshwater Ecotoxicity and Biodegradation Properties of Some Common Ionic Liquids. *Org. Process Res. Dev.,* 10**,** 794-798.

WOOD, N., FERGUSON, J. L., GUNARATNE, H. Q. N., SEDDON, K. R., GOODACRE, R. & STEPHENS, G. M. 2011. Screening ionic liquids for use in biotransformations with whole microbial cells. *Green Chem.,* 13**,** 1843-1851.

WU, B., ZHANG, Y. & WANG, H. 2008a. Phase Behavior for Ternary Systems Composed of Ionic Liquid + Saccharides + Water. *J. Phys. Chem. B,* 112**,** 6426-6429.

WU, B., ZHANG, Y. M. & WANG, H. P. 2008b. Aqueous Biphasic Systems of Hydrophilic Ionic Liquids + Sucrose for Separation. *J. Chem. Eng. Data,* 53**,** 983-985.

WU, M., ZHAO, D., ZHONG, W., YAN, H., WANG, X., LIANG, Z. & LI, Z. 2013. High-density distributed electrode network, a multi-functional electroporation method for delivery of molecules of different sizes. *Sci. Rep.,* 3**,** 3370.

XIE, W. H., ZHU, C. C., ZHANG, N. S., LI, D. W., YANG, W. D., LIU, J. S., SATHISHKUMAR, R. & LI, H. Y. 2014. Construction of novel chloroplast expression vector and development of an efficient transformation system for the diatom *Phaeodactylum tricornutum*. *Mar. Biotechnol.,* 16**,** 538-546.

YAMADA, T. & SAKAGUCHI, K. 1982. Comparative studies on *Chlorella* cell walls: Induction of protoplast formation. *Arch. Microbiol.,* 132**,** 10-13.

YANG, J., LIAN, H., LIANG, W., NGUYEN, V. P. & CHEN, Y. 2018. Experimental investigation of the effects of supercritical carbon dioxide on fracture toughness of bituminous coals. *Int. J. Rock Mech. Min. Sci.,* 107.

YAO, X., JERICHO, M., PINK, D. & BEVERIDGE, T. 1999. Thickness and Elasticity of Gram-Negative Murein Sacculi Measured by Atomic Force Microscopy. *J. Bacteriol.,* 181**,** 6865-6875.

YEFREMOVA, Y. & PURTON, S. 2018. The algal chloroplast as a synthetic biology platform for production of therapeutic proteins. *Microbiology,* 164**,** 113-121.

YOO, B., ZHU, Y. & MAGINN, E. J. 2016. Molecular Mechanism of Ionic-Liquid-Induced Membrane Disruption: Morphological Changes to Bilayers, Multilayers, and Vesicles. *Langmuir,* 32**,** 5403-5411.

ZHANG, F., CHENG, L.-H., GAO, W.-L., XU, X.-H., ZHANG, L. & CHEN, H.-L. 2011a. Mechanism of lipid extraction from *Botryococcus braunii* FACHB 357 in a biphasic bioreactor. *J. Biotechnol.,* 154**,** 281-284.

ZHANG, F., CHENG, L.-H., XU, X.-H., ZHANG, L. & CHEN, H.-L. 2011b. Screening of biocompatible organic solvents for enhancement of lipid milking from *Nannochloropsis sp*. *Process Biochem.,* 46**,** 1934-1941.

ZHANG, F., CHENG, L.-H., XU, X.-H., ZHANG, L. & CHEN, H.-L. 2013a. Application of memberane dispersion for enhanced lipid milking from *Botryococcus braunii* FACHB 357. *J. Biotechnol.,* 165**,** 22-29.

ZHANG, G., LIU, J. & LIU, Y. 2013b. Concentration of Omega-3 Polyunsaturated Fatty Acids from Oil of *Schizochytrium limacinum* by Molecular Distillation: Optimization of Technological Conditions. *Ind. Eng. Chem. Res.,* 52**,** 3918-3925.

ZHANG, J. & LEE, H. K. 2010. Headspace ionic liquid-based microdrop liquid-phase microextraction followed by microdrop thermal desorption-gas chromatographic analysis. *Talanta,* 81**,** 537-542.

ZHAO, D., HUANG, D., LI, Y., WU, M., ZHONG, W., CHENG, Q., WANG, X., WU, Y., ZHOU, X., WEI, Z., LI, Z. & LIANG, Z. 2016. A Flow-Through Cell Electroporation Device for Rapidly and Efficiently Transfecting Massive Amounts of Cells *in vitro* and *ex vivo*. *Sci. Rep.,* 6**,** 18469.